AD-A167 695 INJECTION OF DRAG REDUCING ADDITIVES INTO TURBULENT WATER FLOWS TECHNIQUE..(U) PURDUE UNIV LAFAYETTE IN SCHOOL OF MECHANICAL ENGINEERING W G TIEDERMAN ET AL. 1/2

UNCLASSIFIED APR 86 PME-FM-86 N00014-83-K-0183 F/G 20/4 NL

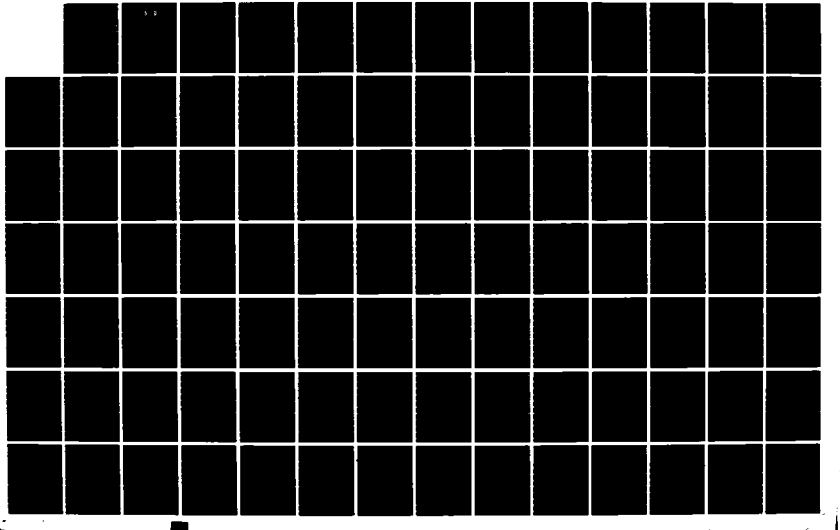

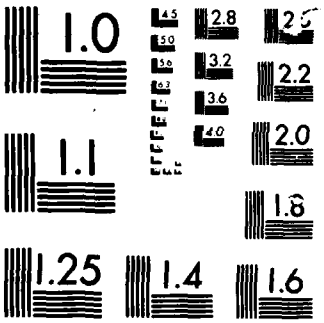
1.0
1.1
1.25
1.4
1.6
1.8
2.0
2.2
2.8
3.2
3.6
4.0
4.5
5.0
5.6
6.3
MICROCOPY
CHART

(12)

Report PME-FM-86

DTIC
S ELECTE
MAY 07 1986
D
D

INJECTION OF DRAG REDUCING ADDITIVES INTO TURBULENT WATER FLOWS

Techniques for Concentration Measurements and Reynolds Number Scaling

AD-A167 695

William G. Tiederman, David T. Walker, Thomas S. Luchik and Amer Abdallah
School of Mechanical Engineering
Purdue University
West Lafayette, Indiana 47907

April 1986

Technical Report for Period 01 March 1985 - 28 February 1986

Approved for public release; distribution unlimited

Prepared for

OFFICE OF NAVAL RESEARCH
800 North Quincy Street
Arlington, VA 22217-5000

86 5 6 121

SECURITY CLASSIFICATION OF THIS PAGE (When Data Entered)

REPORT DOCUMENTATION PAGE

READ INSTRUCTIONS BEFORE COMPLETING FORM

1. REPORT NUMBER: PME-FM-86	2. GOVT ACCESSION NO.: AD-A167695
3. RECIPIENT'S CATALOG NUMBER	
4. TITLE (and Subtitle): INJECTION OF DRAG REDUCING ADDITIVES INTO TURBULENT WATER FLOWS: Techniques for Concentration Measurements and Reynolds Number Scaling	5. TYPE OF REPORT & PERIOD COVERED: Annual Report for March 1, 1985 through February 28, 1986
	6. PERFORMING ORG. REPORT NUMBER
7. AUTHOR(s): William G. Tiederman, David T. Walker, Thomas S. Luchik and Amer Abdallah	8. CONTRACT OR GRANT NUMBER(s): N00014-83K-0183
9. PERFORMING ORGANIZATION NAME AND ADDRESS: School of Mechanical Engineering, Purdue University, West Lafayette, Indiana 47907	10. PROGRAM ELEMENT, PROJECT, TASK AREA & WORK UNIT NUMBERS: NR 062-754
11. CONTROLLING OFFICE NAME AND ADDRESS: Office of Naval Research, 800 North Quincy Street, Arlington, VA 22217-5000	12. REPORT DATE: April 1986
	13. NUMBER OF PAGES: 123
14. MONITORING AGENCY NAME & ADDRESS (if different from Controlling Office)	15. SECURITY CLASS. (of this report)
	15a. DECLASSIFICATION/DOWNGRADING SCHEDULE

16. DISTRIBUTION STATEMENT (of this Report)

APPROVED FOR PUBLIC RELEASE: DISTRIBUTION UNLIMITED

17. DISTRIBUTION STATEMENT (of the abstract entered in Block 20, if different from Report)

18. SUPPLEMENTARY NOTES

19. KEY WORDS (Continue on reverse side if necessary and identify by block number)

Drag reduction; turbulent wall flows; concentration measurements

20. ABSTRACT (Continue on reverse side if necessary and identify by block number)

The basic goals of this project are to determine the mechanisms by which drag-reducing additives modify the turbulent transport near walls and to develop optimum methods for injecting these additives into flows of water. The purpose is to develop methods for controlling and manipulating turbulent wall flows.

This report describes a technique for deducing both time-average and instantaneous values of local additive concentration. The technique is based on measurement of the fluoresced radiation from dye-marked additive.

DD FORM 1 JAN 73 1473 EDITION OF 1 NOV 65 IS OBSOLETE
S/N 0102-014-6601

SECURITY CLASSIFICATION OF THIS PAGE (When Data Entered)

20. Abstract (continued)

The flow-rate capacity of the flow loop has been increased by the addition of two pumps. One-component laser velocimeter measurements are presented that verify the standard character of the flow in the 2.5 x 25 cm, two dimensional channel at a Reynolds number of 49,300. This increase in Reynolds number capability will be used to verify scaling relationships for the time between wall-layer bursts for flows with and without additives.

CONTENTS

Accesion For
NTIS CRA&I ☑
DTIC TAB ☐
Unannounced ☐
Justification .....
By .....
Distribution /
Availability Codes
Dist | Avail and / or Special
A-1

INTRODUCTION

The basic goals of this project are to determine the mechanisms by which drag-reducing additives modify the turbulent transport near walls and to develop optimum methods for injecting these additives into wall bounded flows of water. The purpose is to develop methods for predicting, controlling and manipulating turbulent wall flows.

During this past year Eulerian, single-point methods were developed to determine the time scales and structure of the principal momentum transport event (the burst event) using one-component velocity sensors. The procedure for and verification of these one-component methods are summarized in Appendix A. These methods are based on clearly defining the differences between ejections and bursts using techniques similar to those presented by Bogard and Tiederman (1986).

These Eulerian burst detectors were applied to two-component laser velocimeter data from drag-reducing flows where very low concentrations of additives were well mixed with water in fully developed channel flows (see Appendix B). In these very low concentration (1-3 ppm) flows, the average time between bursts increases the same amount as the average spacing of the low-speed, wall layer streaks. This is one of several results that indicate there are differences between the well mixed, low concentration region well downstream of an injector and the region near the injector where substantial concentration gradients occur normal to the wall.

Prior to this year the maximum Reynolds number that could be achieved in our flow loop was 17,800 (based on channel height and mass average velocity). Results from the limited Reynolds number range of 9,400 to 17,800 indicate

that the average time between bursts, $\overline{T}_B$, scales with inner variables such that

$$\frac{\overline{T}_B \, u_\tau^2}{\nu} = 90 \qquad (1.1)$$

(see Appendix A). During this year the flow loop was modified to increase the maximum Reynolds number. These modifications and the data verifying the standard character of the channel flow at Re = 49,300 (2.5×25 cm channel) are presented in Chapter 2. One of the primary goals that we hope to achieve soon is verification of the inner scaling relationship for $\overline{T}_B$.

Concentration measurements will be an essential part of our experimental program as we begin to make velocity measurements in the region near the injector. Techniques for deducing both time-average and instantaneous values of local additive concentration are presented in Chapter 3. These techniques are based on measurement of the fluoresced radiation from dye-marked additives. Chapter 3 also includes a description of a new test section built this year for the 6×60 cm channel. This new test section was designed specifically for experiments in which simultaneous measurement of two velocity components and additive concentration will be made.

INCREASE IN REYNOLDS NUMBER CAPABILITY

The primary objective of the modifications to increase the flow rate in the channel flow loop was to make it possible to study the turbulent wall structure, particularly the bursting rate at higher Reynolds number. The basic plan was to add two pumps in parallel with the existing two pumps and to reduce losses in the piping system by: 1) removing flow restrictions, and 2) increasing the pipe diameter from two inches to four inches throughout the system. These modifications increased the Reynolds number to about 75,000 in the 2.5 cm channel, and to 39,000 in the 6.0 cm channel. Figure 1 shows how the Reynolds number varies in both channels when one to four pumps are used in the modified flow loop.

The upstream tank was reinforced to accommodate the increased pressure drop in the entrance. Even so, for the small channel, when more than two pumps are used simultaneously, the side walls of the upstream reservoir deflect and the reservoir leaks badly. In the future, we will need to redesign and replace the upstream reservoir to take full advantage of the increased pump capacity with the smaller channel.

Velocity measurements were made at a Reynolds number of 49,300 to confirm the standard character of the flow, and to establish that accurate measurements could be made at the higher Reynolds number.

A single component configuration of the laser velocimeter was used to measure the streamwise velocity component. The scattered radiation was collected in the forward scatter mode. Table 1 gives all laser velocimeter parameters used in this experiment.

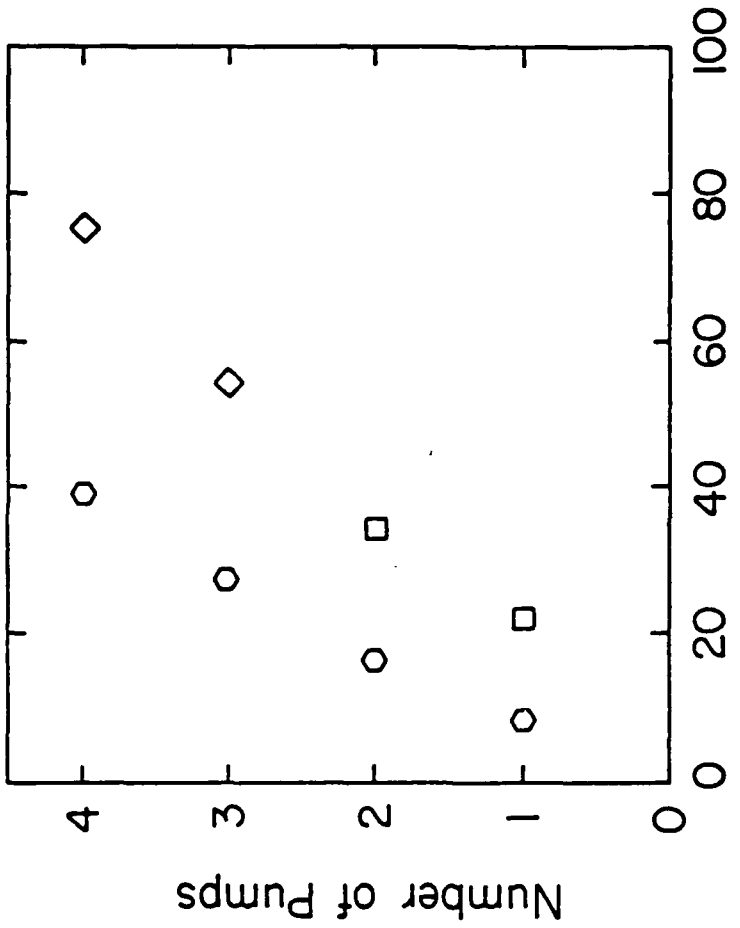

Figure 1. Channel Reynolds Number in Modified Flow Loop as a Function of Number of Pumps Operated; ○ - 6 cm channel, □ - 2.5 cm channel, ◇ - predicted for 2.5 cm channel.

Table 1. One-component laser velocimeter parameters	
Wave length (green) (nm)	514.5
Probe volume length based on beam crossing (mm)	.682
Probe volume length based on receiving optics (mm)	5.50
Probe volume diameter based on beam crossing (μm)	61.8
Probe volume diameter based on receiving optics (μm)	500
Fringe spacing (μm)	2.680
Effective frequency shift (MHz)	-1.0
Beam spacing (mm)	50.0

Figure 2 shows the mean streamwise velocity profile for both the top and bottom half of channel. Clearly the flow field was symmetric.

In Figure 3, the mean streamwise velocity data normalized with inner variables of shear velocity (u_τ) and kinematic viscosity (ν) were plotted as a function of y^+, $y^+ = y\, u_\tau/\nu$. The present results were compared with data from Luchik (see Appendix A) at Re = 17,800. The comparison of most interest is in the log region where Luchik's data is fit best by

$$U^+ = 2.44 \ln y^+ + 6.0 \qquad (2.1)$$

The agreement is very good in this region.

Figure 4 shows the root-mean-square of the streamwise velocity component as function of y^+. Again, comparison was made with Luchik's data and there is good agreement for $y^+ > 25$. The data in Figures 2, 3 and 4 confirm the standard nature of the flow at Re = 49,300.

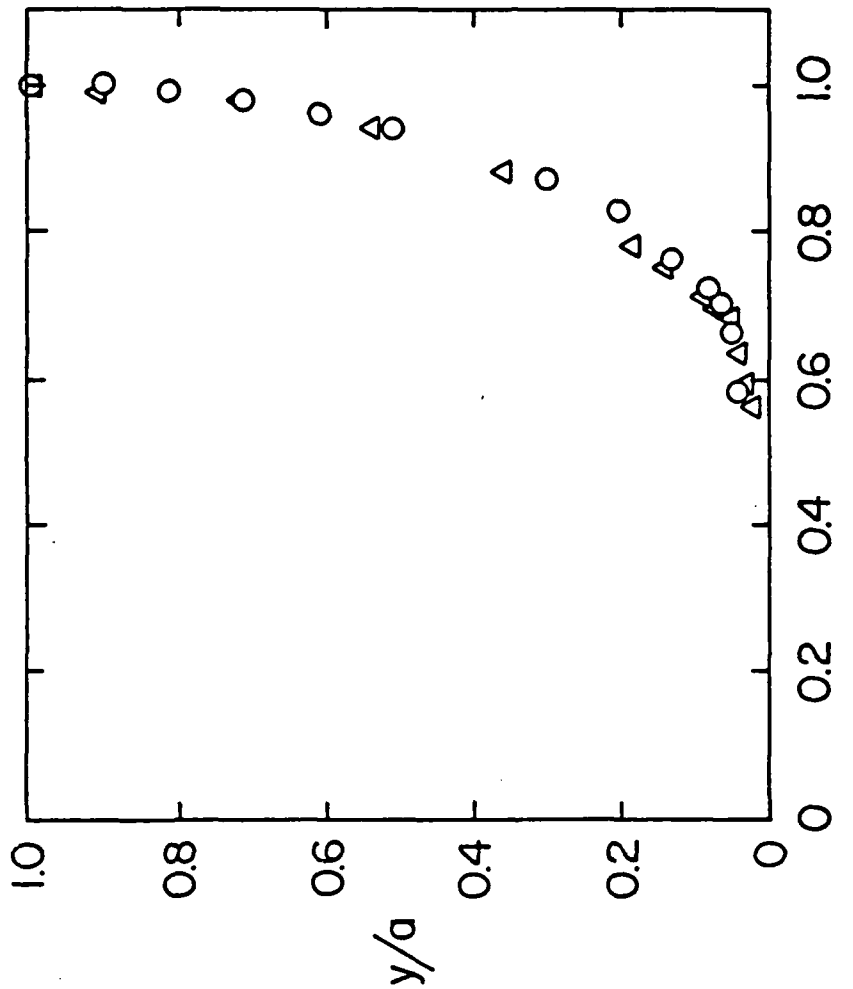

Figure 2. Mean Streamwise Velocity Profile; Δ - top half of channel, O - bottom half of channel.

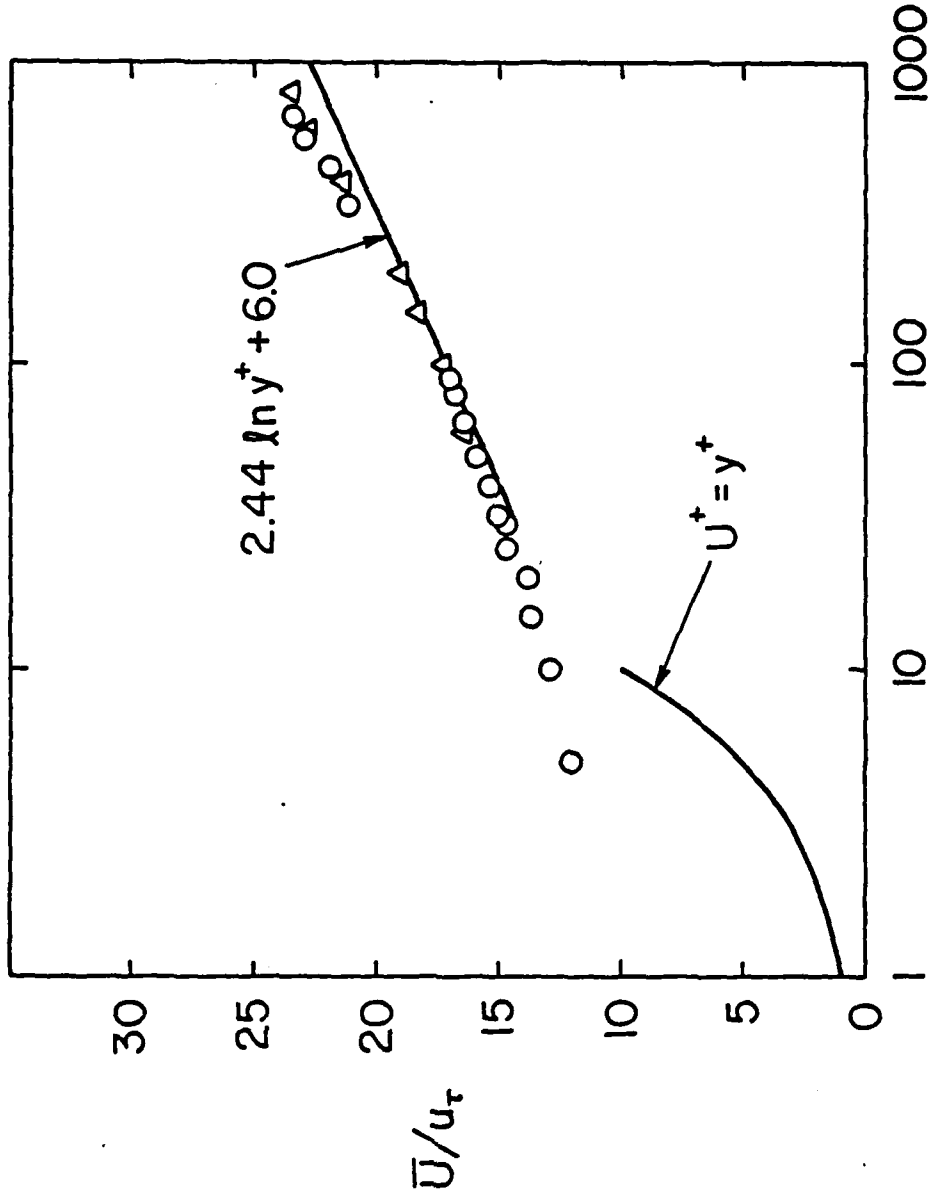

Figure 3. Mean Streamwise Velocity Profile Normalized with Inner Variables; Δ - top half of channel, O - bottom half of channel.

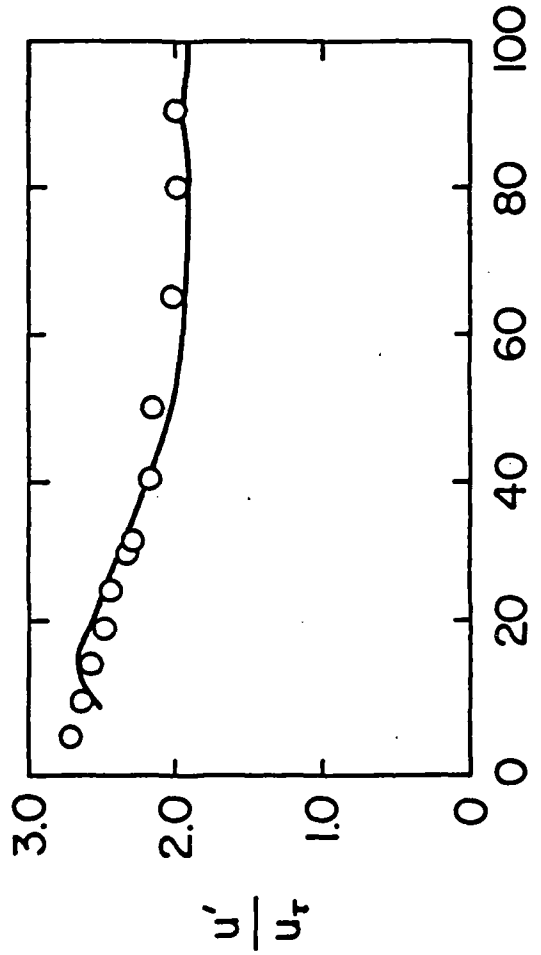

Figure 4. Root-Mean-Square of Velocity Normalized with Inner Variables; O - bottom half of channel.

As a final note, the present data diverge from the standard character of the flow when $y^+ < 25$ or $y < 0.008$ inches. This appears to be a problem associated with the close proximity of the wall and is a laser velocimeter, not a channel flow, problem. Fortunately, to confirm bursting rate scaling, ,we can use the modified u-level method at $y^+ = 30$ where the present methods are accurate.

CONCENTRATION MEASUREMENT TECHNIQUE

Measurements of instantaneous local polymer concentration will be made by marking the additive with a fluorescent dye. The dye will be excited by the green beam from an Argon-ion laser and the instantaneous fluorescence intensity from a small volume will be monitored. This technique has been used to obtain simultaneous measurements of one velocity component and scalar concentration in coaxial mixing jets (Robak et al., 1984; Owen, 1976). Laser-induced fluorescence has also been used to determine instantaneous concentration profiles in a plane mixing layer by Koochesfahani and Dimotakis (1985). The proposed measurements represent the first application of this concept to a turbulent wall flow, simultaneous two-component velocity and concentration measurement, and flows with polymer injection.

3.1 Theoretical Considerations

The theory for this technique begins by considering a light beam propagating in an absorbing medium. The change in intensity is given by

$$dI = - I\alpha ds \tag{3.1}$$

(Jenkins and White, 1976) where I is the intensity of the beam, α is the absorption coefficient of the dye and s is the coordinate in the propagation direction. For several dyes at concentrations between 0.01 and 1 ppm, Weidemann (1974) shows that the absorption coefficient is proportional to dye concentration

$$\alpha = kC_D \; ; \tag{3.2}$$

combining this with Equation (3.1) yields

$$dI = - IkC_D \, ds. \tag{3.3}$$

If we integrate Equation 3.3 and take $I = I_o$ at $s = 0$, then the intensity of the light at any location $s = S$ is given by

$$I = I_o \exp[- \int_0^S kC_D \, ds]. \tag{3.4}$$

Space-averaged dye concentration, $\tilde{C}_D$, is defined as

$$\tilde{C}_D = \frac{1}{S} \int_0^S C_D(s) \, ds. \tag{3.5}$$

Recognizing that k in Equation 3.4 is a constant and substituting Equation 3.5 into Equation 3.4 yields

$$I(S) = I_o \exp[- Sk\tilde{C}_D]. \tag{3.6}$$

Equation 3.6 shows that the intensity of a laser beam propagating in an absorbing dye field is a function of the initial intensity of the beam, I_o, the length of the beam path, S, and the space-averaged dye concentration along the path, $\tilde{C}_D$.

For a fluorescent dye, the amount of energy contained in the fluorescent emission is a fraction (typically 80-85 percent) of the absorbed radiation and has no preferred direction in space. Hence, the fluorescent light emitted from a small length of the excitation beam is proportional to the change in intensity of the excitation beam over that length. If this length (ℓ_m) is sufficiently small, Equation 3.3 is valid and the intensity of the fluorescent emission is given by

$$I_F = - \phi dI = \phi[IkC_D\ell_m] \tag{3.7}$$

where ϕ accounts for the omni-directional nature of the fluorescent emission and the efficiency of the dye. Combining Equations 3.6 and 3.7 yields

$$I_F = \left[k\phi \ell_m I_o e^{-Sk\tilde{C}_D} \right] C_D \ , \tag{3.8}$$

or, equivalently

$$I_F = \left[A\ e^{-Sk\tilde{C}_D} \right] C_D \tag{3.9}$$

where

$$A = k\phi \ell_m I_o \ . \tag{3.10}$$

Equations 3.9 and 3.10 demonstrate that the instantaneous intensity of the fluorescent emission from a small segment of the excitation beam is proportional to the instantaneous dye concentration at that location. It also shows that the constant of proportionality depends on the space-averaged dye concentration along the beam path.

If the beam path is chosen so that the time-averaged concentration at all points along that path is constant (i.e., along the span of a two-dimensional channel flow), the space-averaged dye concentration along the path $\tilde{C}_D$ does not change with time. Furthermore, the space-averaged dye concentration, $\tilde{C}_D$, is equal to the time-averaged dye concentration, $\overline{C}_D$, where

$$\overline{C}_D = \frac{1}{T} \int_0^T C_D(t)\ dt. \tag{3.11}$$

Hence, Equation 3.9 can be written as

$$I_F = A\left[e^{-Sk\overline{C}_D}\right]C_D \tag{3.12}$$

Time-averaging Equation 3.12 yields

$$\overline{I}_F = A\left[e^{-Sk\overline{C}_D}\right]\overline{C}_D \tag{3.13}$$

which defines an implicit relationship for the time-averaged dye concentration in terms of the time-averaged fluorescent intensity. The value of $\overline{C}_D$ determined from Equation 3.13 can then be used in Equation 3.12 to relate the instantaneous fluorescence intensity to the instantaneous dye concentration in the measurement volume, C_D.

As shown in the previous analysis, the ability to measure the instantaneous dye concentration at a point in the flowfield requires that the space-averaged dye concentration *along the beam path* leading to that point does not vary with time. To accomplish this, the path of the excitation beam through the dye-field must be significantly longer than the largest scale dye-concentration variations in the flowfield.

In the near-wall region of a turbulent channel flow, the dominant mass transport mechanism is the turbulent burst. The spanwise length scale of these structures is the spacing of the low-speed streaks which form in the viscous sublayer. The proposed concentration measurements will be made in a 6 cm × 57.5 cm rectangular channel at a Reynolds number (based on channel height) of 39,000. For a water flow at this Reynolds number, the spanwise length of the channel is about one hundred times the average spanwise streak spacing.

When dilute polymer solutions are present in the flow, drag reduction results in an increase in the physical size of the scales present in the near-wall region of the flow. For this reason, a method of determining whether the intensity of the excitation beam is invariant with time at the measurement volume is needed. This can be accomplished by injecting a dye-marked polymer solution over a spanwise length equal to the path length to be used for the instantaneous dye concentration measurement. The intensity of the excitation beam can be measured after passing through this shortened dye-field. If the measured intensity of the excitation beam does not vary with time, the proposed path length is sufficiently long for use in instantaneous dye concentration measurements.

3.2 New Test Section

A new test section for the 6 cm × 57.5 cm rectangular channel has been completed recently and will be in use soon. The test section is 20 channel heights in length and has spanwise slots in the top and bottom plates for injection of dilute polymer solutions. This section along with the two existing sections (each 40 channel heights in length) will yield an overall channel length of 100 channel heights. By varying the way that the three sections are arranged, the polymer injection slots can be located either 40, 60 or 80 channel heights from the channel inlet.

The new test section is constructed almost entirely of polycarbonate sheet which absorbs less water, and therefore suffers less warpage, than acrylic sheet. The section was assembled with screws and silicone sealer rather than bonding the pieces together; this will allow replacement of individual components of the test section if necessary and the seams should be

less prone to failure due to fatigue.

The assembly of the section is such that good optical access to the near-wall region is attainable and the section has a removable top to facilitate cleaning.

REFERENCES

Bogard, D.G. and W.G. Tiederman 1986. Burst detection with single point velocity measurements, J. Fluid Mech., 162, 389.

Jenkins, F.A. and H.E. White 1976. Fundamentals of Optics, McGraw-Hill, New York, p. 231.

Koochesfahani, M.M. and P.E. Dimotakis 1985. Laser induced fluorescence measurements of mixed fluid concentration in a liquid plane shear layer, AIAA J., 23, 1700.

Owen, F.K. 1976. Simultaneous laser measurements of instantaneous velocity and concentration in turbulent mixing flows. In: Application of non-intrusive instrumentation in fluid flow research, AGARD Conference Proceedings No. 193, p. 271.

Roback, R., B.V. Johnson and J.C. Bennet 1984. Turbulent transpoirt measurements using a combined laser velocimeter laser induced fluorescence technique. In: Preprints for the ninth symposium on turbulence; X.B. Reed, G.K. Patterson and J.L. Zakin, eds., Rolla, MO.

Weidemann, H. 1974. Use of fluorescent dyes for turbulence studies in the sea. In: Optical aspects of oceanography; N.G. Jerlov and E.S. Neilson, eds., Academic Press, London and New York, p. 257.

APPENDIX A

Manuscript entitled "Time scale and structure of ejections and bursts in turbulent channel flows," submitted to Journal of Fluid Mechanics on November 15, 1985 and revised in April 1986.

Time scale and structure of ejections and bursts in turbulent channel flows

T.S. Luchik* and W.G. Tiederman

School of Mechanical Engineering

Purdue University

West Lafayette, Indiana 47907, U.S.A.

Burst structures in the near wall region of turbulent flows are associated with a large portion of the turbulent momentum transport from the wall. However, quantitative measures of the time scales associated with the burst event are not well defined largely due to ambiguities associated with the methods used to detect a burst.

In the present study, Eulerian burst detection schemes were developed through extensions of the uv quadrant 2, VITA, and u-level techniques. Each of the basic techniques detect ejections. One or more ejections are contained in each burst and hence the key idea is to identify and to group those ejections from a single burst into a single burst detection. When the ejection detections were grouped appropriately into burst detections, all of the extended techniques yielded the same average time between bursts as deduced from flow visualization for fully developed channel flow in the range $8700 \leq Re_h \leq 17{,}800$. The present results show that inner variables (wall shear stress and kinematic viscosity) are the best candidates for the proper

---

* Present Address: Jet Propulsion Lab, California Institute of Technology, Pasadena, California 91109

scaling of the average time between bursts. Conditional velocity sampling during burst and ejection detections shows that these burst events are closely correlated with slower than average moving fluid moving both away from the wall and toward the wall.

1. Introduction

The ejection of low momentum fluid from the near wall region to the outer portion of the flow has been identified as a coherent structure associated with a large portion of turbulent kinetic energy and Reynolds stress production (Corino and Brodkey, 1969, and Kim et al., 1971). These ejection structures contain fluid from low speed streaks in the viscous sublayer.

A streak is a long narrow region of low speed fluid very near the wall $(y^+ < 5)^*$. Streaks remain stable for some streamwise distance before they begin to oscillate and lift away from the wall. Finally, all or part of the streak filament ejects away from the wall in a coherent manner. This entire process is termed a burst. Within the burst, there may be one or more ejection structures (Offen and Kline, 1975, Bogard and Tiederman, 1985). Thus, a working definition of a burst is one or more ejections resulting from the same streak instability. The burst event occurs in a quasi-periodic manner and therefore experimentalists have concentrated their efforts on determining statistical quantities such as the average time between bursts and the average spanwise spacing of sublayer streaks. It is well known that for Newtonian flows the average streak spacing when normalized with inner variables, shear velocity and kinematic viscosity, has a nondimensional value of about 100

* Superscript + denotes that the quantity was made dimensionless using wall shear velocity, u_τ and kinematic viscosity, ν.

independent of Reynolds number. However, there is no consensus about the scaling of the average time between bursts.

Flow visualization has been effective in giving a good qualitative description of the burst process. Even though the technique of Bogard and Tiederman (1983), gives an accurate estimate of the average time between bursts, it, like all other flow visualization techniques, is limited to rather low Reynolds numbers and does not readily yield statistical quantities based on conditional probabilities. Thus, several techniques for the detection of the Lagrangian burst event with velocity probes have been proposed and used. Most of these techniques require only the measurement of the streamwise component of velocity which is a desirable feature since multi-component velocity measurements in the near wall region of a turbulent flow are difficult to obtain. The techniques are based on the principle that there is some recognizable pattern or level in the velocity signal associated with a burst event. However, the burst rate results obtained from the various techniques have conflicted among themselves and with those obtained from flow visualization. This occurred because each of the techniques has at least one adjustable parameter or threshold with no clear way to determine an appropriate value for it.

In an attempt to explain some of these differences, Bogard and Tiederman (1985) used simultaneous flow visualization and velocity probe measurements to show that each of the more popular techniques were detecting ejection-related phenomena. However, on a one-to-one basis none of the techniques were detecting all of the ejections regardless of the value of the adjustable threshold. They did find that the "best" correspondence, on a one-to-one basis, was obtained with the uv quadrant 2 technique of Lu and Willmarth (1973). Using

this technique with a second filtering parameter, the maximum time between ejections from the same burst, they were able to group probe "ejection" detections into probe "burst" detections. Furthermore, there was a range of the adjustable threshold over which the number of probe "burst" detections remained constant and was equal to the number detected by flow visualization. However, as the name implies, the uv quadrant 2 technique requires accurate two-component velocity measurements. Bogard and Tiederman did not attempt to use any of the single component techniques with the grouping technique. One objective of the present study is to build on the ideas of Bogard and Tiederman (1985) and to develop additional velocity probe "burst" detection techniques.

Recently, several authors (Blackwelder and Haritonidis, 1983; Willmarth and Sharma, 1984; and Alfredsson and Johansson, 1984) have used the variable interval time average (VITA) technique of Blackwelder and Kaplan(1976) with a positive gradient condition at the center of detection to study the scaling of the turbulent wall layer structure. However, the results of these studies have been somewhat conflicting. While Blackwelder and Haritonidis (1983) and Willmarth and Sharma (1984) have shown that the burst rate scales with inner variables, Alfredsson and Johansson have used a mixed time scale to scale the wall layer structure. The second objective of the present study was to give additional data for evaluating the appropriate time scaling of the burst event.

Finally, conditional statistics based on the detection of burst and ejection structures for the streamwise fluctuating velocity u, the fluctuating velocity component normal to the wall, v and the uv product are presented. These statistics are used to determine which technique yields an accurate

estimate of the burst and ejection process by direct comparison to the conditional statistics presented by Bogard (1982) who used flow visualization to detect these structures.

2. Experimental considerations

2.1 Flow loop

The experiments were performed in a recirculating flow loop with a rectangular cross section channel as the test section. Provisions were made in an upstream stilling tank such that the fluid entered the test section without any large scale vorticity (Tiederman et al., 1985). At the downstream end of the flow channel, a large stilling tank provided damping of disturbances created from the outlet. Located in this stilling tank was a cooling coil that maintained the water temperature in the channel at 24^{o}C during an experiment.

The two-dimensional flow channel had an internal cross section of 2.5 by 25.0 cm. Located in the bottom plate of the test section were a thin (0.127 mm wide) slot used for flow visualization and a series of pressure taps, which were used to monitor the pressure gradient throughout an experiment. Velocity measurements were made in the center 1/3 of the channel span, more than 125 channel heights downstream of the inlet and more than 70 channel heights upstream of the outlet. These measurements were made at $y^{+} = 30$ for a range of Reynolds numbers, $9400 < Re_{h} < 17800$. The Reynolds number is based on mass averaged velocity and the channel height of 2.5 cm.

Two micrometer manometers with carbon tetrachloride as the manometer fluid were used to measure the pressure gradient in the test section. With

this manometer fluid, pressure drop measurements could be made with a sensitivity of 0.015 mm of water. Additional details of the experimental apparatus appear in Luchik (1985).

2.2 Velocity measurements

Simultaneous measurements of the streamwise velocity component, U, and the normal velocity component, V, were made using a forward scatter version of a Thermo-Systems Incorporated (TSI) model 9100-8 three-beam, two-color laser velocimeter. The system included frequency shifting at 40 Mhz with electronic down mixing, 2.27 beam expansion, and dual aperture collection to minimize optical noise and to allow finer focusing on the probe volume.

The photomultiplier tubes outputs were processed using TSI model 1980 counter type processors. Each processor was operated in the N-cycle mode with N = 8. Only one data point was taken per Doppler burst. A coincidence window was used to insure that the measurements of U and V were obtained from the same particle.

The data collection electronics included a Digital Equipment Corporation PDP 11/03 minicomputer and TSI model 1998 interfaces. Data were stored temporarily on floppy disk prior to being transferred to a VAX 11/780 for initial data reduction. Data were then transferred to CDC 6500 and 6600 computers for further analysis and permanent storage.

The two-component data were taken at angles of $\pm 45^{\circ}$ to the main flow direction so that the three beam system could be traversed as close to the wall as possible. Velocities at these angles were calculated using

$$U_i\Big|_{+45} = f_R\Big|_{+45} \left(f_{Di}\Big|_{+45} - f_s\Big|_{+45} \right) \qquad (1)$$

and

$$U_i\big|_{-45} = -f_R\big|_{-45}\left(f_{Di}\big|_{-45} - f_s\big|_{-45}\right) \tag{2}$$

Here f_R is the fringe spacing, f_{Di} is the Doppler frequency, f_s is the frequency shift, U_i is the measured velocity component and the subscripts ±45 are the angles in degrees with respect to the streamwise direction at which the measurements were made. Note the sign difference is due to the fact that positive frequency shifting had to be used on one color of the velocimeter. These direct measurements were decomposed into streamwise and normal velocity components using a standard rotation of axes such that

$$U_i = 0.7071\left(U_i\big|_{+45} + U_i\big|_{-45}\right) \tag{3}$$

$$V_i = 0.7071\left(U_i\big|_{+45} - U_i\big|_{-45}\right) \tag{4}$$

where U_i is the instantaneous streamwise velocity component and V_i is the instantaneous velocity component normal to the wall. This arrangement of beams does have the advantage of allowing measurements close to a wall. However, the disadvantage is that the normal component of velocity is calculated from the difference between two numbers of nearly the same magnitude. The LDV parameters used in the present study are listed in Table 1.

The velocity data that were used in probe detection algorithms were taken as fast as possible. Typically the data rate was greater than 2000 Hz. The time between adjacent data points was recorded also. These data were used to reconstruct the real time velocity signal which was sampled at a rate equal to the viscous time scale, u_τ^2/ν. Because of the data storage limitation of the PDP minicomputer, multiple data records were taken in this fashion so that the

total velocity record was longer than 400 average burst periods.

3. Probe detection algorithm

Velocity probe techniques for the detection of the Lagrangian burst event have been devised because flow visualization yields limited quantitative information about the burst event and is limited to relatively low Reynolds numbers. In the present study, three basic probe techniques were examined; the uv quadrant 2, the variable interval time average (VITA) and the u-level techniques. In the following sections, the techniques will be discussed and evaluated on a one-to-one basis as well as an average basis. The one-to-one evaluation uses the simultaneous flow visualization and hot-film data at $y^+ = 15$ of Bogard (1982). These simultaneous measurements were made at a Reynolds number of 8700 based on mass average velocity in a channel with a height of 6.0 cm.

3.1 Description of the probe detection techniques

The uv quadrant 2 technique has a broader physical base than the other techniques used in this study. Since an ejection is defined as low momentum fluid that is lifting away from the wall, it follows that when an ejection passes through the detection point there will be an instantaneous defect from the mean in the streamwise component of velocity and a positive normal component of velocity, thus a quadrant 2 uv event in the velocity fluctuation coordinates (u,v).

The quadrant 2 technique is a simple level detector because an ejection event is said to have occurred when the instantaneous uv product is in the second quadrant and is greater in magnitude than the product of the RMS

streamwise and normal velocities and a threshold, H, or

$$|uv|_2 > H\, u'v' \tag{5}$$

where the superscript, ′ denotes an RMS value. One major advantage of this technique is that it detects the physical situation associated with an ejection, however it does require accurate measurements of both U and V near a wall. Measurement of V increases the experimental difficulty and cost considerably.

The VITA technique introduced by Blackwelder and Kaplan (1976) is the most widely used probe technique for detecting bursts. The basic idea is that when an ejection passes through the detection point, there will be a rapid change in the instantaneous streamwise velocity component. This rapid change will produce a high level of the variance of the streamwise velocity which is detected by the technique. However, Johansson and Alfredsson (1982) noted that a high level of variance was associated with both acceleration and decelerations. They identified the acceleration as the event of interest because it was associated with high levels of uv. The technique in its functional form is given by

$$VAR = \tilde{U^2} - \tilde{U}^2 \tag{6}$$

where

$$\tilde{U} = \frac{1}{T_A} \int_{t-\frac{T_A}{2}}^{t+\frac{T_A}{2}} U\, dt \tag{7}$$

An event is detected when

$$VAR > k\overline{u^2} \tag{8}$$

and validated as an ejection related event when

$$\frac{dU}{dt} > 0 \tag{9}$$

at the center of detection. Here k is a threshold level, $\overline{u^2}$ is the long time variance and T_A is a relatively short time chosen to filter the velocity signal. One advantage of this technique is that only the streamwise component of velocity is required for its implementation. However, the major disadvantage of the technique is that two adjustable parameters, k and T_A, must be fixed.

The u-level technique of Lu and Willmarth (1973) is the least commonly used technique of those studied here. The implementation of the technique is quite simple and the amount of data required for its use is minimal. This probe technique merely looks for deficits from the mean streamwise velocity component and identifies an event when

$$u < -L\,\overline{u^2} \tag{10}$$

where L is a threshold level. An interesting point is that for strongly negative correlated uv data, as is found near a wall, this technique should detect nearly the same number of events as the uv quadrant 2 technique. Because of this similarity, the ease of use of the u-level technique and the findings of Bogard (1982), that both quadrant 2 and quadrant 3 uv are associated with the ejection event, this technique was investigated with more vigor than has been given to it in the past.

3.2 Analysis of techniques

The evaluation of these techniques on a one-to-one basis requires the definition of two new variables (Bogard, 1982). They are

$$P(E) = \frac{N_{ED}}{N_E} \tag{11}$$

and

$$P(D) = \frac{N_{DV}}{N_D} \tag{12}$$

where N_E is the total number of visually marked events, N_D is the total number of probe detections, N_{ED} is the number of visually marked events that correspond to probe detected events and N_{DV} is the number of probe detections that corresponds to a visually marked event. An additional factor for this evaluation is the comparison of P(E) and P(D) when the total number of probe detections, N_D, is equal to the total number of visually marked events, N_E. The number of visually marked ejection events was 164 and the corresponding probabilities are indicated by an arrow in Figures 1 and 2.

Figure 1 shows the probability profiles for the quadrant 2, VITA and u-level techniques. At very low threshold levels, all of the probe techniques except VITA detected nearly all of the visually marked events and P(E) approaches 1; however, there were also a large number of probe detections which did not correspond to a visual ejection and P(D) is low. At high threshold levels, nearly all of the probe detections corresponded to a visual ejection and P(D) = 1; however, a large percentage of the visual events were not detected. It is important to note that when $P(E) < P(D)$ at $N_D = 164$, the probe detection techniques are yielding multiple detections per visual ejec-

tion. In the ideal case, the probe technique would detect each ejection only once while detecting all of the ejections.

For the VITA technique, the averaging time, T_A, was fixed using $\frac{U_o T_A}{a} = 0.9$ where U_o is the centerline velocity and a is the channel half-height. For this averaging time the number of detections was maximized independent of threshold. A similar result was noted by Johansson and Alfredsson (1982). It is also worth noting that at any level of threshold, the VITA technique yields a much lower probability of detecting an ejection, P(E), than the other two methods.

Because the quadrant 2 and u-level techniques were yielding multiple probe detections per visual ejection when $N_D = N_E$, it was desirable to modify both of these techniques such that each technique would yield one probe detection per visual ejection. The modification was to turn the detector function on at one level and turn it off at a second lower level. This concept produced no improvement for the quadrant 2 technique due to the rather large, highly intermittent excursions in the uv signal.

The u-level technique did yield better results when modified. "Off" threshold levels ranging from 0.0 to 1.0 L were investigated. The best results were found when the detector function was turned on when

$$u < -Lu' \tag{13}$$

and turned off when

$$u > -0.25\ Lu' \tag{14}$$

This technique will be referred to as the modified u-level or mu-level technique throughout the rest of the text.

Figure 2 shows the probability profiles for this technique. As can be seen by comparing Figure 1 and 2, there is a substantial improvement in the probability of detecting an ejection, P(E), while P(D) only decreased slightly when $N_D = 164$, indicated by the arrow on the figure. Since P(E) = P(D) at this location, the technique is yielding one probe detection per visual ejection. The probability results for all of the techniques are summarized in Table 2 for the situation when $N_D = 164 \pm 2$.

As noted by Bogard and Tiederman (1985) the probe techniques studied here are ejection detectors. Further inspection of the velocity records reveals that the two level detectors are detecting the leading edge of the ejection while the VITA technique detects the trailing edge. Since each of the techniques detects some sub-event of the burst, which is the event of interest, any of these techniques may be worthwhile burst detectors.

3.3 Methods for deducing time between bursts

The method for separating or grouping ejection detections into burst detections is a filtering technique originated by Bogard and Tiederman (1985). A new parameter, τ_E, the maximum time between ejections from the same burst is defined. The appropriate value of this new parameter can be determined using various methods based on the concept that ejections may be grouped into two temporal distributions; one for ejections from the same burst and one for ejections from different bursts. Ideally, the combined distribution would be like the one shown in Figure 3, where there is a clear distinction between the two types of events. However, the actual distributions overlap enough such that there is no clear break in the distribution for all ejections. Therefore, techniques were developed to obtain an appropriate deterministic method

for obtaining a value of the grouping parameter such that the two distributions are separated properly.

In the following sections, methods of separating ejection detections into burst detections for the four probe detection techniques are presented. These methods of separation were developed at $y^+ = 15$ and $Re_h = 8700$ and verified at $y^+ = 30$ and $Re_h = 8700$ (see Luchik, 1985) prior to application at higher Reynolds numbers. The results presented are for $y^+ = 30$ and $Re_h = 17800$.

3.3.1 Quadrant 2 and u-level techniques

The quadrant 2 and u-level techniques both yielded multiple probe detections per visual detection. This skewed the distribution of the time between ejections (T_E) toward zero which resulted in this distribution resembling an exponential distribution. Because of this, a slight variation on the technique of Bogard and Tiederman (1985) was used to group probe ejection detections into probe burst detections.

When the cumulative probability of $T > T_E$ as a function of T_E was plotted in semi-log coordinates for a given threshold level, three straight lines emerged. A typical example for the quadrant 2 technique with $H = 1.0$ and $Re_h = 17800$ is shown in Figure 4. Similar results were obtained for the u-level technique. From this graph, two distributions are clearly present, one for $T_E < 0.01$ s (region 1) and one for $T_E > 0.04$ s (region 2). The middle straight line, referred to as the overlap region, is some combination of the other two. The appropriate value for τ_E exists within the overlap region; however, as can be seen from Figure 4, this region is rather large. The method for choosing the value of τ_E was to use the value of T_E at the intersection of a line extrapolated from region 1 and a line extrapolated from

region 2, indicated by the arrow on Figure 4.

The data in Figure 4 are for H = 1.0 which is an appropriate first estimate of the correct threshold for the quadrant 2 technique. The first estimate threshold for the u-level technique was L = 1.0. These choices were based on the probability profiles shown in Figure 1. Once an appropriate value for the grouping parameter, τ_E, is obtained, its incorporation into the basic probe detection technique is quite simple. By knowing the time between adjacent ejections and comparing this time to the value of τ_E, one can determine whether any two ejections adjacent in time are from the same burst or from different bursts. By incorporating the grouping procedure into the basic probe detection algorithm, a region of threshold level over which the number of burst detections remain constant or have a slight minimum will result. This region of threshold independence should include the threshold level used to determine the value of τ_E. If this does not occur, the level of threshold should be iterated until the threshold independent range includes the threshold used to determine τ_E.

The variation in the average time between bursts with threshold at $Re_h = 17800$ and $y^+ = 30$ for the quadrant 2 technique is shown in Figure 5. From this figure it is clear that there is good agreement between the flow visualization data of Luchik and Tiederman (1984) and the present probe data. The grouping parameter varied less than ±10% for threshold levels $0.25 < H < 1.25$ for the quadrant 2 technique which resulted in approximately a 7% variation in the number of burst detections.

Similar results were obtained using the u-level technique. However, agreement with flow visualization was not quite as good for this technique.

Also, τ_E varied about ±15% for $0.25 \leq L \leq 1.25$ which changed the average time between bursts about the same amount. For both the quadrant 2 and the u-level technique the uncertainty of the results was significant when data records shorter than 200 burst periods were used. The present results were obtained using data records longer than 400 burst periods.

3.3.2 Modified u-level and VITA techniques

Examination of the data of Bogard and Tiederman (1985) for flow visualization marked events reveals that the distribution of ejections from the same burst resembles that of a Poisson distribution. Further examination of these data show that quantitative agreement between the experimental data and the Poisson distribution is good. The Poisson distribution predicts that 95% of the ejections from the same burst will occur for $T_E \leq 0.9$ sec. while 95% of the experimental data occurs for $T_E \leq 0.8$ sec.

Since the modified u-level technique was in good agreement on a one-to-one basis with flow visualization and also gave a reasonable estimate of the average duration of an ejection at a point in the flow, it was hypothesized that the mu-level technique would yield a distribution of time between ejections similar to the one obtained from flow visualization. Since the modified u-level and VITA ejection detections were distributed similarly, a Poisson distribution method for estimating τ_E was used for both techniques.

Implementation of the Poisson distribution separation technique is quite simple. The mode of the experimental distribution is set equal to the mean value of a hypothesized Poisson distribution. τ_E is then chosen as the value of T_E where $P(T \leq T_E) = .95$ for the Poisson distribution. As a starting point for the mu-level technique, the threshold level was chosen equal to unity

since the probability profile for this technique (Figure 2) indicated good correspondence with flow visualization at this level. The initial threshold level for the VITA technique was chosen to be that threshold where P(E) = P(D) which was k = 0.3 - 0.4 in the present study. The same criterion for determining the correct combination of grouping parameter and threshold level was used for the mu-level and VITA techniques as for the $uv|_2$ and u-level techniques. Use of the value of τ_E with the mu-level and VITA techniques to group ejections into bursts is identical to that for the quadrant 2 and u-level techniques. The grouping parameter varied less than 10% for $0.5 < L < 1.25$ for the modified u-level technique which resulted in approximately ±10% variation in $\overline{T}_B$. For the VITA technique the variation in the grouping with threshold level for $0.2 < k < 0.4$ was 10% which also resulted in an uncertainty of ±10% in $\overline{T}_B$ over the same range of threshold. When using the Poisson separation technique, it is important to note that the resolution of the grouping parameter is a function of the bin width used in the histograms. Finally, it should be noted that the VITA technique yielded consistent results with data records as short as 80 burst periods. This was a substantially shorter record than those required by the other techniques.

The results in terms of average time between bursts for the modified u-level and VITA techniques are presented in Figures 6 and 7.

3.3.3 Summary of detection algorithms

Each of the techniques discussed exhibit good correspondence with flow visualization in terms of determining an average time between bursts. However, some of the techniques are more accurate than others. The $uv|_2$ technique is the best of the techniques used in the present study when large data sets are available (more than 200 bursting periods). It yields the smallest

amount of error associated with the grouping parameter and thus the smallest uncertainty in the value of the average time between bursts. The modified u-level and VITA technique were tied for second. Each of these techniques has the advantage of requiring only single-component data. Moreover, the VITA technique with T_A set such that the maximum number of detections are obtained for any threshold, yields a more consistent value for $\overline{T}_B$ when smaller data sets are used. The shortcoming of the VITA technique is the small range of threshold independence. For the VITA technique this range changed from $0.1 \leq k \leq 0.6$ at $Re_h = 8700$ to $0.2 \leq k \leq 0.5$ at $Re_h = 17800$. This trend is clearly not favorable. Studies at higher Reynolds numbers are needed to verify this trend over a larger range of Reynolds numbers.

In cases where larger data sets are available, the modified u-level technique is quite desirable. This technique exhibits no flat region although the rate of change in $\overline{T}_B$ over the range $0.25 \leq L \leq 1.25$ was small. The accuracy of these data were nearly the same as the $uv|_2$ technique. However, the existence of a threshold independent region makes the $uv|_2$ technique more desirable.

Finally, the u-level technique, although it showed good agreement with the visual data at $Re_h = 17800$, had the largest amount of uncertainty associated with the proper value of the grouping parameter and the largest uncertainty in the estimate of the average time between bursts.

3.4 Average time between bursts for channel flows of water

Part of the rationale for developing a probe burst detection algorithm was to determine how the average time between bursts scales at high Reynolds numbers where flow visualization is impractical. Figure 8 shows the variation

in the average time between bursts determined using the various probe techniques, with Reynolds number scaled with outer variables. Flow visualization data are also shown on this plot. It is clear that each of the probe techniques yield results which are in good agreement with the flow visualization results. Figures 9 and 10 show representative values of the average time between burst normalized with inner variables and the mixed time scale recommended by Alfredsson and Johansson (1984) as a function of Reynolds number. The results presented in Figures 8, 9 and 10 show similar trends for all three methods for normalizing the average time between bursts. For $Re_h < 10{,}000$ dimensionless times increase because the favorable pressure gradient in the channel is substantial. For $Re_h > 10{,}000$, the pressure gradient is no longer a factor and all three normalizations appear to approach constant values. For outer scaling,

$$T_{BO} = \frac{U_o}{h/2} \overline{T}_B \simeq 4 \tag{15}$$

for inner scaling,

$$T_B^+ = \frac{u_\tau^2}{\nu} \overline{T}_B \approx 90 \tag{16}$$

and for mixed scaling,

$$T_{BM} = \frac{\overline{T}_B}{\left[\frac{\nu}{u_\tau^2} \frac{h/2}{U_o}\right]^{1/2}} \simeq 20 \tag{17}$$

However, since the flow field is fully developed, there is a unique relationship between shear velocity and the Reynolds number as well as a unique relationship between the ratio of center-line velocity to bulk average velocity,

U_m, and Reynolds number. As a result, at most only one of the three trends given by Equations 15-17 can be correct. For example, if Equation 15 is correct, then correlations for u_τ and U_o/U_m for fully developed channel flows can be used to renormalize $\overline{T}_B$ with either inner or mixed variables. The results from this type of argument yield a rather sensitive test of Equations 15, 16 and 17.

In the following paragraphs, one of Equations 15, 16 and 17 will be assumed to be correct and the implications of that assumption will be investigated. The relevant correlations for fully developed smooth channels recommended by Dean (1978) are

$$u_\tau^2 = 0.073 \frac{1}{2} U_m^2 Re_h^{-1/4} \tag{18}$$

and

$$\frac{U_o}{U_m} = 1.28\ Re_h^{-0.0116} \tag{19}$$

If Equation 15 is correct, then Equations 18 and 19 may be used to renormalize $\overline{T}_B$ in Equation 15. The results are

$$\frac{u_\tau^2 \overline{T}_B}{\nu} = 0.057\ Re_h^{0.762} \tag{20}$$

and

$$\left[\frac{U_o u_\tau^2}{h/2\ \nu}\right]^{1/2} \overline{T}_B = 0.479\ Re_h^{0.381} \tag{21}$$

The trends estimated by Equations 20 and 21 are shown by the solid lines on Figures 9 and 10. Clearly Equations 20 and 21 do not agree with the data.

If Equation 17 is correct, then similar use of Equations 18 and 19 yields

$$\frac{U_o \overline{T}_B}{h/2} = 167.5\ Re_h^{-0.381} \tag{22}$$

and

$$\frac{u_\tau^2 \overline{T}_B}{\nu} = 2.39\ Re_h^{0.381} \tag{23}$$

Equations 22 and 23 are shown as the long-short-long dashed lines on Figures 8 and 9. The agreement with the data in Figure 8 is good but the assumption does not predict the trend shown by the data in Figure 9.

Finally, if Equation 16 is correct, then Equations 20 and 21 may be used to give

$$\frac{U_o \overline{T}_B}{h/2} = 6313\ Re_h^{-0.762} \tag{24}$$

and

$$\left[\frac{U_o}{h/2}\frac{u_\tau^2}{\nu}\right]^{1/2} \overline{T}_B = 754\ Re_h^{-0.381} \tag{25}$$

This assumption that inner scaling is correct is compared to the data in Figures 8 and 10 (see dotted lines). In both cases, the predictions agree well with the experimental data.

Obviously, the best test of the scaling procedures will occur when reliable results are obtained at higher Reynolds number. The present range includes the maximum Reynolds number attainable in our flow facility with current pumps. Nonetheless, the present data, as tested in preceding para-

graphs, indicates that outer scaling is not correct and that inner scaling is more appropriate than mixed scaling.

4. Conditionally sampled velocity characteristics

In the previous section, each of the probe detection techniques was shown to give a reasonable estimate of the average time between bursts when used with an appropriate value of the grouping parameter, τ_E. However, when obtaining conditional velocity averages, it is not only important for the probe technique to have a high probability of detecting an ejection, but it is equally important that the technique detect the entire event. Otherwise the technique will yield conditional velocity signatures which are not characteristic of the visual event. Therefore each of the four probe techniques was evaluated further using the data of Bogard (1982) at $Re_h = 8700$ and $y^+ = 15$ and the conditionally averaged quantities deduced by Bogard (1982) when flow visualization was the detector of ejections.

For this evaluation the thresholds of the probe techniques were chosen such that the number of probe detections was approximately equal to the number of visual ejections, the thresholds at which probe techniques yielded the correct value for the average time between ejections. High thresholds, where the probability of a valid detection is high but the probability of detecting an ejection is low, were not used because at these thresholds only the stronger events are detected and this would yield unrealistically high conditional averages. Low thresholds, where nearly all ejections are detected with a large number of invalid probe detections, were not used because the invalid detections would scramble with the valid detections resulting in unrealistically low conditional averages. The parameters chosen for comparison were:

1) the average duration of the event which is given by

$$\overline{T}_D = \frac{1}{N_D} \Sigma T_{Di} \tag{26}$$

where T_{Di} is the duration of a probe detected event; 2) the percent contribution of uv in a given quadrant during all ejections compared to the total uv in that quadrant which is given by

$$100 \times \frac{\Sigma(uv_D)_i}{\Sigma(uv)_i} \tag{27}$$

where $(uv_D)_i$ is the uv in quadrant i during a detection and $\Sigma(uv)_i$ is the total uv in quadrant i; 3) the percent contribution to the time average $\overline{uv}$ from each quadrant during an ejection given by

$$100 \times \frac{\Sigma(uv_D)i}{\Sigma(uv)} \tag{28}$$

and 4) the ensemble average of the streamwise fluctuating velocity, the ensemble average of the normal fluctuating velocity and the ensemble average of the turbulent shear stress during an ejection.

A comparison of the conditionally sampled quantities obtained using the four probe detection techniques with the conditional samples based on flow visualization of Bogard (1982) is given in Table 3. From this table it is clear that the modified u-level technique yields the best estimate of the values obtained using flow visualization as the detector. By having an "off" level lower than the "on" level, the modified u-level technique is much better at capturing most of the visual detections as shown by the good correspondence in the duration of the events. There is also good correspondence in the amount of uv measured with modified u-level and visual detection of the events. It is also worth noting that the uv_2 technique detects that portion

of the ejection event associated with the occurrence of a high level of quadrant 2 uv; however, the duration of this detection is less than 25% of the duration of the average ejection event. The u-level and VITA techniques also detect some portion of the ejection event however, from this table it is unclear upon what portion of the event these techniques are focusing. The rather poor correspondence of VITA with the quantities obtained from flow visualization is not surprising since the technique was only detecting about one-half of the visual ejections when $N_D = 164$.

Average signal characteristics using the modified u-level technique are shown in Figure 11. In the figure and throughout the rest of the text, a conditionally averaged quantity is shown by that quantity located within the operator $\langle\ \rangle$. Characteristics using flow visualization to detect ejections are shown in Figure 12. A comparison of Figures 11 and 12 shows that steeper gradients in u and uv are obtained at the leading and trailing edge of the events using the modified u-level than were obtained from flow visualization. This was not unexpected since the visual data had a broader distribution in the duration of events than did the probe detection data and thus would yield increased phase scrambling at the extremities of the event. This is also shown by the broader peak in the u signal centered on the middle of the detection of the ejection. However, the average signal patterns obtained using the modified u-level technique are reasonable estimates of those obtained using flow visualization. Because of this and the good comparison with the flow visualization in the ensemble quantities presented in Table 3 as well as the fact that the modified u-level technique had the highest probability for detecting an ejection, P(E), when $N_D \simeq N_E$, the modified u-level technique was used to obtain ejection and burst characteristics at $y^+ = 30$.

4.1 Average signal levels associated with an ejection

Since there is a continuous variation of the number of probe detections with threshold level, it was necessary to determine the appropriate threshold level for the detection technique prior to obtaining the conditional averages. At $y^+ = 15$ and $Re_h = 8700$ the threshold level was L = 1 which was determined from both the probability profile and a prior knowledge of the average time between ejections. Since the leading edge of the visual ejection was associated with a strong -u component and a second quadrant uv product, the threshold level of the detector function should be associated with the same level of second quadrant u level. At $y^+ = 15$ it was also noted that

$$\frac{|\overline{u}_2|}{u'} = 1.004 \tag{29}$$

which is effectively the value of unity that was used in the prior probe detections and that yielded $P(E) \simeq P(D)$. Thus the threshold level chosen to obtain ejection and burst characteristics was

$$L = \frac{|\overline{u}_2|}{u'} \tag{30}$$

It is interesting to note that for all of the data used in the present study, $8700 < Re_h < 17800$, this threshold level was nearly equal to one.

Table 4 gives the same conditionally sampled quantities as those given in Table 3 when ejection detections were made using the modified u-level technique, with the threshold level determined by Equation 30, at the highest and lowest Reynolds numbers used in the present study. At $Re_h = 8700$ and $y^+ = 30$ a greater number of probe detections are made than at $y^+ = 15$ resulting in a lower value of $\overline{T}_E$; however, the duration of the event decreases correspond-

ingly resulting in nearly the same value of intermittency, about 0.235. Thus, the uv contribution due to a randomly occurring event would be about 23.5%. The occurrence of higher levels in quadrants 2 and 3 indicate that the ejection event is correlated with second and third quadrant turbulent momentum transport. Also at $y^+ = 30$, although larger portions of second and third quadrant uv occur during an ejection event, the second quadrant uv contribution to $\overline{uv}$ during an ejection is about the same as at $y^+ = 15$ while there is a marked decrease in quadrant 3 contribution to $\overline{uv}$ at $y^+ = 30$. The average streamwise velocity defect, relative to u', and the average uv, relative to $\overline{uv}$ are about the same at $y^+ = 30$ as $y^+ = 15$ while $\frac{\langle v \rangle}{v'}$ is seen to increase at $y^+ = 30$ indicating much stronger fluid movement normal to the wall at this location than at $y^+ = 15$.

As Reynolds number increases from $Re_h = 8700$ to $Re_h = 17800$, there is a slight increase in the intermittency of ejections, a slight increase in the negative contribution of quadrant 3 uv to $\overline{uv}$ and small decreases in u, v and uv relative to u', v' and $\overline{uv}$, respectively. However, the changes that take place are rather small in all cases which indicates that there is very little change in the relationship between the flow structure and the mean flow quantities in this Reynolds number range.

Figure 13 shows conditionally averaged velocity traces for the flow at $Re_h = 17800$ centered on the leading edge, middle and trailing edge of an ejection detection. Care must be taken when drawing conclusions from these conditional averages since phase scrambling will occur when $T^+ \neq 0$. In the present study, times less than 1/2 the average duration of the event away from the center of the conditional averages ($T^+ \simeq \pm 6$) were considered relatively good representations of individual signals. At the leading edge of the event sharp

negative gradients in u and uv occur while a sharp positive gradient of the normal component of velocity occurs. The converse is true at the trailing edge of the event. The magnitude of the gradient of the streamwise component of velocity is slightly greater near the trailing edge of the event than at the leading edge. The opposite is true of the v and uv signals. Similar results were noted by Bogard (1982) at $y^+ = 15$ for visually detected ejections. Upon comparing the conditional averages at $y^+ = 15$ and $Re_h = 8700$ (Figure 11) with those at $y^+ = 30$ and $Re_h = 17800$ (Figure 13), it is apparent that the time gradients in u, v, and uv associated with an ejection at both the leading edge and trailing edge of the event increases as Reynolds number increases when time is normalized with inner variables. A similar effect is seen when time is normalized with outer variables.

4.2 Average signal levels associated with a burst

The conditionally sampled quantities obtained during a burst detection at $y^+ = 30$ for $Re_h = 8700$ and 17800 are given in Table 5. Similar trends are obtained for the burst structure as were obtained for the ejection structure. This again indicates that the relationship of the burst structure to the time-averaged flow properties does not change much with increasing Reynolds number.

Figures 14 and 15 show conditional velocity traces centered on the leading and trailing edge of a burst respectively. Comparing these figures with Figure 13(a) and (c) shows that both the magnitudes and gradients of the u, v and uv signals are the same for the burst as they are for the ejection event. However positive u fluctuations and negative v fluctuations, usually associated with the sweep event, are seen both leading the burst event and trailing

the burst event. Bogard (1982) also noted these trends at $y^+ = 15$ using flow visualization to detect the ejection events. These results indicate that sweep-type motions are related to the burst event, not the ejection event and that the sweep structure can be found at either extreme of a burst.

5. Conclusions

The burst detection techniques developed in the present study as well as the $uv|_2$ technique with the grouping parameter determined using the exponential distribution all yield accurate estimates for the average time between bursts. In terms of accuracy, the uv quadrant 2 technique gave the most accurate estimate of the average time between bursts; however, the technique did not detect the entire burst or ejection event. Overall, the modified u-level technique did yield a good estimate of the average time between bursts when used with the appropriate value of the grouping parameter as well as yielding representative conditional averages when the threshold level was set using Equation 30. The VITA technique with the grouping parameter also yielded an accurate estimate of the average time between bursts even when only small data sets were available. However, the present results were obtained with significantly lower threshold values than are commonly used with this technique. Critical comparison of the three alternatives (inner, mixed, outer) for scaling the average time between bursts showed that outer scaling does not work. Inner scaling appears to be more appropriate than mixed scaling. Results at higher Reynolds numbers are needed to remove any doubt about the dimensionless value of $\overline{T}_B$.

This research was supported by a David Ross Grant from Purdue University and the Office of Naval Research, Contract number N00014-8316-183, NR062-754.

References

Alfredsson, P.H. and Johansson, A.V. 1984 Time scales for turbulent channel flows, Phys. Fluids Vol. 27, No. 8, p. 1974.

Blackwelder, R.F. and Haritonidis, J.H. 1983 Scaling of the bursting frequency in turbulent boundary layers, J. Fluid Mech., 132, 87.

Blackwelder, R.F. and Kaplan, R.E. 1976 On the structure of the turbulent boundary layer, J. Fluid Mech., 76, 89.

Bogard, D.G. 1982 Investigation of burst structures in turbulent channel flows through simultaneous flow visualization and velocity measurements, Ph.D. thesis, Purdue University.

Bogard, D.G. and Tiederman, W.G. 1983 Investigation of flow visualization techniques for detecting turbulent bursts. In Symposium on Turbulence, 1981 (ed. X.B. Reed, G.K. Patterson and J.L. Zakin), p. 289. Univ. of Missouri - Rolla.

Bogard, D.G. and Tiederman, W.G. 1986 Burst detection with single point velocity measurements, J. Fluid Mech., 162, 389.

Corino, E.R. and Brodkey, R.S. 1969 A visual study of turbulent shear flow, J. Fluid Mech., 37, 1.

Dean, R.B. 1978 Reynolds number dependence of skin friction and other bulk flow variables in two-dimensional rectangular duct flows, Trans. ASME J. Fluids Engr., 100, 215.

Johansson, A.V. and Alfredsson, P.H. 1982 On the structure of turbulent chan-

nel flow, J. Fluid Mech., 122, 295.

Kim, H.T., Kline, S.J. and Reynolds, W.C. 1971 The production of turbulence near a smooth wall in a turbulent boundary layer, J. Fluid Mech., 50, 133.

Lu, S. and Willmarth, W.W. 1973 Measurements of the structure of Reynolds stress in a turbulent boundary layer, J. Fluid Mech., 60, 481.

Luchik, T.S. 1985 The effect of drag-reducing additives on the turbulent structure in channel flows, Ph.D. thesis, Purdue University.

Luchik, T.S. and Tiederman, W.G. 1984 Bursting rates in channel flows and drag-reducing channel flows, In Symposium on Turbulence, 1983, (ed. X.B. Reed, G.K. Patterson and J.L. Zakin), p. 15, Univ. of Missouri - Rolla.

Offen, G.R. and Kline, S.J. 1975 A comparison and analysis of detection methods for the measurement of production in a boundary layer, In Proc. 3rd Biennial Symposium on Turbulence in Liquids, (ed. G.K. Patterson and J.L. Zakin), p. 289, Univ. of Missouri - Rolla.

Tiederman, W.G., Luchik, T.S. and Bogard, D.G. 1985 Wall-layer structure and drag reduction, J. Fluid Mech., 156, 419.

Willmarth, W.W. and Sharma, L.K. 1984 Study of turbulent structure with hot wires smaller than the viscous length, J. Fluid Mech., 142, 121.

Table 1. Two-component laser velocimeter parameters

	Blue	Green
Probe Volume Length (mm)	1.024	1.080
Probe Volume Diameter (μm)	52.4	55.2
Fringe Spacing (μm)	3.402	3.624
Frequency Shift (MHz)	-1.0	+1.0
Beam Spacing (mm)	35.3	35.3

Table 2. Results for all techniques with $N_D \simeq 164$.

Technique	Threshold	N_{ED}	P(E)	N_D	N_{DV}	P(D)
$uv\|_2$	1.209	106	.646	163	140	.859
VITA	0.4	95	.579	166	102	.613
u-level	1.28	104	.634	163	126	.773
mu-level	1.00	124	.756	166	124	.747

Table 3. Comparison of conditionally sampled quantities during an ejection to detected by various probe detection algorithms at $y^+ = 15$

		visual	mu level	u level	uv_2	VITA
Number of detections		163	163	163	161	162
$\overline{T}_E$ (sec)		1.23	1.23	1.23	1.24	1.23
$\overline{T}_{DE}$ (sec)		0.386	0.286	0.161	0.091	0.120
Intermittency		.313	.232	.130	.073	.098
Percent contribution	1	16	0	0	0	3
to uv in a quadrant	2	79	82	65	73	25
by quadrant	3	62	76	42	0	32
	4	12	0	0	0	2
Percent contribution	1	-4	0	0	0	-1
to $\overline{uv}$	2	79	83	65	73	25
by quadrant	3	-23	-28	-16	0	-12
	4	7	0	0	0	1
$\langle u \rangle / u'$		-0.756	-1.38	-1.75	-1.59	-0.980
$\langle v \rangle / v'$		0.300	0.356	0.561	1.84	0.188
$\langle uv \rangle / \overline{uv}$		1.87	2.33	3.78	10.02	1.36

Table 4. Conditionally sampled quantities at $y^+ = 30$ during an ejection detection using the modified u-level technique with $L = |\overline{u}_2|\, u'$

Re_h		8700	17800
$\overline{T}_E$		0.876	0.0301
$\overline{T}_{DE}$		0.208	0.079
T^+_{DE}		13.8	12.4
Intermittency		.237	.262
Percent contribution to $\overline{uv}$ in a quadrant by quadrant	1	0	0
	2	87	84
	3	67	66
	4	0	0
Percent contribution to $\overline{uv}$ by quadrant	1	0	0
	2	76	83
	3	-16	-25
	4	0	0
$\langle u \rangle / u'$		-1.362	-1.224
$\langle v \rangle / v'$		0.546	0.399
$\langle uv \rangle / \overline{uv}$		2.56	2.30

Table 5. Conditionally sampled quantities at $y^+ = 30$ during a burst detection using the modified u-level technique with $L = |\overline{u}_2|/u'$

Re_h		8700	17800
$\overline{T}_B$		2.00	0.0632
Average number of ejections/burst		2.28	2.10
$\overline{T}_{DB}$		0.784	0.0235
T^+_{DB}		52.6	36.8
Intermittency		.392	.372
Percent contribution to $\overline{uv}$ in a quadrant by quadrant	1	14	37
	2	93	89
	3	82	76
	4	13	7
Percent contribution to $\overline{uv}$ by quadrant	1	-2	-2
	2	81	88
	3	-19	-29
	4	7	5
$\langle u \rangle / u'$		-0.786	-0.865
$\langle v \rangle / v'$		0.288	0.244
$\langle uv \rangle / \overline{uv}$		1.664	1.680

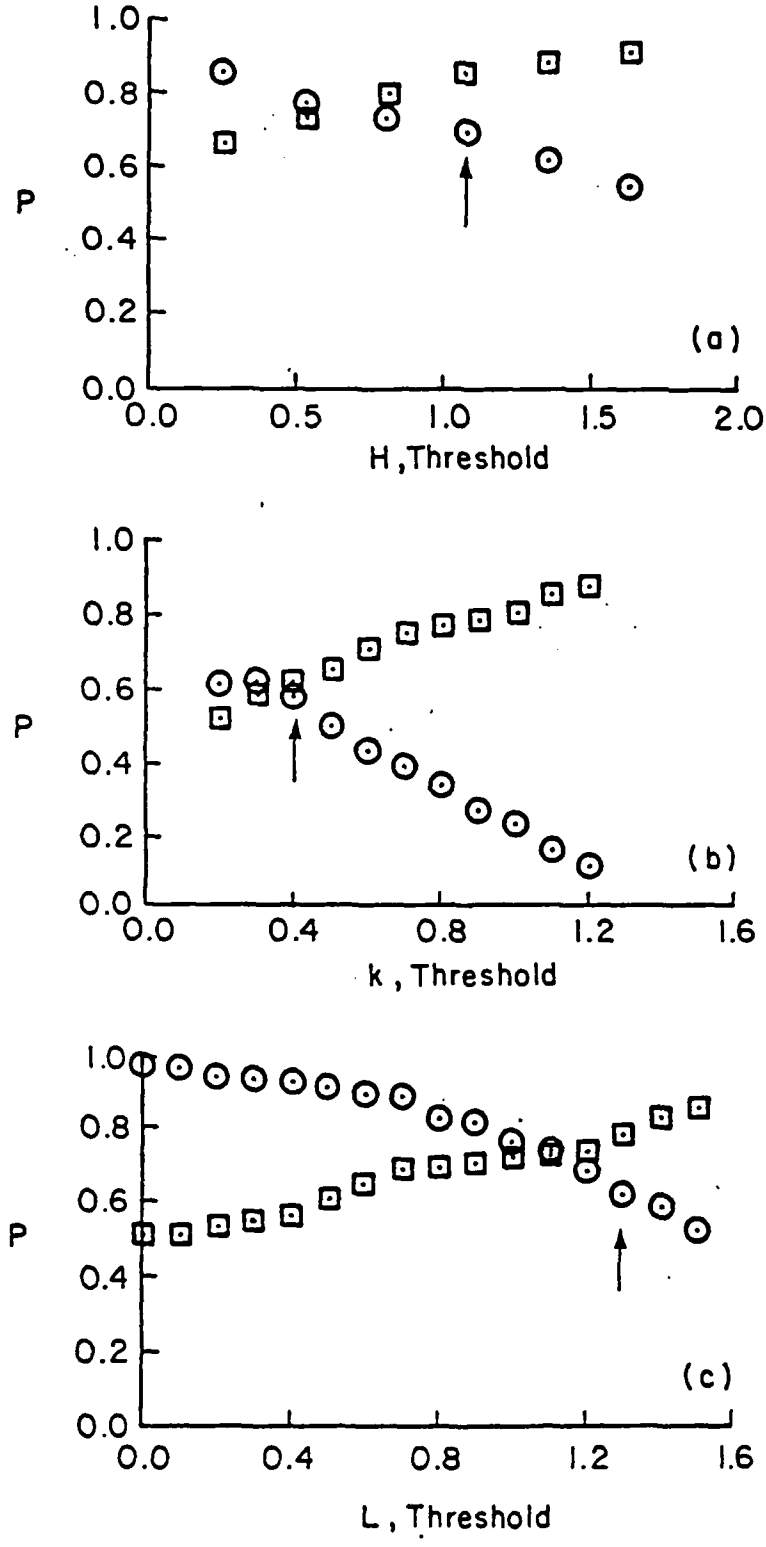

Figure 1. Probability variation with threshold for a) uv quadrant 2, b) VITA, c) u-level techniques; □ - P(D), ○ - P(E).

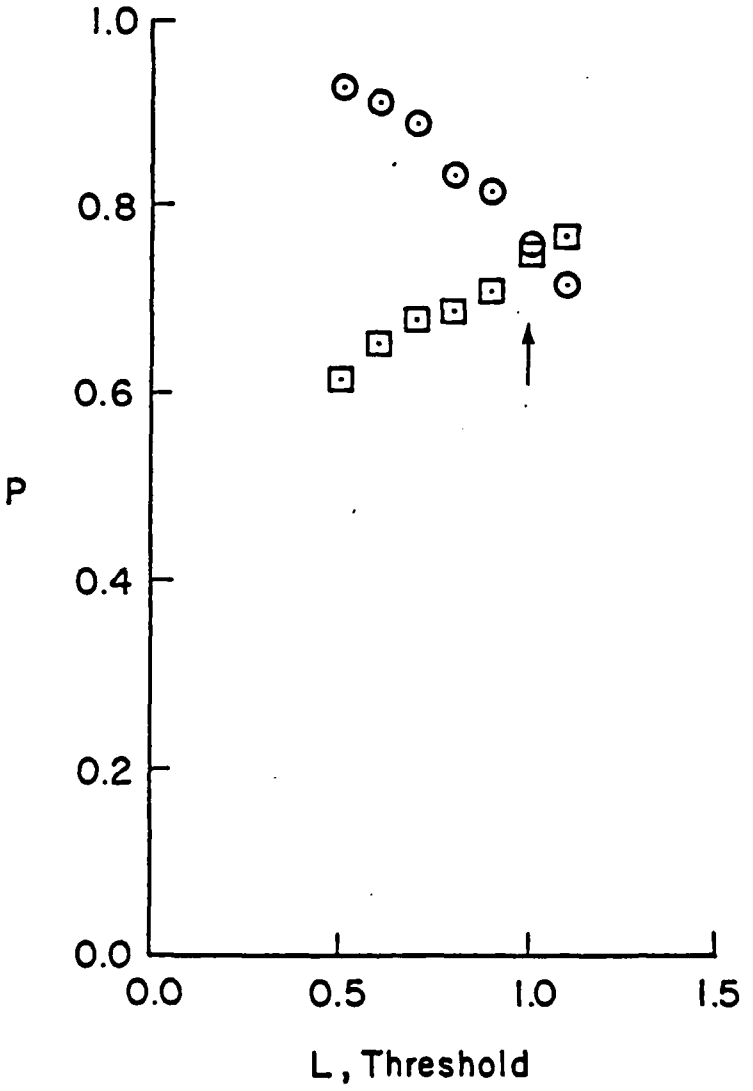

Figure 2. Probability variation with threshold for the modified u-level technique; □ - P(D), ○ - P(E).

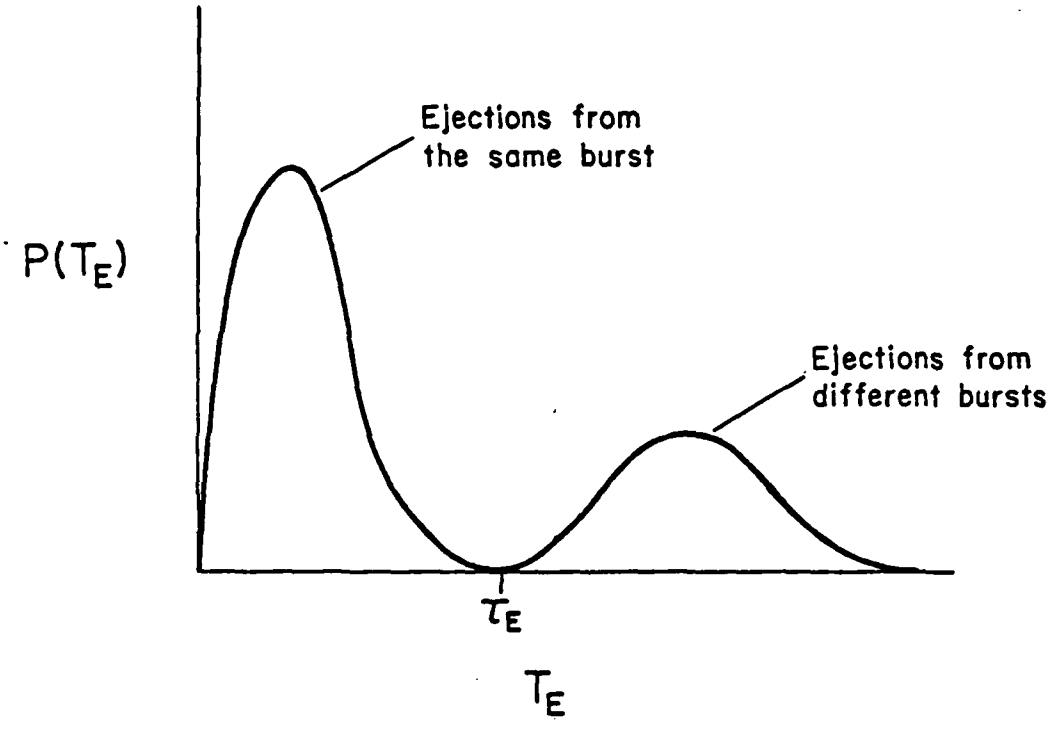

Figure 3. Schematic showing idealized probability distribution of time between ejections..

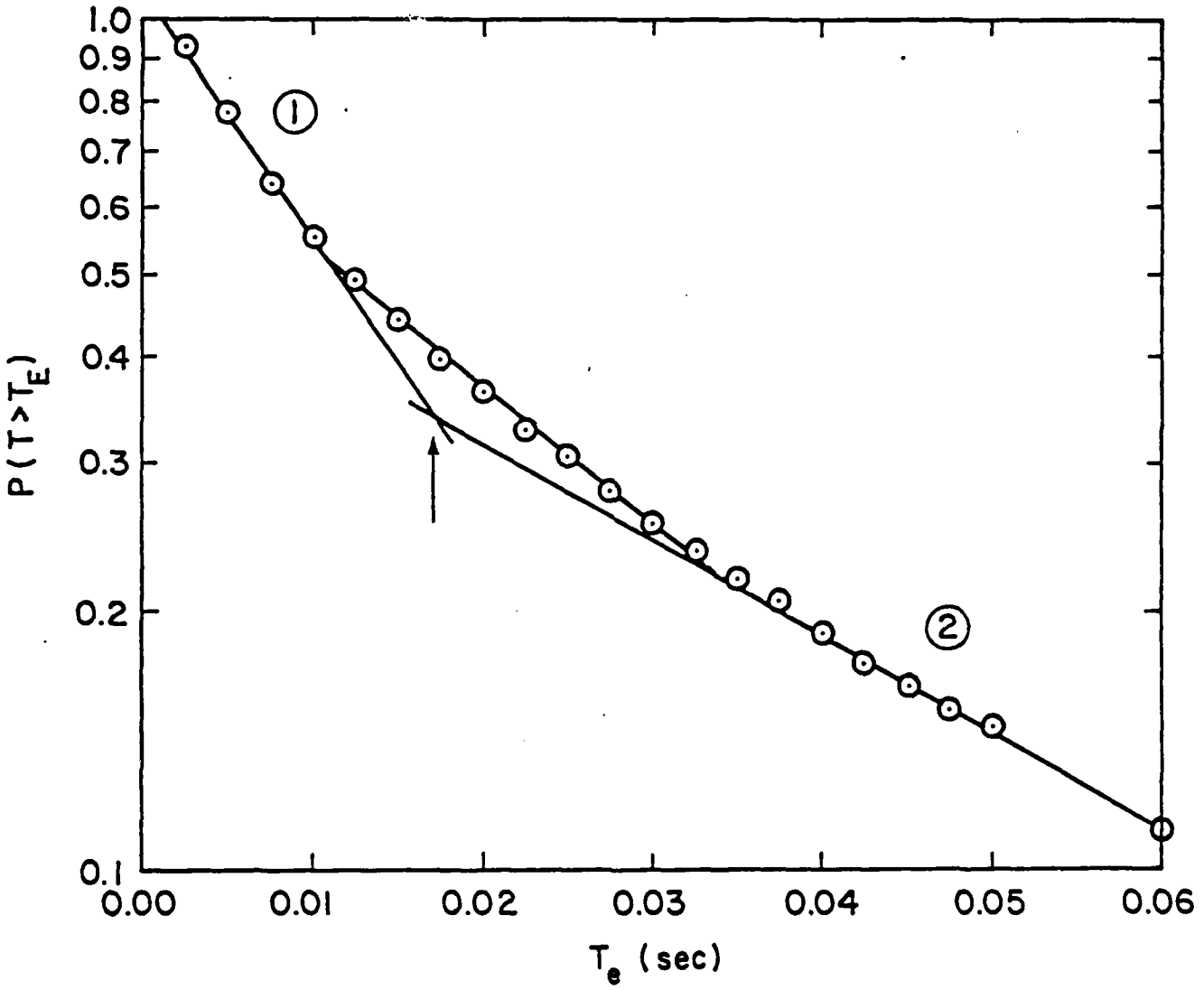

Figure 4. Cumulative probability distribution of time between ejections using the uv quadrant 2 technique with H = 1.0.

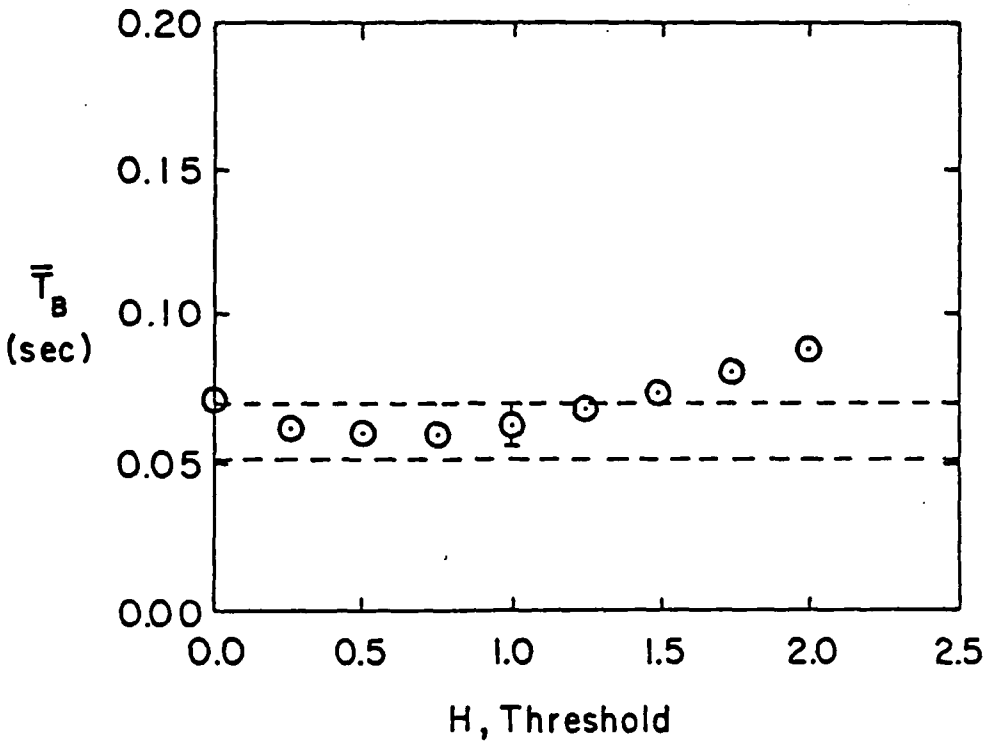

Figure 5. Variation in the average time between bursts using the uv quadrant 2 technique with τ_E determined using the exponential distributions and H = 1.0, τ_E = 0.018 sec. I - 95% confidence interval, = = = 95% confidence interval of flow visualization data from Luchik and Tiederman (1984).

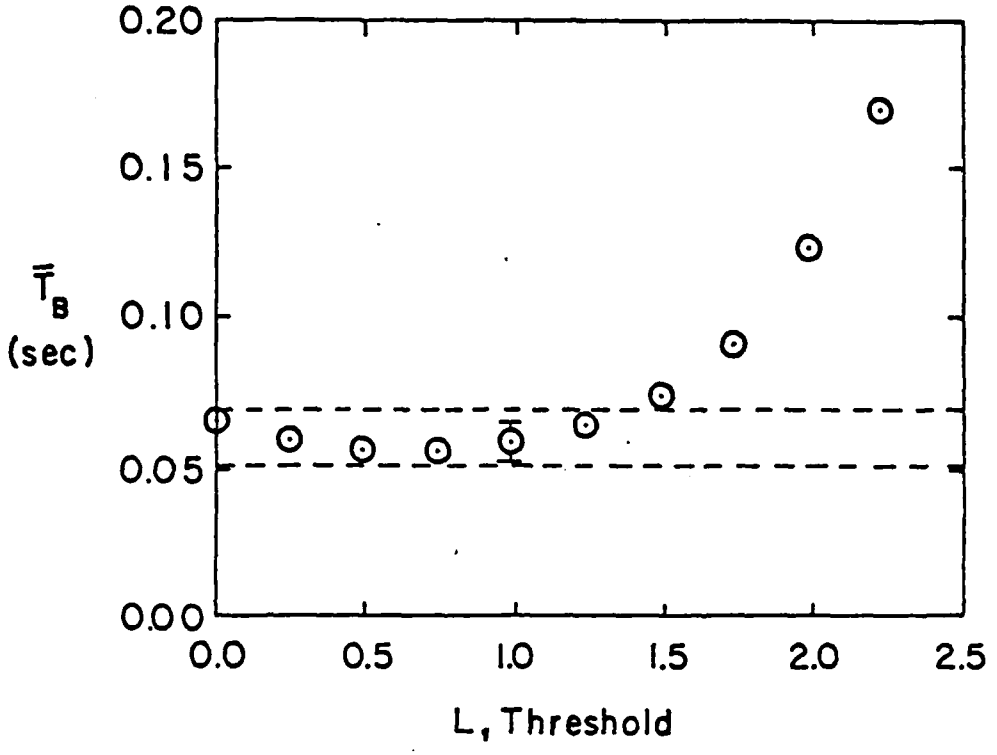

Figure 6. Variation in the average time between bursts for the mu-level technique with τ_E determined using the Poisson method, and L = 1.0, τ_E = 0.02 sec., I - 95% confidence interval, = = = 95% confidence interval of flow visualization data from Luchik and Tiederman (1984).

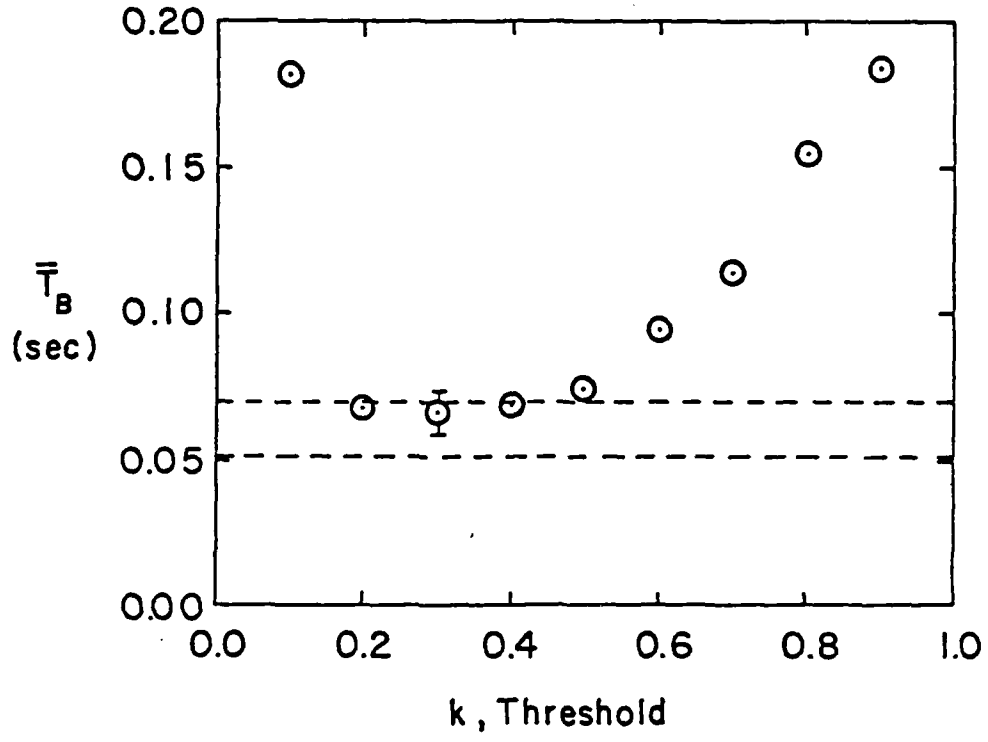

Figure 7. Variation in the average time between bursts for the VITA technique with τ_E determined using the Poisson method and k = 0.4, τ_E = 0.022 sec., I - 95% confidence interval, = = = 95% confidence interval of flow visualization data from Luchik and Tiederman (1984).

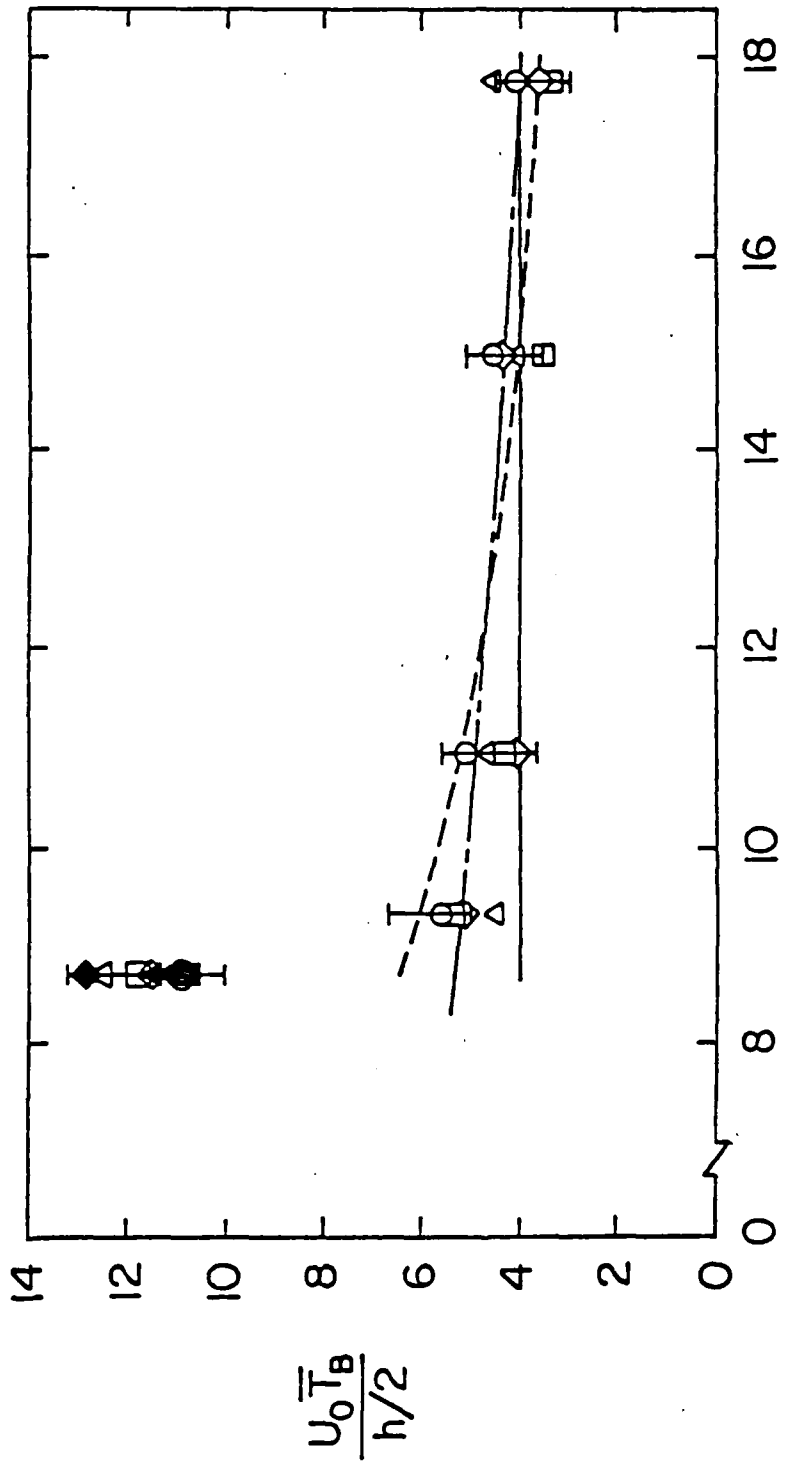

Figure 8. Effect of Reynolds number on the average time between bursts normalized with outer variables for the various probe detection algorithms with the appropriate value of τ_E, ◇ - uv quadrant 2, △ - u-level, □ - modified u-level, O - VITA, I - 95% confidence interval of flow visualization data, closed symbols - $y^+ = 15$, open symbols - $y^+ = 30$. ——— , $T_{BO} = 4$; - - - , $T_B^+ = 90$; —·—·—, $T_{BM} = 20$.

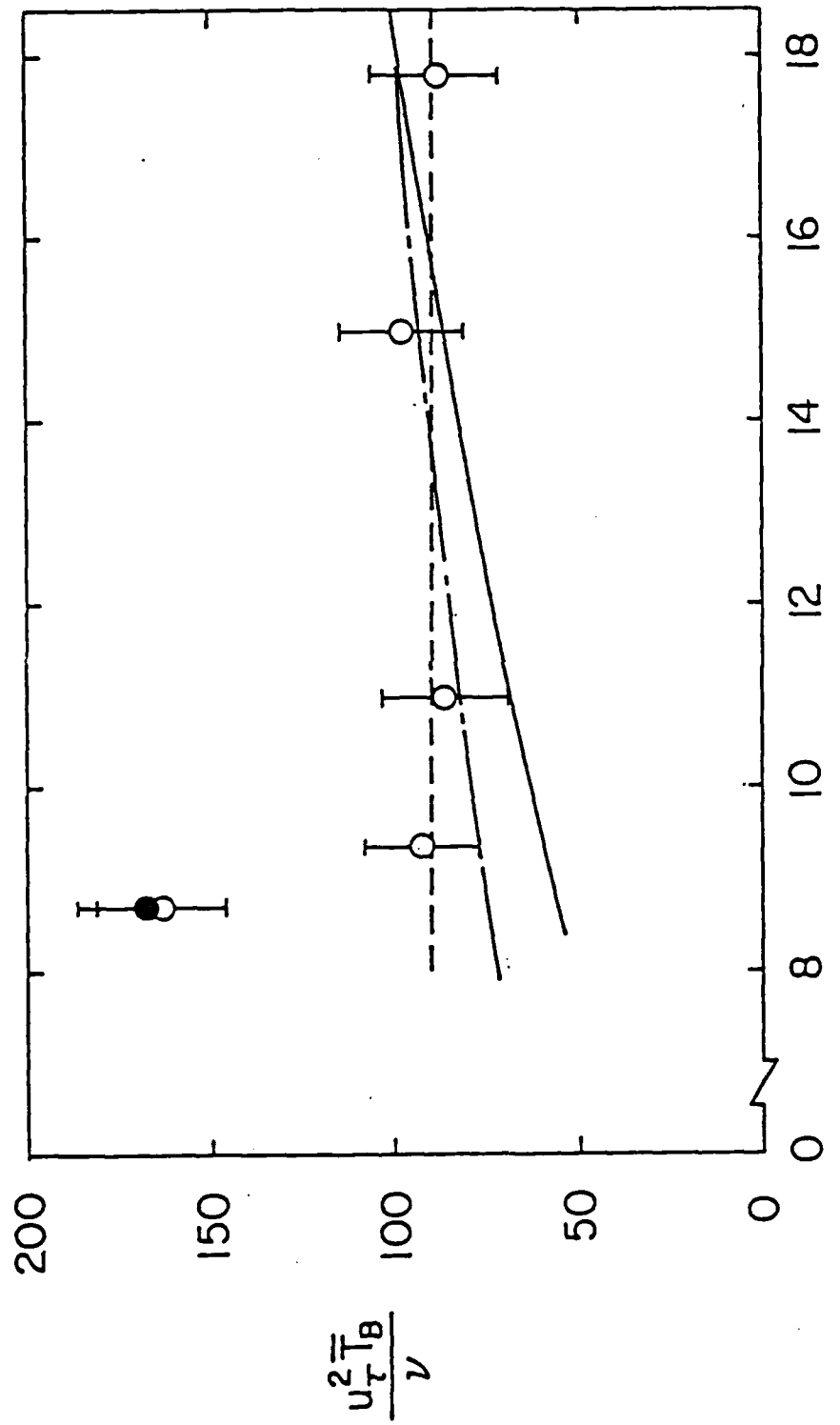

Figure 9. Effect of Reynolds number on the average time between bursts scaled with inner variables, representative values, shaded symbols - $y^+ = 15$, open symbols $y^+ = 30$. ——— , $T_{BO} = 4$; - - - , $T_B^+ = 90$; —— - —— , $T_{BM} = 20$.

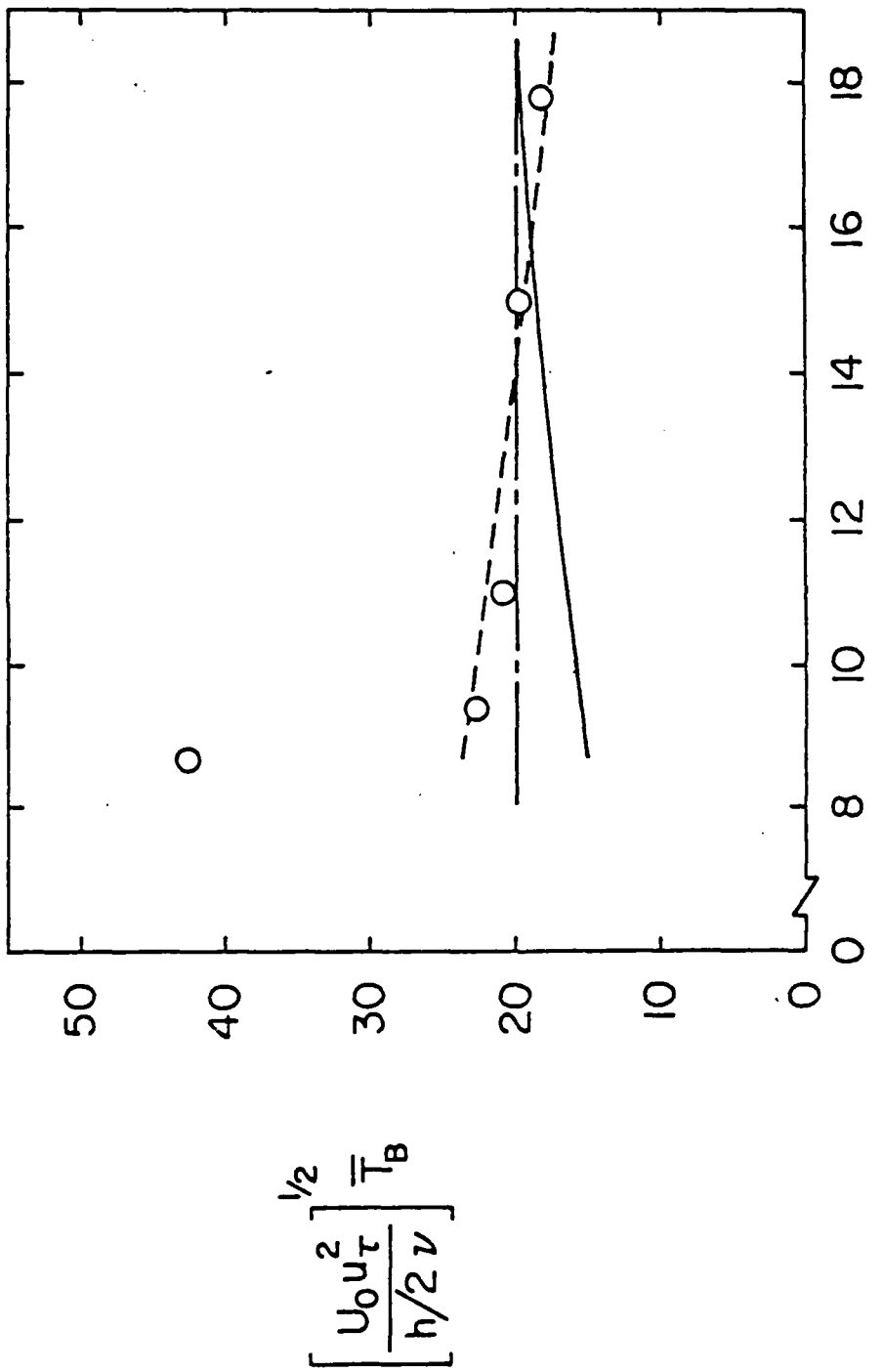

Figure 10. Non-dimensional burst period normalized with a mixed time scale as a function of Reynolds number; Typical data from $y^+ = 30$. ——, $T_{BO} = 4$; – – –, $T_B^+ = 90$; — – —, $T_{BM} = 20$.

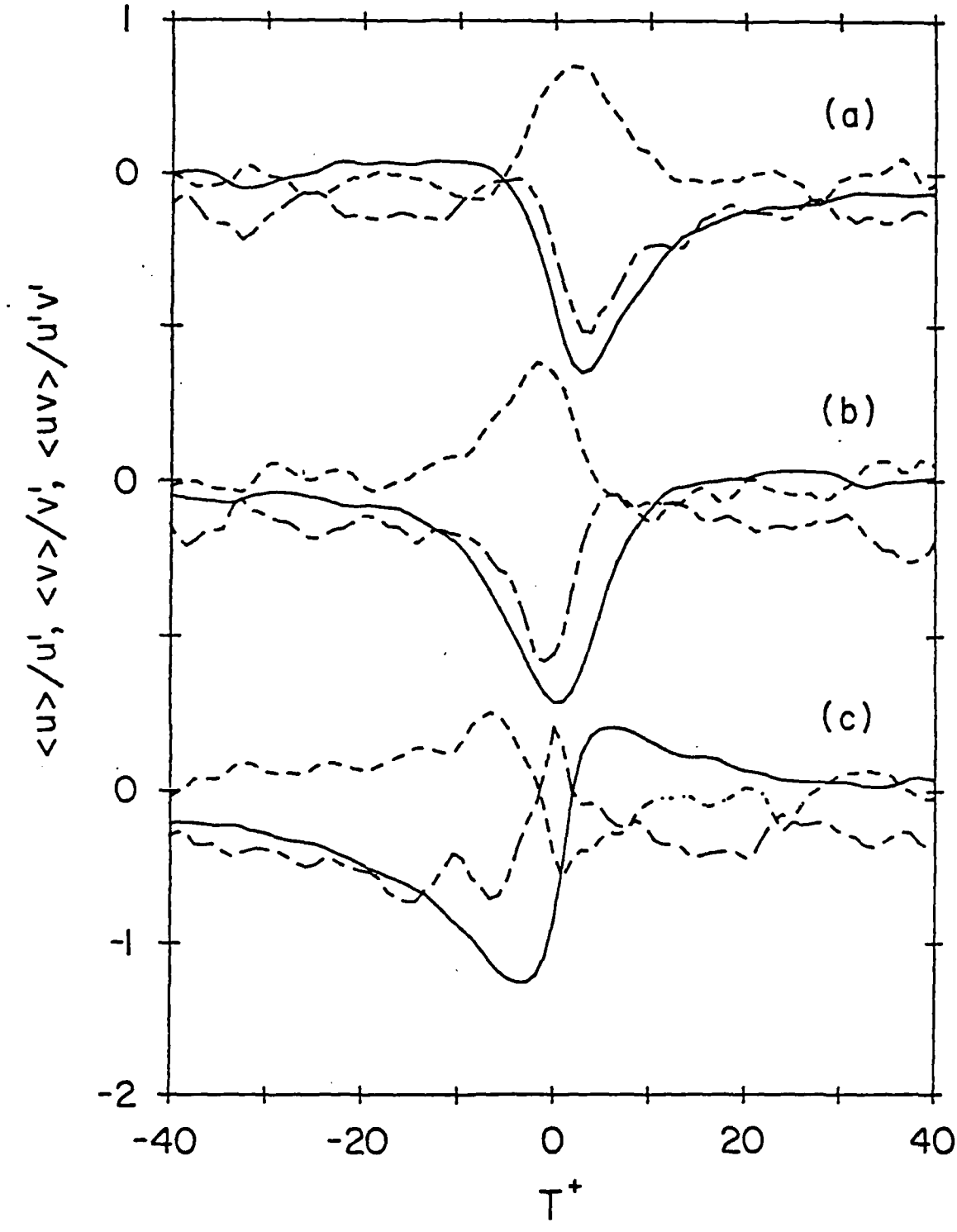

Figure 11. Conditionally averaged velocity signals using the modified u level technique centered on a) leading edge, b) middle, c) trailing edge; —— <u> , ---- <v>, —·— <uv>.

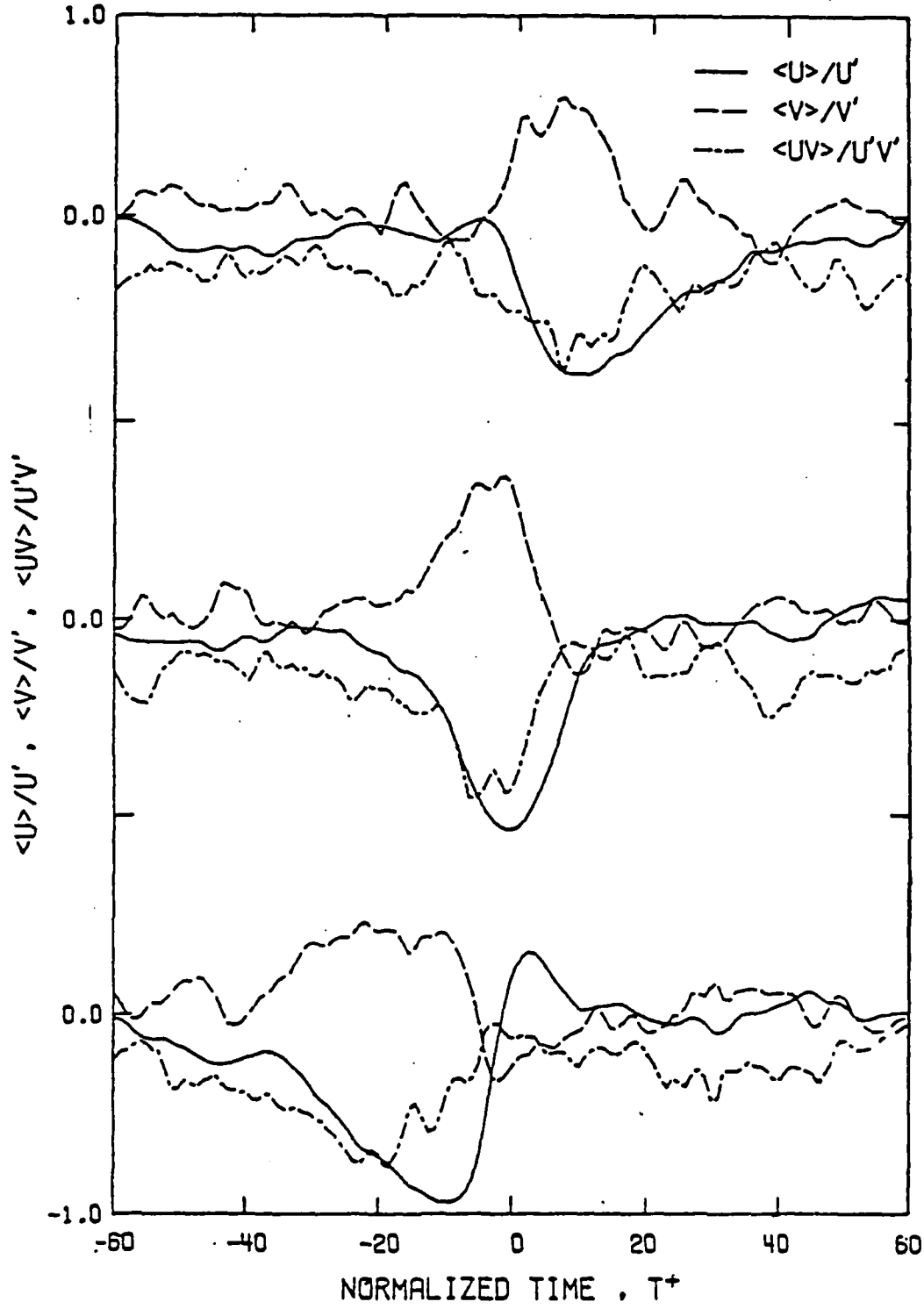

Figure 12. Conditionally averaged velocity signals using flow visualization (after Bogard; 1982) centered on a) leading edge, b) middle, c) trailing edge; —— <u> , ----- <v>, —·— <uv>.

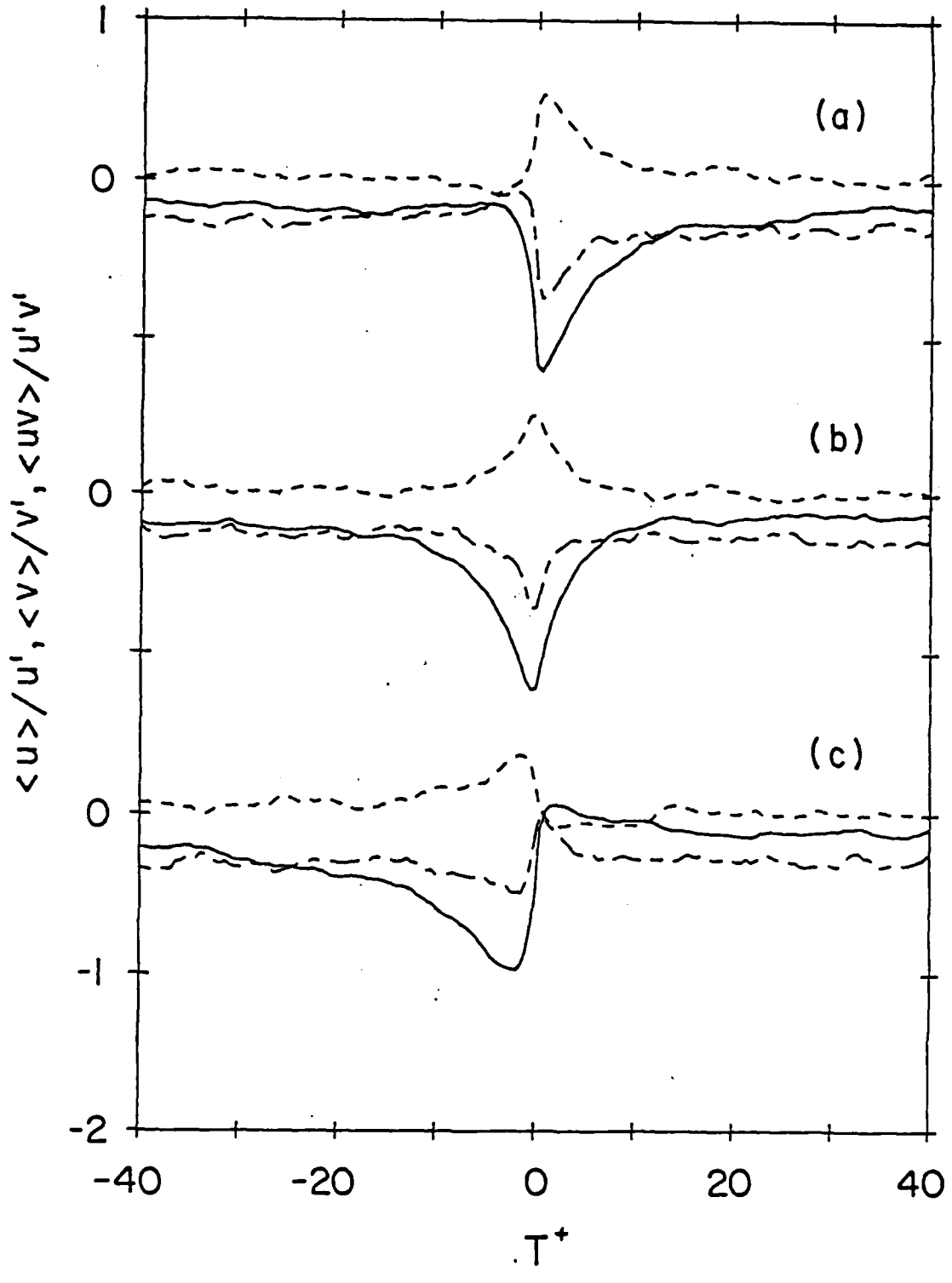

Figure 13. Conditionally averaged velocity signals for the water flow centered on a) leading edge, b) middle, c) trailing edge; —— <u> , ---- <v>, —·— <uv>.

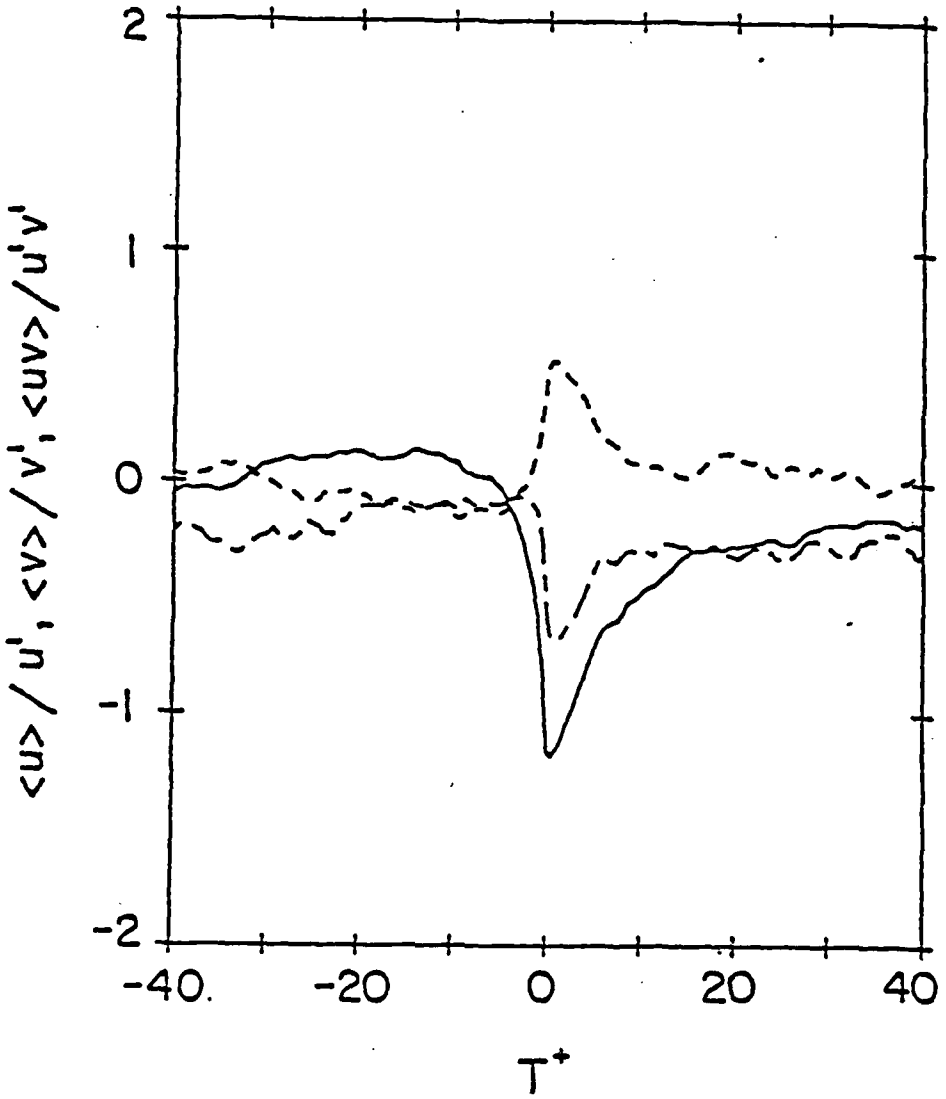

Figure 14. Conditionally averaged velocity signals for the water flow centered on the leading edge of the first ejection in a burst; ——— <u>, - - - - <v>, —— —— <uv>.

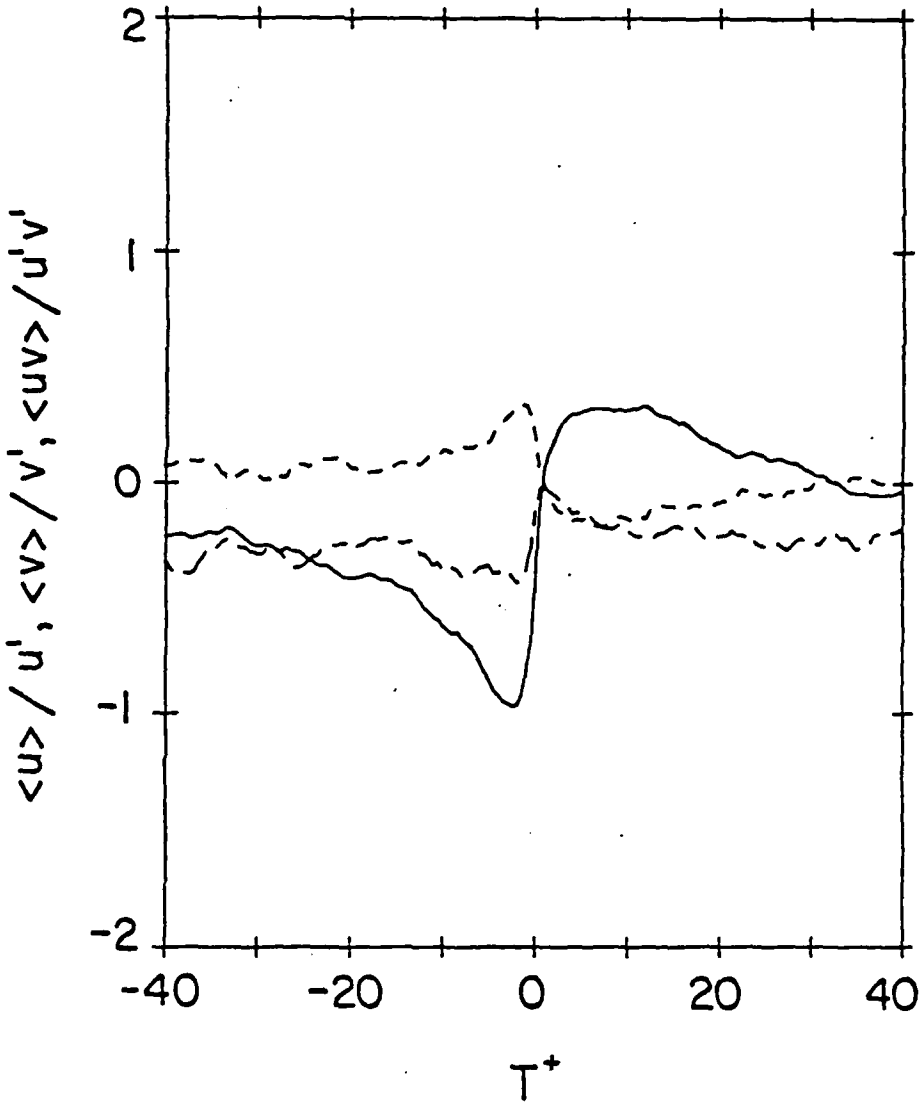

Figure 15. Conditionally averaged velocity signals for the water flow centered on the trailing edge of the last ejection in a burst; ——— <u> , ---- <v>, —·—<uv>.

APPENDIX B

Manuscript entitled "Turbulence structure in low concentration, drag-reducing channel flows," submitted to Journal of Fluid Mechanics on December 18, 1985.

Turbulent structure in low concentration, drag-reducing channel flows

T. S. Luchik* and W. G. Tiederman

School of Mechanical Engineering

Purdue University

West Lafayette, Indiana 47907

A two-component laser Doppler velocimeter was used to measure simultaneously velocity components parallel and normal to the wall in two fully developed, low concentration (1-3 ppm) drag-reducing channel flows and one turbulent channel flow of water. The mean velocity profiles, root-mean-square velocity profiles and the distributions of the $\overline{uv}$ turbulent correlation confirm that the additives modify the buffer region of the flow. The principal influence of the additives is to damp velocity fluctuations normal to the wall in the buffer region.

The average time between bursts increased for the drag-reducing flows. When compared to a water flow at the same wall shear stress, this increase in the time scale was equal to the increase in the average streak spacing. This is one of several results that indicates that the drag reduction mechanism for very low additive concentrations (1-3 ppm) may be different than the mechanisms for solutions with concentrations about 20 to 50 ppm.

---

* Present Address: Jet Propulsion Lab, California Institute of Technology, Pasadena, California 91109

Conditionally averaged velocity signals at $y^+ = 30$ centered on the leading edge of a burst as well as those centered on the trailing edge have the same general characteristics in all three flows. The signals from the drag-reducing flows demonstrate more coherence which is consistent with damping of the smaller scale motions.

1. Introduction

The addition of small amounts of soluble, high molecular weight polymer molecules to water flows has been one of the most successful methods of reducing viscous drag. The flow must be turbulent and the additives must be in the wall region in order for these polymer solutions to reduce the wall shear stress (Wells & Spangler, 1967 and Wu and Tulin, 1972). Reischman and Tiederman (1975) showed that the non-dimensional thickness of the drag-reducing viscous sublayer was unchanged compared to water flows and that the buffer region ($10 \leq y^+ \leq 100$)* of the flow was the region where the polymer solutions had their largest effect on the mean velocity profile. McComb and Rabie (1982) observed similar changes in the velocity profile and established that the buffer region is the only portion of the flow where the polymer molecules must be in order to reduce viscous drag. These results were verified by Tiederman et al. (1985).

Walker et al. (1986) attempted to take advantage of this knowledge of the region where the polymer molecules are effective in an experimental study to optimize the additive injection process. Using flush mounted injectors, Walker et al. (1986) found that drag reduction peaked about 10 channel heights downstream of the injection slot. The wall-layer polymer concentration in the vicinity of this peak in drag reduction was nearly one order of magnitude larger than the fully mixed concentration showing that there were appreciable concentration gradients normal to the wall at this streamwise location. In the present study, drag-reducing flows with concentration gradients normal to

* The distance from the wall, y, has been normalized with the wall shear velocity, $u_\tau = \tau_w/\rho)^{1/2}$ and the kinematic viscosity, ν. Here τ_w is the wall shear stress and ρ is the fluid density.

the wall are referred to as inhomogeneous drag-reducing flows. Walker et al. also showed that for distances greater than 30 channel heights downstream of the injection slot, drag reduction was nearly constant and the polymer concentration was equal to the fully mixed polymer concentration. The flow in this fully mixed region is referred to as a homogeneous drag-reducing flow in the present study.

An important result in the study of Walker et al. (1986) motivated this study. In the fully mixed region, 20 to 30 percent drag reduction was achieved with polymer concentrations of only 1 to 3 ppm. Since these experiments were performed in a 2.5 cm × 25.0 cm channel, the amount of drag reduction was quite good considering the polymer concentration. The flow in this region is an ideal drag-reducing flow to investigate because the flow is fully developed and the differences in the rheological properties of the drag-reducing solution and solvent are minimal at these very low polymer concentrations.

The important issues are how do these low concentration polymer solutions alter the turbulent flow field and cause drag to be reduced. In this study, both the time-average character of the streamwise and normal velocity components as well as the modifications to the time scale of the coherent wall-layer structure were measured.

For the most part velocity measurements in turbulent drag-reducing flows have been limited to single component measurement of the streamwise velocity component in flows where the polymer concentration was about 50 to 100 ppm (McComb and Rabie, 1982 and Reischman and Tiederman, 1975). These measurements have shown an increase in the thickness of the buffer region and an

increase in the peak value of the root-mean-square (RMS) of the streamwise velocity component. This peak is broader in extent and located farther from the wall in drag-reducing flows than in water flows. The first objective of the present study was to obtain a more detailed description of the time-averaged flow field in a low concentration drag-reducing flow and compare those results with those of a water flow. The flow quantities of particular interest are the RMS of the normal velocity component, v', and the uv turbulent correlation. Here u and v are the fluctuating velocities in the streamwise and normal directions. These flow quantities give the best indication of how the drag-reducing additives alter the turbulent transport normal to the wall.

The portion of the study related to the wall-layer coherent structure was motivated by the experiments of Kim et al. (1971) and Corino and Brodkey (1969) who found that essentially all of the turbulent kinetic energy and most of the turbulent transport occurs during the burst events associated with this structure. The burst event is a sudden outrush of low momentum fluid away from the wall. Associated with each burst is a sweep or inrush of high momentum fluid toward the wall. Since the burst event involves major changes in the near-wall region where drag-reducing solutions have an effect on the time-average flow field, the changes that take place in the burst events in drag-reducing flows are of particular interest.

The burst event includes the break-up and ejection of all or part of a wall-layer streak which is a long, narrow region of low speed fluid very near the wall ($y^+ < 5$). Streaks remain stable for some streamwise distance, lift away from the wall, and break up by ejecting low momentum fluid away from the wall. Within the burst there are one or more coherent filaments of low

momentum fluid which are called ejections. The burst event occurs in a quasi-periodic manner. Therefore, experimentalists have concentrated their efforts on measuring statistical quantities such as the average time between bursts and the average spanwise spacing of the streaks.

There have been previous studies of these coherent structures in drag-reducing flows where the polymer concentration was 50 ppm or higher. Oldaker and Tiederman (1977) showed that the average nondimensional spacing between streaks, λ^+, increases linearly with increasing drag reduction for homogeneous drag-reducing flows. They also noted that the viscous sublayer was more stable when polymer solutions were present. Donohue et al. (1972), Achia and Thompson (1977) and Tiederman et al. (1977) all reported that the ratio of the average time between bursts for a drag-reducing flow to that for a water flow at the same wall shear stress was equal to the ratio of the streak spacings for the two flows. This led those authors to the conclusion that the burst event was not directly affected by the drag-reducing solutions. In contrast, Tiederman et al. (1985) showed that the sublayer streak spacing in inhomogeneous polymer flows correlated with percent drag reduction in the same manner as for homogeneous flows while the burst rate decreased more than the increase in streak spacing. These results were considered more accurate than earlier studies because the flow visualization was understood better and the data reduction method was more accurate. Similar results for burst rates were obtained by McComb and Rabie (1982). Furthermore, using flow visualization, Tiederman et al. (1985) noted that the burst event was physically larger and more distinct in drag-reducing flows.

Although the flow visualization technique used by Tiederman et al. (1985) yields accurate values for the average time between bursts, it does not lend

itself well to obtaining statistical velocity quantities based on conditional probabilities. Because of this, the modified u-level technique of Luchik and Tiederman (1985) was used to detect the burst and ejection structures. This technique has been verified by comparison of both the average time between bursts and the conditionally averaged velocity signals associated with ejections with the burst periods and signals obtained by Bogard (1982) when flow visualization was the detector. In addition the method gives the best estimate of the burst duration (see Luchik and Tiederman, 1985).

The major experimental devices were a three-beam, two-color laser velocimeter and a long two-dimensional flow channel described in the next section. Discussion of the results will occur in two major parts. The first will center on the time-average statistics of the velocity field while the second will be concerned with a comparison of the burst structures.

2. Apparatus and procedure

2.1 Flow loop.

The experiments were performed in a recirculating flow loop with a rectangular cross section test section. Upstream of the test section was a large stilling tank which contained a perforated plate, a screen-sponge-screen section and a series of two two-dimensional nozzles which reduced the flow area to 2.5 cm × 25 cm. The flow then passed through a section of closely packed 5.6 mm I.D. plastic tubes. With these provisions, the flow entered the test section without any large scale vorticity. At the downstream end of the test section, a large stilling tank with a cooling coil for temperature control provided damping of disturbances created from the outlet.

The two-dimensional flow channel had an internal cross section of 2.5 × 25.0 cm. Located in the channel were a pair of polymer injection slots and a thin (0.127 mm wide) slot used for flow visualization. The polymer injection slots spanned the center 22.5 cm of the channel walls and were located 60 channel heights downstream of the channel inlet and 136 channel heights upstream of the outlet. These slots made an angle of 25° with the main flow direction and were 0.13 cm wide. The flow visualization slot was 123 channel heights downstream of the channel inlet and was used to mark ejection and burst structures. Velocity profiles were measured more than 65 channel heights downstream of the polymer injection slots where the injected solutions had become well mixed with the channel flow of water (see Walker et al., 1986). Polymer solutions flowed by gravity from an overhead reservoir to the injection slots. The flow to each slot was regulated by a separate rotameter and flow control valve.

The bottom plate of the test section was also lined with a series of pressure taps used to monitor the local pressure gradient. Two micrometer manometers with carbon tetrachloride as the manometer fluid were used to measure the pressure drop. With this manometer fluid, pressure drop measurements could be made with a sensitivity of 0.015 mm of H_2O.

2.2 Experimental technique

Prior to each experiment, filtered softened tap water was deaerated by heating it to 50°C in a separate holding tank and then allowing it to cool to room temperature. The water temperature in the channel was held constant at 24°C during an experiment.

The drag-reducing additives were solutions of SEPARAN AP-273, a polyacrylimide manufactured by Dow Chemical Corp., with filtered tap water as the solvent. The polymer solutions were initially mixed to 2560 ppm and 2917 ppm. These concentrated mixtures were allowed to hydrate for 12 to 24 hours prior to dilution to 400 ppm and 700 ppm, respectively.

In order to avoid batch to batch variations, the drag-reducing capability of the polymer solutions was checked in a 14.05 mm I.D. tube. The polymer solutions also were checked for consistency by measuring the viscosity of the solutions at shear rates of 115 s^{-1} and 230 s^{-1} using a Wells-Brookfield LVT-SCP 1.565° cone and plate viscometer.

During an experiment, the amount of drag reduction was deduced from pressure drop measurements. For fully developed flow, the pressure gradient is proportional to the wall shear stress, and the viscous drag. By assuming the flow is two dimensional and fully developed, which are good assumptions in the vicinity of the measurement location, drag reduction was calculated using

$$DR = \frac{\Delta P - \Delta P_i}{\Delta P} \tag{2.1}$$

Here, ΔP is the water flow pressure drop and ΔP_i is the pressure drop with polymer solution present in the flow. Because the fluid is recirculated with intermittant injection of polymer, the water-flow pressure gradient had to be monitored periodically during an experiment to insure that drag reduction due to polymer build-up in the channel did not occur. These checks showed that once the polymer solution had passed the test section, it was no longer an effective drag reducer. It is hypothesized that the polymer molecules were broken down by the high shears in the centrifugal pump and orifice.

2.3 Flow visualization

Ejections were marked by seeping fluid dyed with 2 g/ℓ fluoroscein disodium salt through the small 0.127 mm wide flow visualization slot. The dye marked wall structure was illuminated and recorded on video tape using a Video Logic Corp. INSTAR IV high speed motion analyzer. The system records 120 frames per second on one-inch video tape using a synchronous strobe to give an exposure time of 10 μs. Flow visualization data were used for two purposes. First, the visualization yielded qualitative information from which original hypothesis were formed. Second, the flow visualization information was used to deduce the average ejection period directly and the average burst period assuming two ejections per burst for the water flow (Bogard and Tiederman, 1983, and Offen and Kline, 1975). However, the average number of ejections per burst for the low-concentration flows was unknown. To determine this value, simultaneous visualization of one streak and the number of ejections resulting from each streak instability was determined. This was done at Reynolds numbers of 17800 with 25% drag reduction and 15800 with 20% drag reduction. In all cases the Reynolds number is based on the mass average velocity, U_m, and the channel height, h. These visualization results showed that 2.39 ejections per burst occurred on average at $Re_h = 17800$ and that there were 2.42 ejections per burst at $Re_h = 15800$. Thus, a value of 2.40 ejections per burst was used to reduce all of the homogeneous drag-reducing flow data. This result is significantly different from the 3.45 ejections per burst measured by Luchik and Tiederman (1984) near the location of peak drag reduction downstream of the injection of a high concentration of polymer solution.

The data for the average time between bursts obtained from flow visualization was used as a standard to which the values obtained using the modified

u-level technique were compared.

2.4 Laser velocimeter

Velocity measurements were made using a three-beam, two-component TSI model 9100-8 laser Doppler velocimeter. The system included frequency shifting at 40 mHz with electronic down mixing, 2.27 beam expansion and dual aperture collection (to minimize optical noise and allow finer focusing on the probe volume). To eliminate fringe wash-out due to unequal optical path lengths of the three beams, a path length compensator, consisting of a 50.8 mm long piece of optical quality glass, was placed in the path of the blue-green beam downstream of the color separator and upstream of the beam expander. The scattered light was collected in forward scatter.

The photomultiplier output was processed using TSI model 1980 counter type processors. Each processor was operated in the N-cycle mode with N = 8 fringes. Only one data point was taken per Doppler burst and a coincidence window was imposed on the two outputs. The maximum allowable time for coincidence was calculated by dividing the probe volume diameter by the highest velocity expected in the channel. This would correspond to the minimum time for a particle to pass through the probe volume. Setting the coincidence timer to this minimum value insured that the measurements of the streamwise velocity component and the normal velocity component were obtained from the same particle passing through the probe volume.

The data collection electronics included a DEC PDP 11/03 minicomputer and TSI model 1998 interfaces. Data were stored temporarily on a floppy disk prior to being transferred to a VAX 11/780 for initial data reduction. Data were then transferred to CDC 6500 and 6600 computers for further analysis and

permanent storage.

The velocity data were taken at angles of $\pm 45^{\circ}$ to the main flow direction so that the three-beam system could be traversed as close to the wall as possible. The direct measurements were decomposed into streamwise and normal velocity components using a standard rotation of axes such that

$$U_i = 0.7071\left[U_i\Big|_{+45} + U_i\Big|_{-45}\right] \tag{2.2}$$

$$V_i = 0.7071\left[U_i\Big|_{+45} - U_i\Big|_{-45}\right] \tag{2.3}$$

where U_i with the subscript $\pm 45^{\circ}$ are the measured velocities at $\pm 45^{\circ}$ to the main flow direction, U_i without any additional subscript is the instantaneous streamwise velocity component and V_i is the instantaneous normal velocity component. This arrangement has the advantage of allowing measurements close to a wall. The disadvantage is that additional error, particularly in the normal velocity component, occurs because the difference of two numbers of nearly the same magnitude must be used in Equation 2.3. The LDV parameters used in the present study are given in Table 1.

Movement of the probe volume normal to the wall was accomplished using a traversing system that had a range of 25.4 mm. A position could be located with an accuracy of ±0.013 mm with his system.

Different methods were used to acquire velocity data for the long time-average flow characteristics and the conditionally average signals of the burst structures. The data for the long time-average flow characteristics were taken at a sampling rate of 50 Hz with a particle arrival rate in excess of 3000 Hz. Using this type of sampling technique, the velocity bias is elim-

inated as shown by Stevenson et al. (1982) and Luchik (1982). Ensembles of 5000 samples per component were used to make initial estimates of the mean and RMS velocities. New estimates of the long time-average quantities were calculated using only velocity realizations within four standard deviations of the respective mean. This procedure generally discarded less than 15 samples in either the streamwise velocity or the normal velocity.

The velocity data for the conditionally averaged signal were taken as fast as possible; generally the rate was greater than 2000 Hz. The time between adjacent data points was also recorded. These data were used to reconstruct the real time velocity signal. This signal was then sampled at a rate equal to the viscous frequency (u_τ^2/ν). This procedure was used because the method of Stevenson et al. (1982) requires a 10 to 1 ratio between the particle arrival rate and the sampling rate to remove velocity bias. This criterion could not be met when it was necessary to sample at the viscous frequency rate. Because of the data storage limitation of the PDP minicomputer, multiple velocity records were taken at this fast rate so that the total sampling time was greater than 400 burst periods. For the two-component measurements, 50-60% of the data verified by either processor also met the requirement imposed by the coincidence window.

2.5 Expermental conditions

Three flow situations were studied. The baseline flow was a fully developed water flow. Two drag-reducing flows were compared to this baseline flow. For one, the Reynolds number was matched, and for the second, the wall shear stress of the water flow was matched. The experimental conditions summarized in Table 2 show that the homogeneous polymer concentration, C, for the

drag reducing flows was only 1.3 and 2.1 ppm. A 50 μs and 70 μs coincidence window was used for Re_h = 22000 and Re_h = 17800, respectively.

3. Time-average results

Figure 1 shows the mean streamwise velocity profile for the water flow, the drag-reducing flow that matches the Reynolds number of the water flow (case DR1) and the drag-reducing flow that matches the wall shear stress of the water flow (case DR2). As a verification of the two component technique, one-component measurements of Luchik and Tiederman (1985) are also presented in Figure 1a. Agreement between the two sets of data is excellent showing that the two-component technique yielded accurate results. The data in Figure 1a also agree well with the "law of the wall" using constants in the logarithmic overlap region of κ = 0.41 and B = 6.0. The drag-reducing data shown in Figure 1b and c are in good qualitative agreement with the data of Reischman and Tiederman (1975) whose experiments were conducted with AP-273 concentrations of 100 ppm. In the presence of the drag-reducing additives the buffer region thickens resulting in an additive offset in the logarithmic overlap region. However, the amount of offset in the present drag-reducing flows is less than the amount extrapolated from the experiments of Reischman and Tiederman (1975). A direct comparison of the present data with Reischman and Tiederman is given in Table 3. This difference in the additive constant, ΔB, may be due to either viscosity or viscoelastic differences between the 100 ppm solutions used by Reischman and Tiederman and the 1-3 ppm solutions used in the present study. The rheological properties of the polymer solutions are strong functions of polymer concentration and solution preparation procedures.

Figure 2 shows the RMS of the streamwise velocity component, u', for the three flow situations non-dimensionalized with outer variables (a = channel half-height, U_o = centerline mean velocity). In Figure 2a, the results of Luchik and Tiederman (1985) provide an additional verification of the two-component measurements. It should be noted that Luchik and Tiederman (1985) showed there was no spatial averaging in the one-component LDV data because the data were obtained from individual particles and the long dimension of the probe volume is in the direction of homogeneous turbulence. Since the present two-component data are in good agreement with that of Luchik and Tiederman and since the data again are from individual scattering particles, the present data also have no spatial averaging error. Comparison of the water data with that of the two drag-reducing flows shows that as the percentage drag-reduction increases, the peak in u' broadens as well as moves away from the wall. Also, the peak level of u' for Case DR1 (the drag-reducing flow which matches the Reynolds number of the water flow) has the same value as that for the water flow when u' is normalized with U_o.

Figure 3 shows the same data normalized with inner variables u_τ and ν. In Figure 3a, hot-wire data of Johansson and Alfredsson (1983) are also shown. The data of Johansson and Alfredsson are consistently low by an amount nearly equal to that predicted by Willmarth and Sharma (1984). This difference is due to the spatial averaging of the hot wire. Comparison of the water flow to the drag-reducing flow again shows slightly higher levels of u'/u_τ and a broader region over which peak levels occur. The location of the peak also moves from $y^+ = 15$ for the water flow to $y^+ = 30$ for the drag-reducing flows. Here the peak level of u' for Case DR2 (the drag-reducing flow that matched the wall shear stress of the water flow) has about the same value as that for

the water flow.

These low polymer concentration data are in trendwise agreement with the high concentration data of Logan (1972), Reischman and Tiederman (1975) and McComb and Rabie (1982). The peak in u' occurs further away from the wall and a broader peak region occurs when drag-reducing additives are present in the flow. However, the peak value of u'/u_τ for the high concentration drag-reducing flows was considerably higher than that for a water flow whereas the present results show a peak in u'/u_τ for Case DR1 that is only slightly higher than the water flow and approximately equal to that of a water flow for Case DR2.

The RMS of the velocity component normal to the wall, v', nondimensionalized with outer variables is shown in Figure 4. Also shown in part a of this figure are the hot-wire data of Bogard (1982) and Alfredsson and Johansson (1984). There is good agreement among the shape of the curves for the three water flow cases; however, the data of Bogard are consistently higher while that of Johansson and Alfredsson are lower than the present data. The reason for this will be discussed later in this section. A comparison of the present water flow data with the two drag-reducing flows shows that the fluctuations normal to the wall are being damped throughout the flow field, with the largest damping in the near-wall region.

The same data normalized with inner variables are shown in Figure 5. From these plots damping of the fluid movement normal to the wall is occurring in the drag-reducing flows throughout the buffer region of the flow. However, the most appreciable damping, about 5% when normalized with inner variables, occurs in the thickened portion of the buffer region. Also as the percent

drag reduction increases, a nearly constant level of v' occurred across the buffer region of the flow. Also, contrary to the u' results, the peak values of v' for both of the drag-reducing flows are lower than the peak RMS value for the water flow.

Logan (1972) obtained values of the RMS of the normal velocity by making independent measurements of the average and RMS velocity at three different angles with respect to the main flow direction using a one-component LDV for a drag-reducing flow in a square channel. Although the levels of the RMS of the normal velocity component in the buffer region of his flow are different than those noted in the present study, probably due to secondary flows in his channel, Logan measured a decrease in the normal fluctuations when drag-reducing additives were present.

The turbulent shear stress distributions across the channel half-height are shown in Figure 6. The normalization of $\overline{uv}$ has been done with shear velocity while distance from the wall has been normalized with channel half-height. For both of the drag-reducing flows (Figure 6b and c) the normalized turbulent shear stress in the outer portion of the flow is the same as that of the water flow. However, as the wall is approached, the $\overline{uv}$ profiles of both drag-reducing flows have broader peaks and the peak region occurs farther away from the wall than for the water flow. The peak value of uv does not follow the expected trend as the $\overline{uv}$ peak for the drag-reducing flow that matches the wall shear stress of the water flow has nearly the same peak value of turbulent shear stress ($\simeq .8\ u_\tau^2$) as that for the water flow while the drag-reducing flow at the same Reynolds number has a peak turbulent shear stress of only $0.65\ u_\tau^2$. This is unexpected because Case DR2 had 30.8% drag reduction while Case DR1 had only 22% drag reduction.

These same data, with distance from the wall normalized with inner variables, are presented in Figure 7. Also shown in Figure 7a are results from Bogard (1982) which agree well with the present data. Figure 7 does show the damping of $\overline{uv}$ in the near-wall region ($y^+ < 40$) in both of the flows where drag-reducing additives are present. Notice that there is greater damping of uv for Case DR1 (22% drag reduction) than for Case DR2 (30.8% drag reduction).

The instantaneous flow angle for these fully developed channel flows is given by

$$\beta = \tan^{-1} \frac{V}{U} \tag{3.3}$$

where V is the instantaneous velocity component normal to the wall and U is the instantaneous streamwise velocity component. This information is useful because in a fully developed flow the flow angle shows whether fluid is ejecting away from or moving toward the wall. Therefore, this information yields insight into the coherent wall layer motions associated with high -uv production.

Figure 8 shows the instantaneous flows angle distribution for a water flow at two y locations. The x-wire data of Alfredsson and Johansson (1984) are also presented in this figure. The comparison of the present data with that of Alfredsson and Johansson shows that there is a significant difference between the two data sets near $\beta = 0$. It is believed that the x-wire has an inherent difficulty recognizing a normal velocity component of zero. Since the x-wire has two wires separated in the direction of homogeneity by some distance Δz ($\Delta z^+ = 11$ for Alfredsson and Johansson), the existence of instantaneous streamwise velocity gradients in z will result in a low probability of recognizing a zero normal velocity, and thus a zero flow angle. This gradient

related error will also broaden the flow angle distribution near the zero flow angle. Both of these effects are seen in Figure 8a and b. These same gradients are responsible for the spatial averaging problems noted in single-wire measurements. The present data show a broadening of the distribution of the instantaneous flow angle as the wall is approached which is in qualitative agreement with the data of Alfredsson and Johansson.

The flow angle distributions for Case DR1 and DR2 on the center line of the channel and at $y^+ = 50$ are shown in Figures 9 and 10, respectively. On the center line of the channel there is very little difference between the distribution for the drag-reducing flow and the water flow. However, at $y^+ = 50$, there is a notable increase in the probability of an occurrence of a zero flow angle for the drag-reducing flows. This result is consistent with the decrease in the RMS normal velocity for the drag-reducing flow in this region.

4. Turbulent structure results

Several methods have been proposed to detect the burst or ejection structure using Eulerian velocity information. Luchik and Tiederman (1985) have shown that a modified u-level technique coupled with a filtering parameter yielded a good estimate of both the average time between bursts and conditional averages of the turbulent velocity signals for ejection events. This technique defines the leading edge of an ejection when

$$u < -Lu' \tag{4.1}$$

and the trailing edge of an ejection when

$$u > 0.25\ Lu' \tag{4.2}$$

The threshold level, L, is also defined by

$$L = \frac{|u_2|}{u'} \tag{4.3}$$

where u_2 is the average of the streamwise fluctuation when $u < 0$ and $v > 0$.

With this technique ejection detections are grouped into burst detections using a filtering parameter, τ_E, which is the maximum time between ejections from the same burst. This parameter is determined from the distribution of the time between ejections as described by Luchik and Tiederman (1985). the modified u-level technique was applied to the water flow data and the drag-reducing data of Case DR1 and DR2 at $y^+ \approx 30$.

4.1 Average time between bursts

Figure 11 shows the variation in the average time between bursts with percentage drag reduction for low concentration drag-reducing flows. The average time between bursts in drag-reducing flows has been normalized with the average time between bursts of a water flow at an equal shear velocity. These results show that there is good agreement in the modified u-level results and the flow visualization results. Also, note that the ratio of burst period in the 30.8% drag-reducing flow to a water flow at an equal shear velocity is equal to 1.67. This ratio is essentially the same as the ratio of the streak spacing in the same two flows which is 1.58 (see Oldaker and Tiederman, 1977). A similar result occurs for the 22% drag-reducing flow as shown on Figure 11 where the ratio of T_B is compared to λ^+. Thus, the burst rate from a streak for the low concentration flow is equal to that for a

Newtonian flow.

This result does not necessarily contradict the findings of Luchik and Tiederman (1984), Tiederman et al. (1985) or McComb and Rabie (1982), who all noted that the change in burst period was greater than the change in streak spacing for drag-reducing flows with polymer concentration larger than 20 ppm. For these higher concentration flows the mechanism through which drag-reduction is achieved may include damping of the large scale structures. In contrast, the 1 to 3 ppm flows of this study may achieve drag reduction through damping of only the smaller eddies.

4.2 Ejection and burst characteristics

A comparison of several conditionally sampled quantities during an ejection detection for the three flows is given in Table 4. The parameters chosen for comparison are: 1) the average time from when the detector is turned on to when it is turned off or the average duration of an event which is given by

$$\overline{T}_D = \frac{1}{N_D} \Sigma T_{Di} \tag{4.4}$$

where N_D is the number of detections and T_{Di} is the duration of a probe detected event; 2) the percent contribution of uv in a given quadrant (in u,v coordinates) during all ejections to the total uv in that quadrant which is given by

$$100 \times \frac{\Sigma(uv_D)_i}{\Sigma(uv)_i} \tag{4.5}$$

where $(uv_D)_i$ is the uv in quadrant i during a detection and $\Sigma(uv)_i$ is the total uv in quadrant i; 3) the percent contribution to the time average $\overline{uv}$ from each quadrant during an ejection given by

AD-A167 695 INJECTION OF DRAG REDUCING ADDITIVES INTO TURBULENT WATER FLOWS TECHNIQUE..(U) PURDUE UNIV LAFAYETTE IN SCHOOL OF MECHANICAL ENGINEERING W G TIEDERMAN ET AL. 2/2

UNCLASSIFIED APR 86 PME-FM-86 N00014-83-K-0183 F/G 20/4 NL

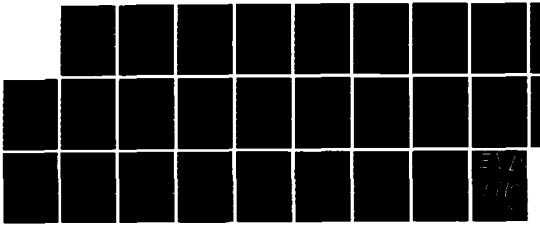

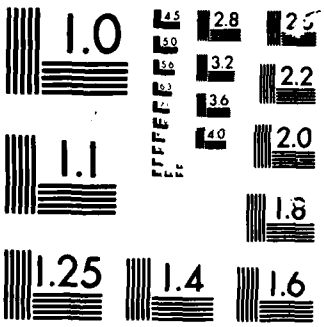

MICROCOPY CHART

$$\frac{100\ \Sigma(uv)_{D_i}}{\Sigma(uv)} \tag{4.6}$$

and 4) the mean streamwise fluctuation, the mean normal fluctuation and the mean turbulent shear stress during an ejection.

In comparing the three flows, it is interesting to note that although the average time between ejections increases for the drag-reducing flows, the average duration of the event increases correspondingly such that the intermittency of the ejection event for each of the three flows is nearly the same (ranging between 0.25 and 0.27). Thus, for each of the three flows, the uv contribution due to a randomly occurring event would be about 26%. The significantly higher contributions to uv in quadrants 2 and 3 indicate that the ejection event is correlated strongly with second and third quadrant turbulent momentum transfer. A similar result was noted by Bogard (1982) at $y^+ = 15$ in a channel flow of water. An ejection is usually thought to be related to fluid with a positive normal component of velocity; however, the present study as well as that of Bogard indicate that the fluid within the ejection can have either a positive or negative velocity component. It is hypothesized that the negative normal velocity within the ejection occurs when an ejection interacts with non-ejecting fluid and is turned toward the wall before the ejecting fluid mixes completely with the non-ejecting fluid. An increase in the quadrant 3 uv associated with an ejection is seen when drag-reducing additives are present in the flow. The increase may be due to the lack of small scale mixing in these flows, which is consistent with flow visualization. These drag-reducing flows had more clearly marked convolutions between the trailing edge of one ejection and the leading edge of the next within a burst. The increased quadrant 3 uv was also a more substantial negative contributor to $\overline{uv}$ in case DR2 during the ejection event, contributing -42%, while the

contribution of quadrant 3 uv to $\overline{uv}$ was about 25% for the water flow and case DR1. It is interesting to note that for all three flows the mean streamwise velocity during an ejection was about 1.2 u' lower than the mean streamwise velocity while the mean normal velocity was nearly the same for case DR1 and the water flow with a value of about 0.38 v'. The average contribution to uv during an ejection event decreased as percent drag reduction increased (Table 4).

Figure 12 shows conditionally averaged velocity traces for the water flow centered on the leading edge, middle and trailing edge of the modified u-level detected ejection. Care must be taken when drawing conclusions from these conditional averages since phase scrambling will occur when $T^+ \neq 0$ due to dispersion in the duration of the events. The amount of phase scrambling is a function of the amount of time displacement from the center of the conditional average. In the present study average signals with times less than one-half the average duration away from the center of the conditional average were representative of the individual signals. From Figure 12 we see that the ejection in a water flow is associated with a sharp negative gradient in u and uv and a positive gradient in the normal velocity component at the leading edge of the ejection. The converse is true at the trailing edge of the event. The magnitude of the gradient of the streamwise component is slightly greater near the trailing edge than that near the leading edge of the ejection. The opposite is true for the u and uv signal. Similar results were noted by Bogard (1982) at $y^+ = 15$ for visually detected ejections.

Figures 13 and 14 show the conditionally averaged velocity signals centered on the leading edge, center and the trailing edge of the ejection detection for case DR1 and DR2, respectively. Sharp negative gradients in u and uv

and a positive gradient in v are associated with the leading edge of the ejection for these drag-reducing flows, as was also noted for the water flow. The opposite is true at the trailing edge of the event. However, for case DR2, the peak level of <v> and <uv> is substantially less than the corresponding peaks for the water flow, which agree well with the peak level of <v> and <uv> for case DR1. This is an indication that the ejection event in a drag-reducing flow is similar to the event in a water flow with the same outer variables as the drag-reducing flow.

From Figures 12, 13 and 14 it appears that the peaks in u, v and uv all occur simultaneously. However, closer examination of the data showed that the negative peak in u leads the peak in v and -uv by approximately one viscous time unit for each of the flows. Also, the peaks in v and -uv occur simultaneously and the peaks in -u, v and -uv are substantially greater than those obtained for the conditional averages centered on either the leading edge, middle or trailing edge of the ejection. Thus, these peaks in -u, v and -uv which occur during the event are not phase aligned with any clearly discernible physical phase of the event.

4.3 Average signal levels associated with a burst

The conditionally sampled quantities obtained during a burst event are given in Table 5. The burst event was detected using the modified u-level technique with the appropriate value of τ_E. From Table 5 it can be seen that this technique yields values for the average number of ejections per burst that are in good agreement with those obtained using flow visualization for each of the flows studied here. The average time between bursts was shown to increase for the drag-reducing flows. This increase in the T_B for the drag-

reducing flows compared to that for a water flow at the same shear velocity was shown to be equal to the change in streak spacing for these low concentration drag-reducing flows. It is interesting to note that the same relationship holds for the average duration of a burst. The intermittency of the ejection event was shown to be a constant for the three flows studied, however the same is not true of the burst. The intermittency of the burst for the water flow and case DR1 are essentially the same while the intermittency of the burst process for case DR2 is somewhat larger than that for the water flow.

The contribution to uv in a given quadrant is much larger than the intermittent value for quadrants 2 and 3 showing that the burst event is strongly correlated with this type of turbulent momentum transfer (recall that the contribution of uv to each quadrant for a random event would be the intermittent value). The contribution to $\overline{uv}$ in each quadrant during a burst event is very similar for the water flow and case DR1, and noticeably different particularly in the amount of quadrant 3 turbulent momentum transfer for case DR2. The conditionally averaged streamwise velocity, normal velocity and turbulent shear stress are also similar for the water flow and case DR1 while somewhat different results in these quantities are shown for case DR2. All of this demonstrates that the burst event in a low concentration, drag-reducing flow is similar to that of water flow at the same Reynolds number. It is also worth noting that it is during the ejection phase of the burst event that the majority of the turbulent momentum transfer from the wall occurs.

Figure 15 shows conditionally averaged velocity signals centered on the leading edge of the burst for the three flow situations. Comparison of this figure with part a of Figures 12, 13 and 14 shows that although the peak

levels of -u, v and -uv are nearly the same, there is a much higher probability of positive u and -v values leading the burst. These types of velocity fluctuations are usually associated with the sweep event. Also in the presence of a drag-reducing solution, the interface between the sweep and burst structures has a sharper gradient in the streamwise velocity signal than in a water flow. This is consistent with the removal of small scale turbulence by the polymer additives.

Results of the conditionally averaged velocity signals centered on the trailing edge of the burst for the three flows are shown in Figure 16. Again, positive u and -v velocity fluctuations are seen trailing the burst and the interface between the burst and the sweep has a sharper gradient in the drag-reducing flows than in the water flow.

The ejection and burst events have been shown to correlate with the occurrence of quadrant 2 and quadrant 3 turbulent momentum transfer, or negative fluctuations in the streamwise velocity component. It therefore seems reasonable that the sweep event would be correlated with the occurrence of quadrant 1 and 4 uv or positive fluctuations in the streamwise velocity component. Thus, the gradient in the streamwise velocity component was used as a measure of the clarity of the interface between the burst and sweep events. Examination of Figure 16 shows that the sweep follows the burst almost immediately. However, the interface at the leading edge of the burst is substantially less distinct and because of this lack of clarity at the leading edge no estimate of the phase relationship between a burst and a sweep can be made at the leading edge .

5. Conclusions

A comparison of the long time-averaged flow quantities of a drag-reducing flow with a water flow showed that the decrease in wall shear stress in low concentration polymer flows is associated with damping of the velocity fluctuations normal to the wall. The turbulent shear stress is also damped in this region ($y^+ < 60$) indicating a decrease in turbulent mixing of the fluid near the wall with fluid in the outer portion of the flow. This decreased mixing is consistent with the flow visualization results of Tiederman et al. (1985) who showed that near the injection of drag-reducing additives that dyed fluid near the wall required twice the distance to mix into the buffer region compared to a corresponding water flow.

Instantaneous flow angle distributions for the water and two drag-reducing flows indicated that the flow on the center line of the channel are very similar. However, in the buffer region, the drag-reducing flows have a narrower distribution of flow angle than a water flow with a higher probability for angles $-0.25^\circ < \beta < 0.25^\circ$ in these drag-reducing flows. This is further evidence of decreased mixing. At the sublayer-buffer region interface there is again a slightly higher probability for small angles in the drag-reducing flows.

In the low concentration drag-reducing flows the average time between bursts increased, which is consistent with the damping of the turbulent shear stress near the wall. However, the change in the average time between bursts for the low concentration drag-reducing flow, when compared to a water flow at the same wall shear stress, was equal to the change in streak spacing. Thus, the average time between bursts from a streak in the low concentration drag-

reducing flows was the same as that for a water flow. The average number of ejections per burst was only 2.25 to 2.46 for the low concentration, well-mixed solutions. Further upstream near the injector where the additive concentration is about 20 ppm or more, the average number of ejections per burst is about 3.5 (Luchik and Tiederman, 1984). This difference and the differences in the time between bursts for the same level of drag reduction indicate that the mechanism by which a very low concentration (1-3 ppm) of additives reduce drag may be different than the mechanism for solutions with concentrations above 20-50 ppm.

Although the average time between bursts from a streak was the same in the low concentration drag-reducing flow as in a water flow with the same shear velocity, the conditionally sampled ejection and burst characteristics showed that both the ejection and burst structures in the low concentration drag-reducing flow were damped. However, in the drag-reducing flow that matched the Reynolds number of the water flow, these events were damped in such a fashion that the average deficit in the streamwise velocity and the average normal velocity of the events relative to the corresponding RMS value were equal to those obtained in a water flow. The contribution to $\overline{uv}$ during the burst and ejection events for these two flows was also similar. The conditional velocity averages also indicated that the ejection interfaces for both of the drag-reducing flows were nearly the same as those for the water flow. However the drag-reducing bursts had more distinct interfaces than those in the water flow.

This research was supported by the Office of Naval Research contract number N00014-83K-0183, NR062-54.

References

Achia, B.U. and Thompson, D.W. 1977 Structure of the turbulent boundary layer in drag reducing pipe flow. J. Fluid Mech., 81, 439.

Alfredsson, P.H. and Johansson, A.V. 1984 On the detection of turbulence generating events. J. Fluid Mech., 139, 325.

Bogard, D.G. 1982 Investigation of burst structures in turbulent channel flows through simultaneous flow visualization and velocity measurements, Ph.D. Thesis, Purdue University.

Bogard, D.G. and Tiederman, W.G. 1983 Investigation of flow visualization techniques for detecting turbulent bursts. In Symposium on Turbulence, 1981 (ed. X.B. Reed, G.K. Patterson and J.L. Zakin), p. 289. University of Missouri - Rolla.

Corino, E.R. and Brodkey, R.S. 1969 A visual study of turbulent shear flow. J. Fluid Mech., 37, 1.

Donohue, G.L., Tiederman, W.G. and Reischman, M.M. 1972 Flow visualization of the near-wall region in a drag-reducing flow. J. Fluid Mech., 56, 559.

Instruction Manual for System 9100-6, Single Channel High Power LDV, Thermo-Systems Incorporated, St. Paul, Minnesota.

Johansson, A.V. and Alfredsson, P.H. 1983 Effects of imperfect spatial resolution on measurements of wall-bounded turbulent shear flows. J. Fluid Mech., 137, 409.

Kim, H.T., Kline, S.J. and Reynolds, W.C. 1971 The production of turbulence near a smooth wall in a turbulent boundary layer. J. Fluid Mech., 50, 133.

Logan, S.E. 1972 A laser velocimeter measurement of Reynolds stress in dilute polymer solutions. Ph.D. Thesis, California Institute of Technology.

Luchik, T.S. 1982 A laser velocimeter investigation of turbulent flow in an axisymmetric sudden expansion. Master's Thesis, Purdue University.

Luchik, T.S. and Tiederman, W.G. 1984 Bursting rates in channel flows and drag reducing channel flows. In Symposium on Turbulence, 1983, (ed. X.B. Reed, G.K. Patterson, and J.L. Zakin), p. 15, University of Missouri - Rolla.

Luchik, T.S. and Tiederman, W.G. 1985 Effect of spanwise probe volume length on laser velocimeter measurements in wall bounded turbulent flows. Exp. Fluids, 3, 339.

Luchik, T.S. and Tiederman, W.G. 1985 Time scale and structure of ejections and burst in turbulent channel flows, Submitted to J. Fluid Mech.

McComb, W.D. and Rabie, L.H. 1982 Local drag reduction due to injection of polymer solutions into turbulent flow in a pipe. Part I: Dependence on local polymer concentration; Part II: Laser-Doppler measurements of turbulent structure. AICHE J. 28, 547.

Offen, G.R. and Kline, S.J. 1975 A comparison and analysis of detection methods for the measurement of production in a boundary layer. In Proc. 3rd Biennial Symposium on Turbulence in Liquids (ed. G.K. Patterson and J.L. Zakin), p. 289, University of Missouri - Rolla.

Oldaker, D.K. and Tiederman, W.G. 1977 Spatial structure of the viscous

sublayer in drag-reducing channel flows. Phys. Fluids 20, No. 10, Pt. II, S133.

Reischman, M.M. and Tiederman, W.G. 1975 Laser Doppler anemometer measurements in drag-reducing channel flows. J. Fluid Mech., 70, 369.

Stevenson, W.H., Thompson, H.D. and Roesler, T.C. 1982 Direct measurements of laser velocimeter bias errors in a turbulent flow. AIAA Journal, 20, 1720.

Tiederman, W.G., Smith, A.J. and Oldaker, D.K. 1977 Structure of the viscous sublayer in drag-reducing channel flows. In Turbulence in Liquids 1975, (ed. J.L. Zakin and G.K. Patterson), p. 312. University of Missouri - Rolla.

Tiederman, W.G., Luchik, T.S. and Bogard, D.G. 1985 Wall layer structure and drag reduction. J. Fluid Mech., 156, 419.

Walker, D.T., Tiederman, W.G. and Luchik, T.S. 1986 Optimization of the injection process for drag reducing additives. Exp. Fluids, 4, 114.

Wells, C.S. and Spangler, J.G. 1967 Injection of a drag-reducing fluid into turbulent pipe flow of a Newtonian fluid. Phys. Fluids 10, 1980.

Willmarth, W. W. and Sharma, L.K. 1984 Study of turbulent structure with hot wires smaller than the viscous length. J. Fluid Mech., 142, 121.

Table 1 Laser Velocimeter Parameters

	Blue	Green
Probe volume length (mm)	1.024	1.080
Probe volume diameter (μm)	52.4	55.2
Fringe Spacing (μm)	3.402	3.624
Effective Frequency Shift (MHz)	-1.0	+1.0
Beam Spacing (mm)	35.3	35.3

Table 2 Experimental Conditions

	Water	Drag Reducing #1 (DR1)	Drag Reducing #2 (DR2)
Re_h	17800	17800	22000
U_m (m/s)	.646	.647	.799
U_o (m/s)	.782	.776	.936
u_τ (cm/s)	3.77	3.33	3.77
ν (m^2/s) $\cdot 10^{+6}$	.907	.907	.907
DR (%)	--	22	31
C (ppm)	--	1.3	2.1

Table 3. Comparison of Additive Constants for Overlap Region*

% Drag Reduction	Reischman and Tiederman (1975)	Present Study
22	4.3	3.0
31	7.4	4.34

* $U^+ = 1/\kappa \ln y^+ + B + \Delta B$

Table 4. Comparison of conditionally sapled quantities during an ejection detection for the three flow situations using the modified u-level technique at $y^+ = 30$.

		water	case DR1	case DR2
Re_h		17800	17800	22000
%DR		0.0	22.0	30.8
$\overline{T}_E$ (sec)		0.030	0.047	0.043
$\overline{T}_{DE}$ (sec)		0.008	0.013	0.011
$\overline{T}^+_{DE}$		12.4	15.8	1.4
Intermittency		0.26	0.27	0.26
Percent contribution	1	0	0	0
to uv in a quadrant	2	84	84	82
by quadrant	3	66	74	77
	4	0	0	0
Percent contribution	1	0	0	0
to $\overline{uv}$	2	83	79	87
by quadrant	3	-25	-26	-42
	4	0	0	0
$\langle u \rangle / u'$		-1.227	-1.241	-1.242
$\langle v \rangle / v'$		0.399	0.374	0.288
$\langle uv \rangle / \overline{uv}$		2.30	2.00	1.76
$\langle uv \rangle / u'v'$		0.585	0.333	0.384

Table 5. Comparison of conditionally sapled quantities during an burst detection for the three flow situations using the modified u-level technique at $y^+ = 30$.

		water	case DR1	case DR2
Re_h		17800	17800	22000
%DR		0.0	22.0	30.8
T_B (sec)		0.063	0.106	0.105
Average number of ejectons/burst		2.10	2.25	2.46
$\overline{T}_{DB}$ (sec)		0.024	0.041	0.045
$\overline{T}^+_{DB}$		37.6	50.0	70.5
Intermittency		0.380	0.387	0.428
Percent contribution to uv in a quadrant by quadrant	1	7	9	14
	2	89	90	90
	3	76	83	88
	4	7	8	11
Percent contribution to $\overline{uv}$ by quadrant	1	-2	-3	-4
	2	88	84	96
	3	-29	-29	-48
	4	5	5	8
$\langle u \rangle / u'$		-0.865	-0.862	-0.729
$\langle v \rangle / v'$		0.244	0.237	0.164
$\langle uv \rangle / \overline{uv}$		1.68	1.52	1.23

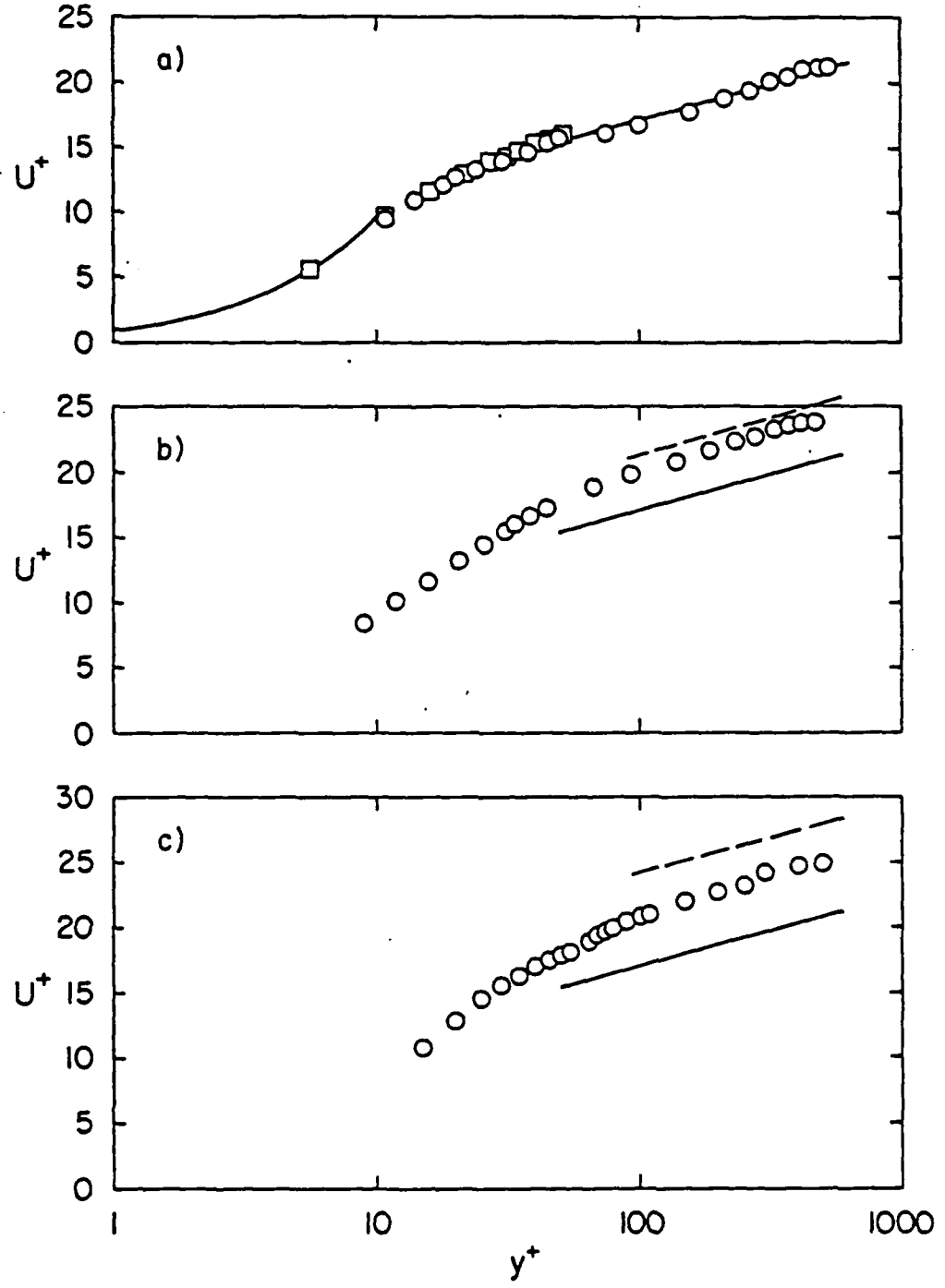

Figure 1. Mean streamwise velocity profile normalized with inner variables for a) water flow, b) Case DR1, c) Case DR2; ○ - Present study, □ - Luchik and Tiederman (1985); —— $U^+ = 2.44 \ln y^+ + 6.0$, ---- ΔB values from Reischman and Tiederman (1975).

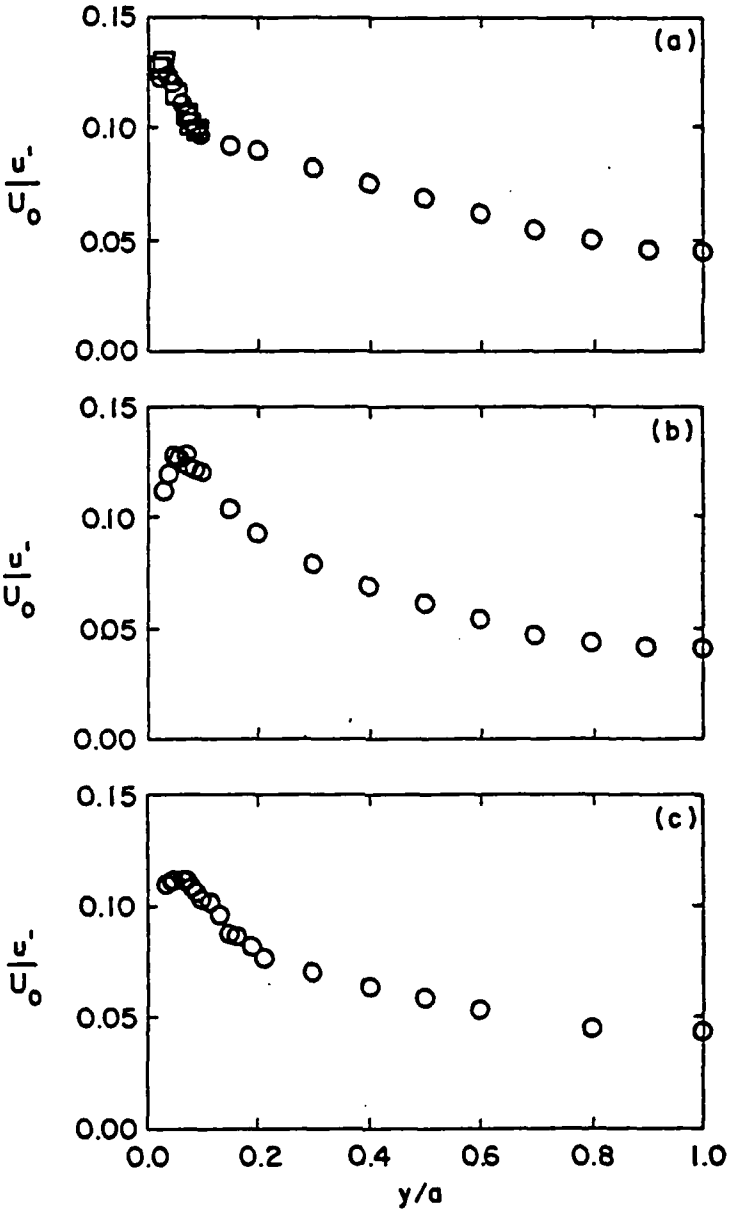

Figure 2. Streamwise RMS velocity normalized with center-line velocity; a) Water flow, b) Case DR1, c) Case DR2; ○ - Present study, □ - Luchik and Tiederman (1985).

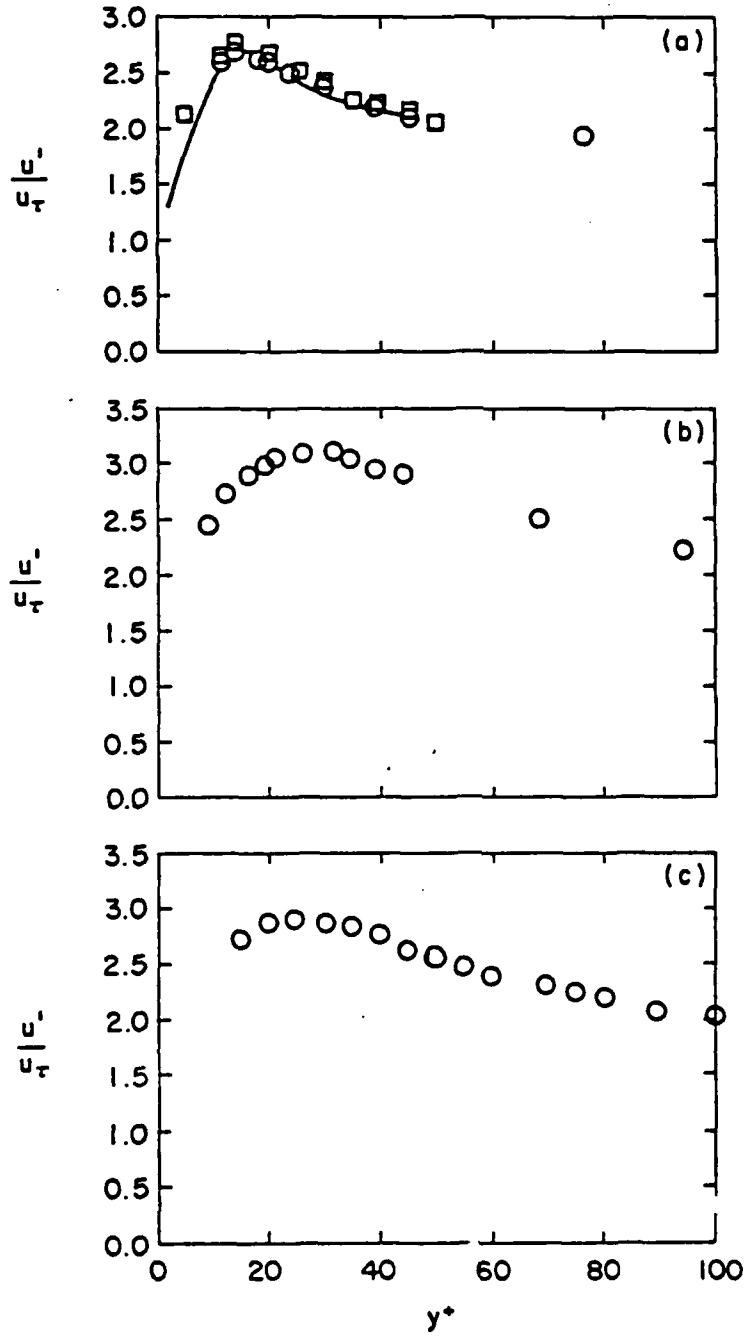

Figure 3. Streamwise RMS velocity normalized with wall shear velocity; a) Water flow, b) Case DR1, c) Case DR2; ——— Johansson and Alfredsson (1983), □ - Luchik and Tiederman (1985), ○ - two component measurement.

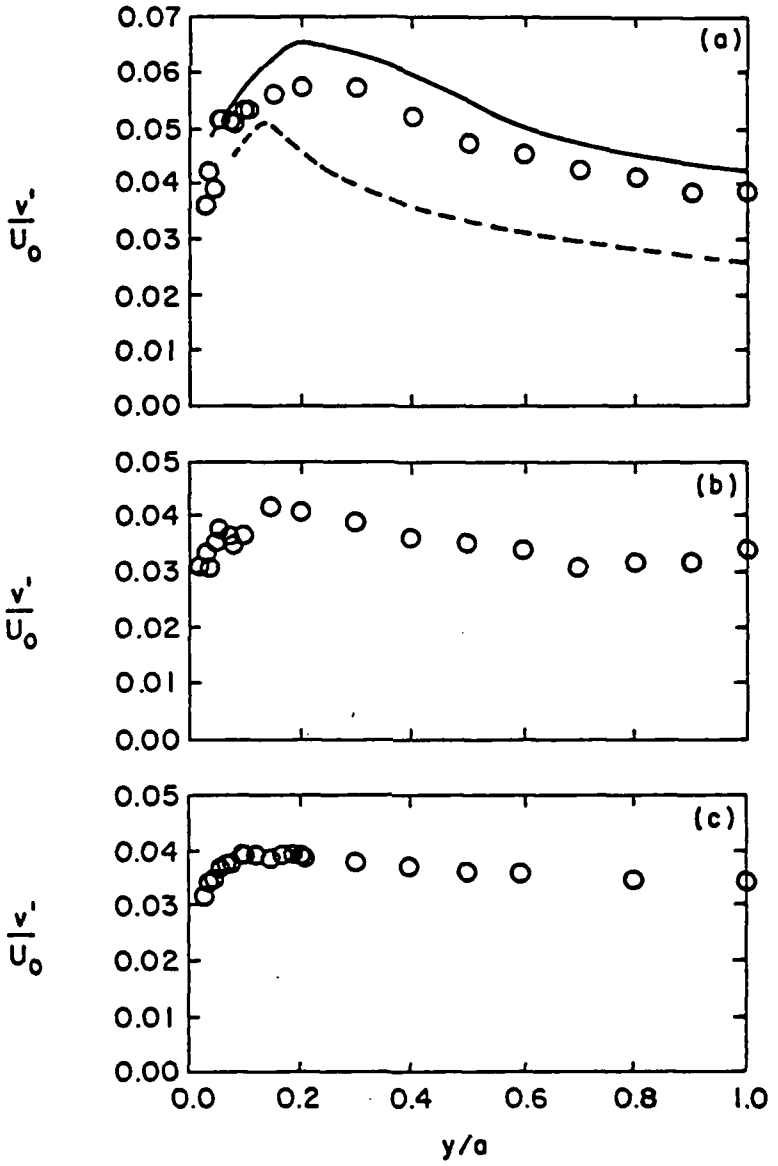

Figure 4. Normal RMS velocity normalized with center-line velocity; a) Water flow, b) Case DR1, c) Case DR2; —— Bogard (1982), - - - - Alfredsson and Johansson (1984).

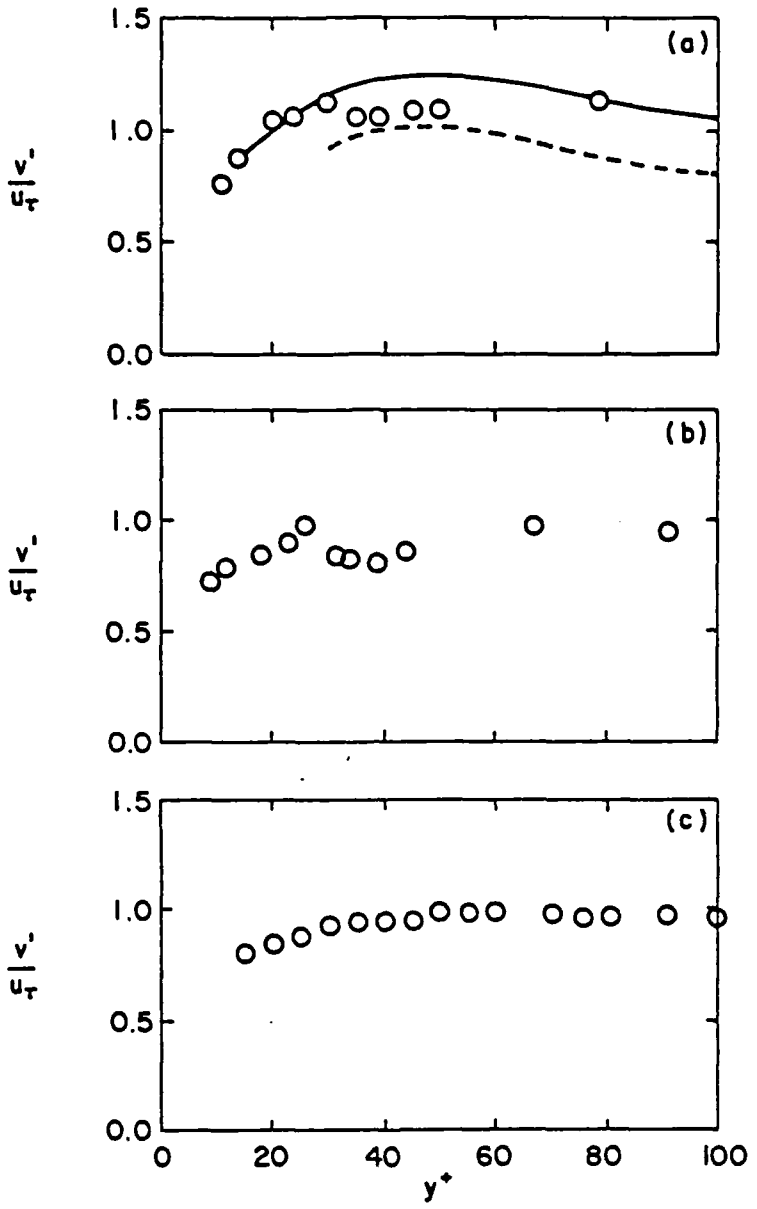

Figure 5. Normal RMS velocity normalized with wall shear velocity; a) Water flow, b) Case DR1, c) Case DR2; —— Bogard (1982), ---- Alfredsson and Johansson (1984).

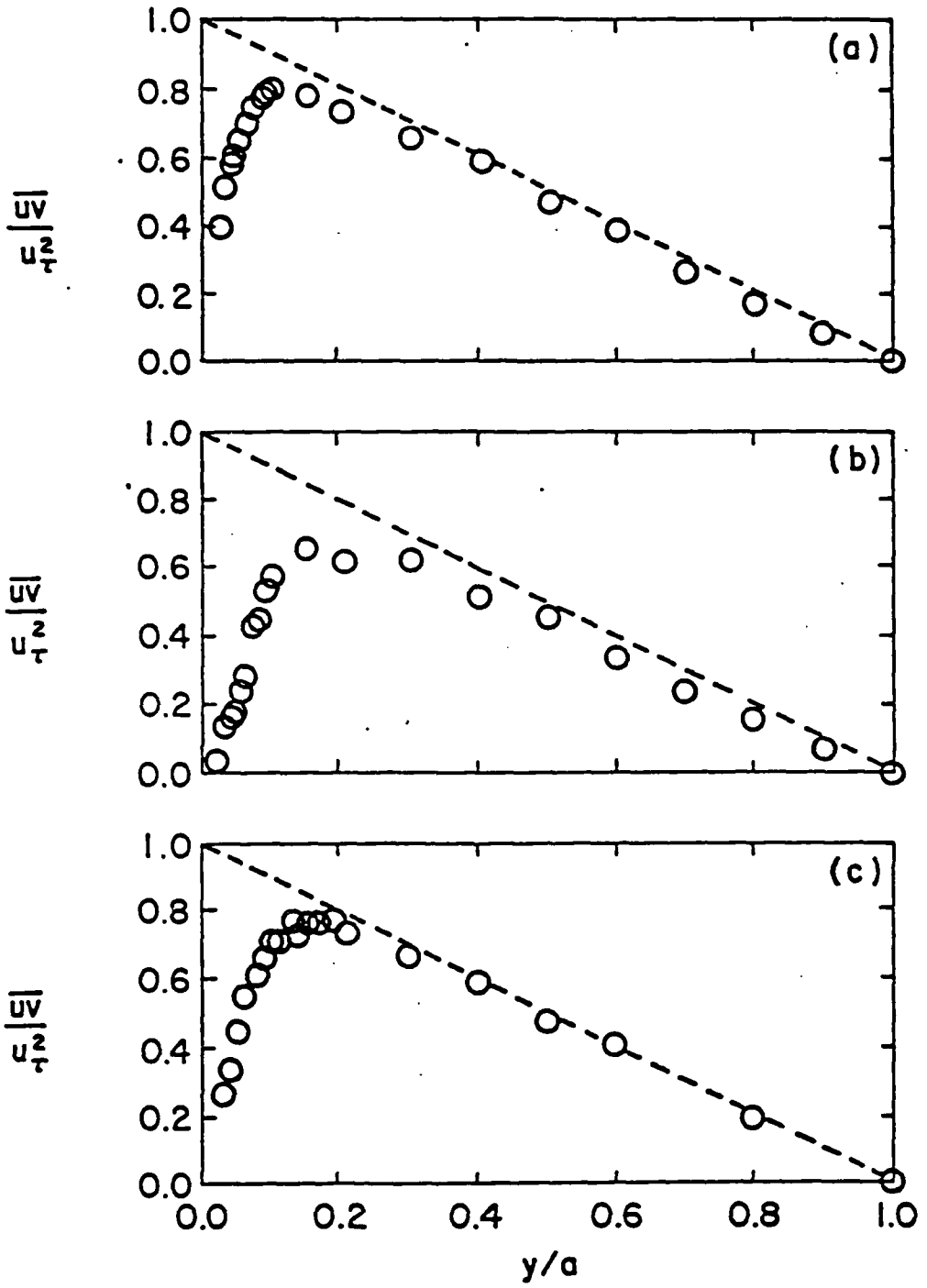

Figure 6. Turbulent shear stress distribution across channel half height; a) Water flow, b) Case DR1, c) Case DR2; ---- total shear stress distribution.

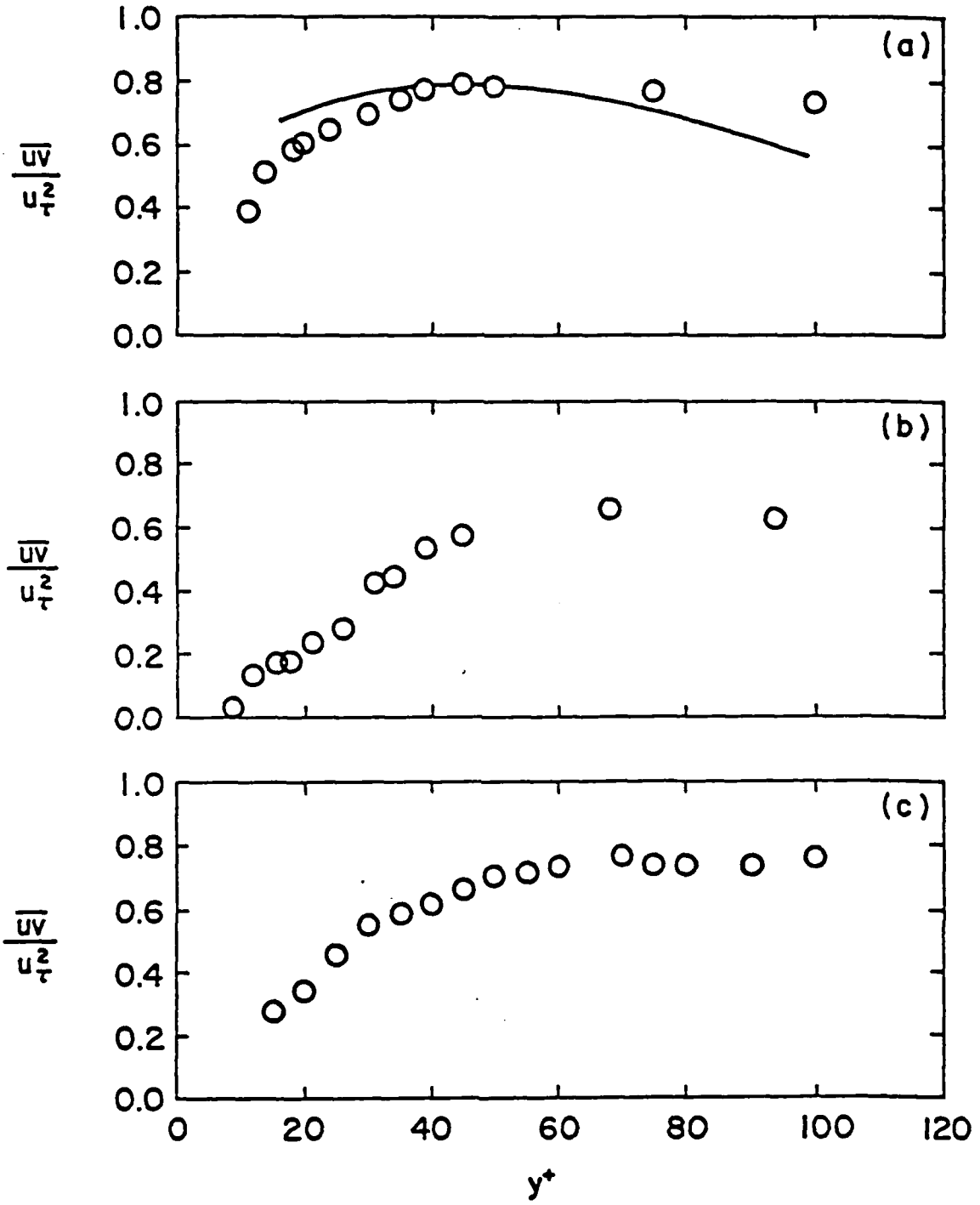

Figure 7. Tubulent shear stress normalized with inner variables; a) Water flow, b) Case DR1, c) Case DR2; ——— Bogard (1982).

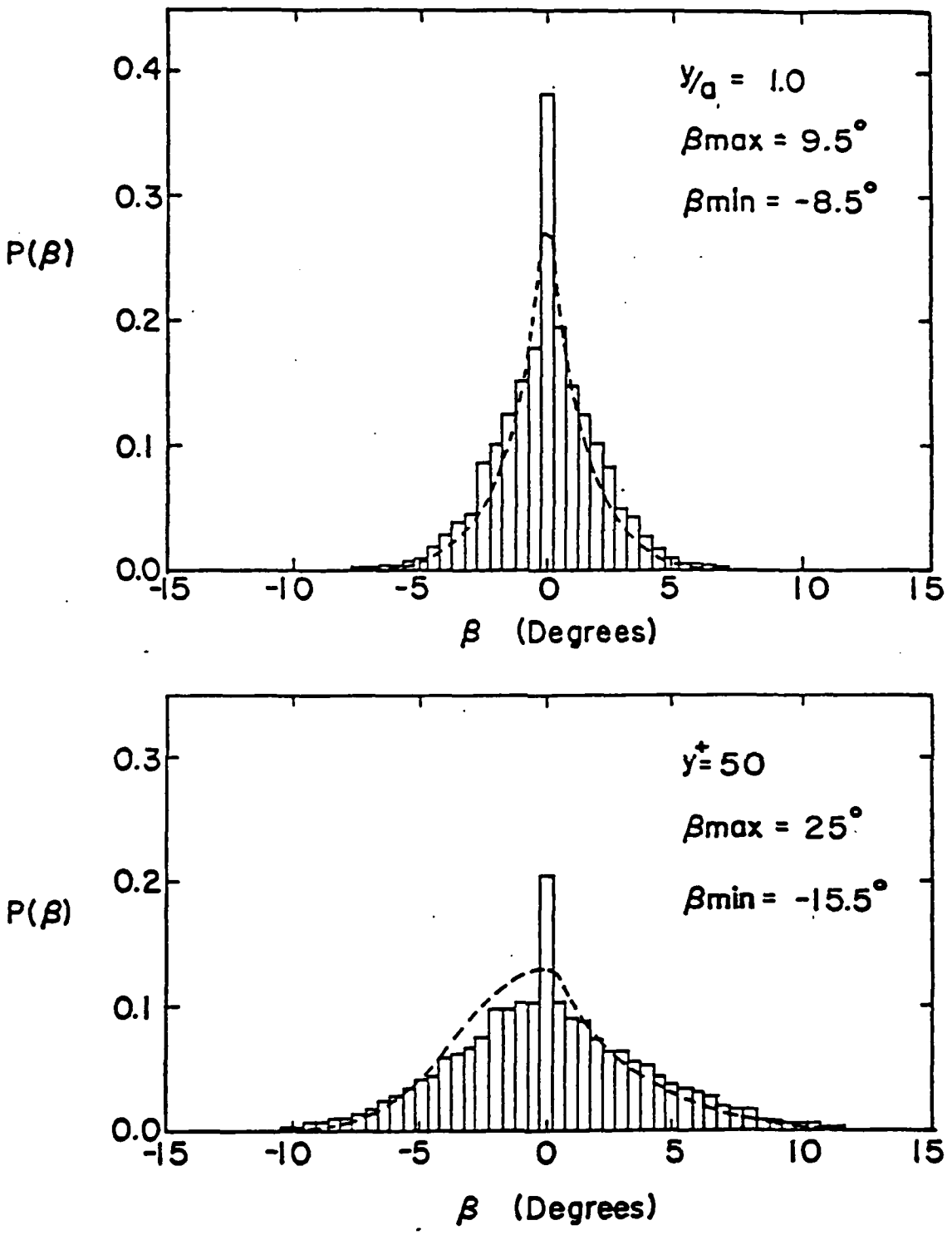

Figure 8. Instantaneous flow angle distribution for the water flow on channel centerline and at $y^+ = 50$, ---- Alfredsson and Johansson (1984).

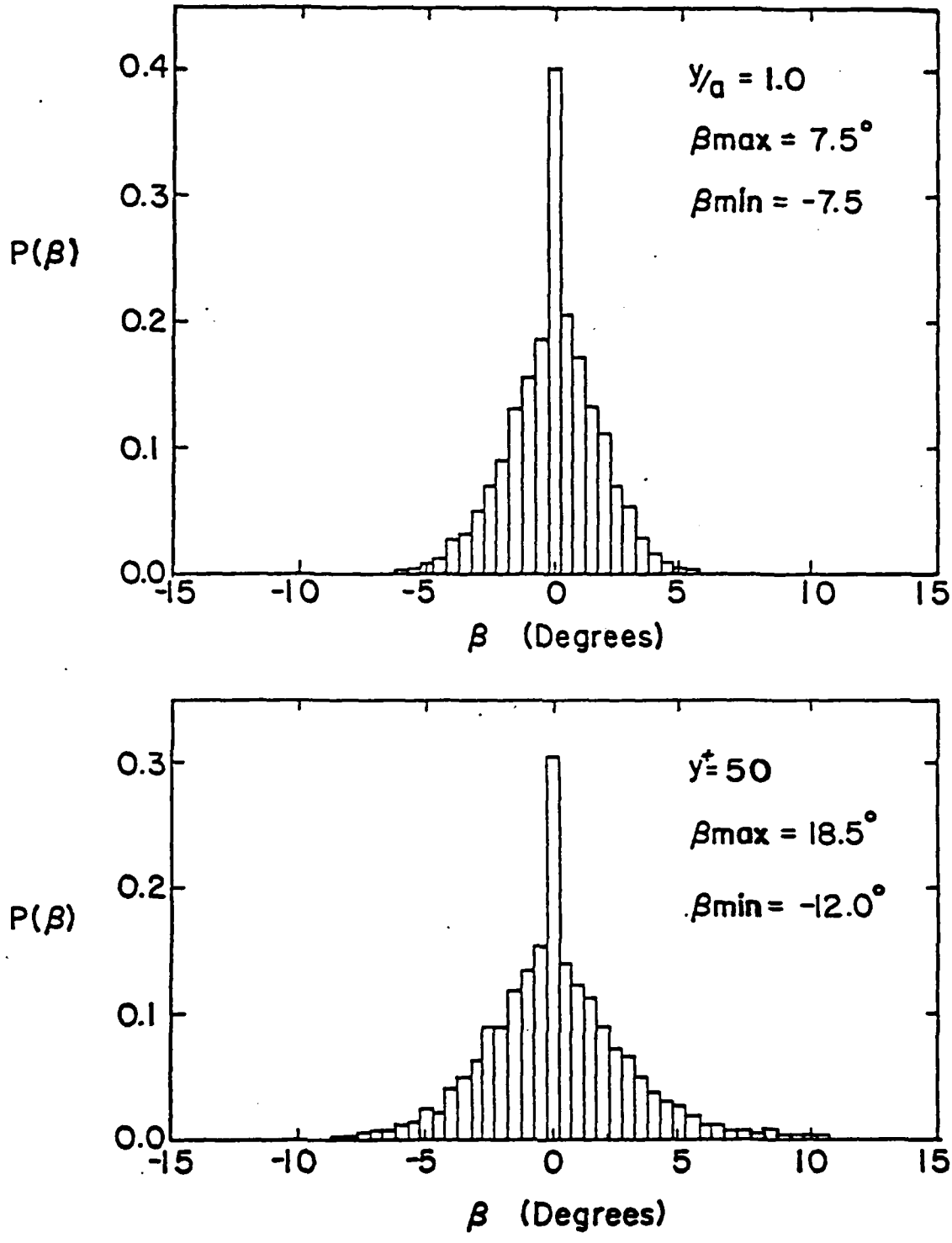

Figure 9. Instantaneous flow angle distribution for Case DR1 on channel centerline and at $y^+ = 50$.

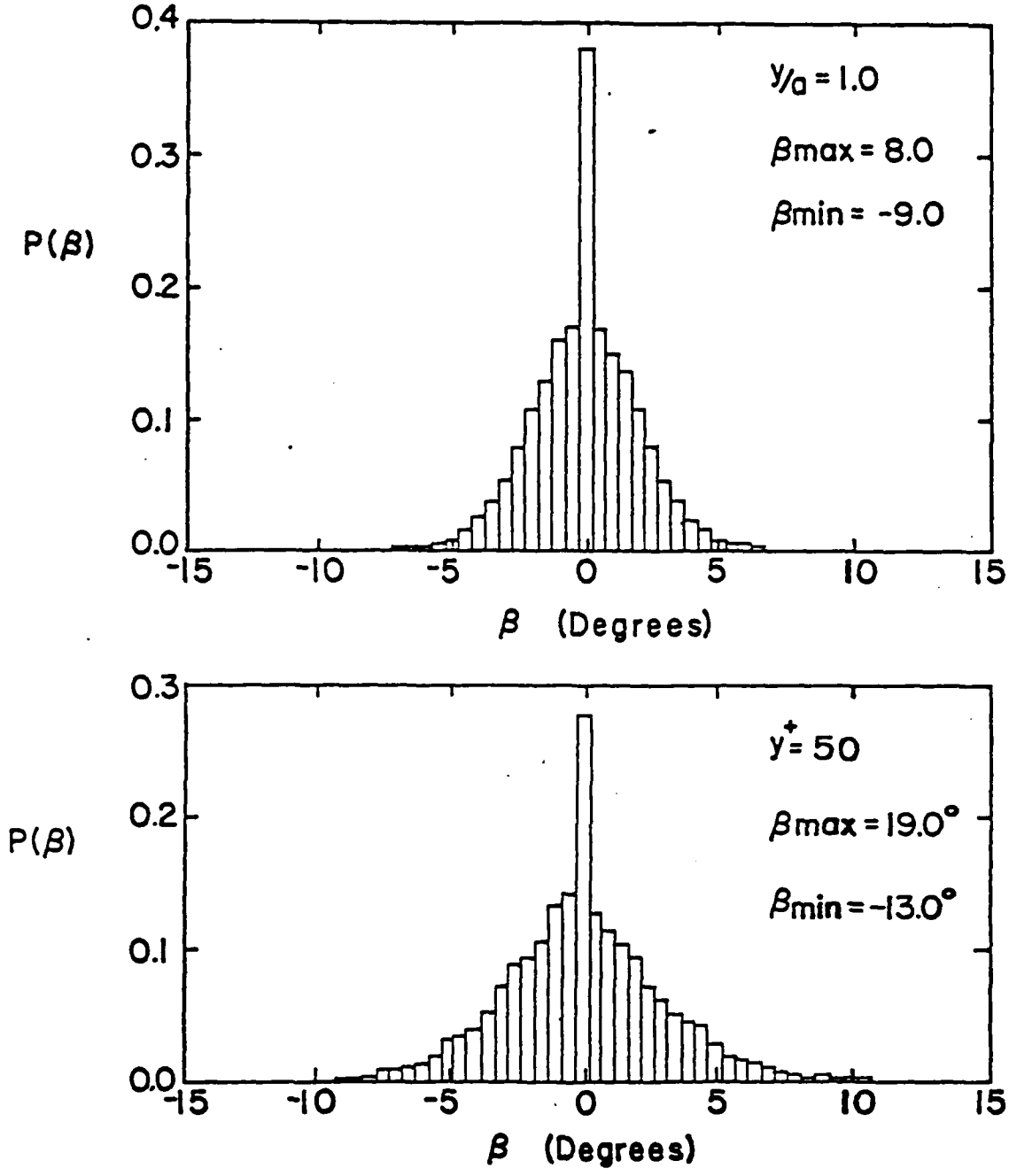

Figure 10. Instantaneous flow angle distribution for Case DR2 on channel centerline and at $y^+ = 50$.

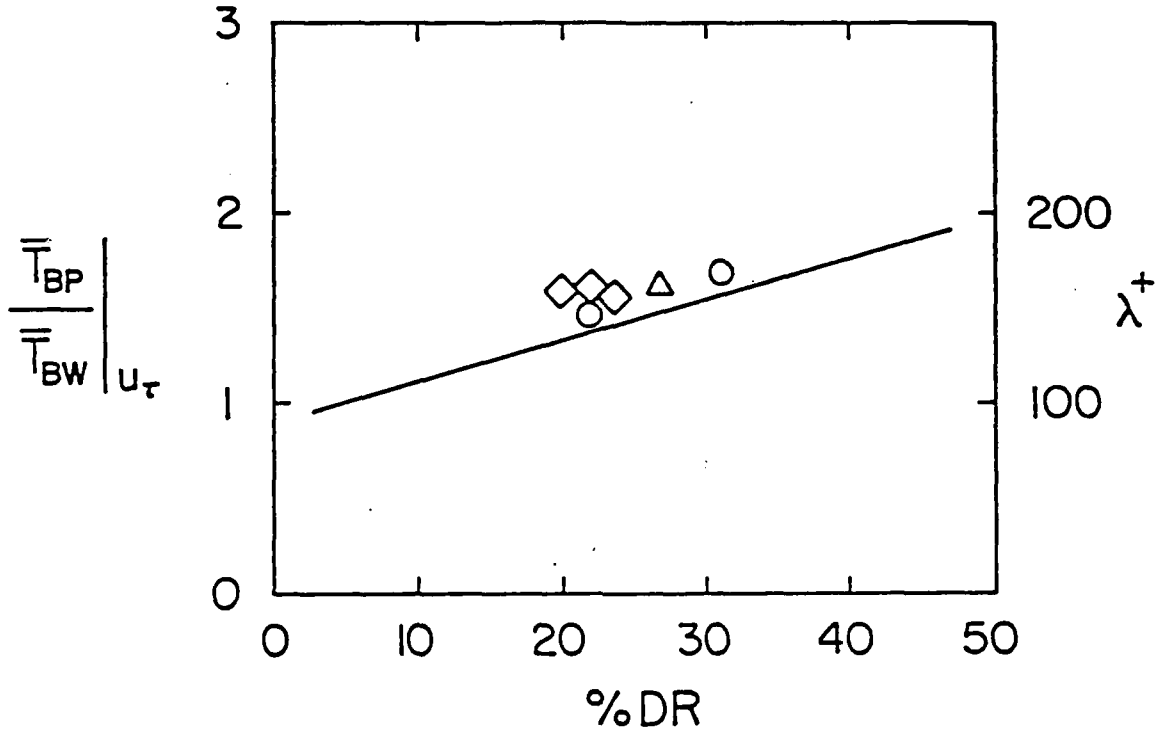

Figure 11. Variation in the ratio of the average time between bursts in a drag-reducing flow to that of a water flow at an equal shear velocity; ◇ flow visualization - present study, ○ modified u-level - present study, △ flow visualization - Walker et al. (1985); ——, $\lambda^+ = 99.7 + 1.9$ DR.

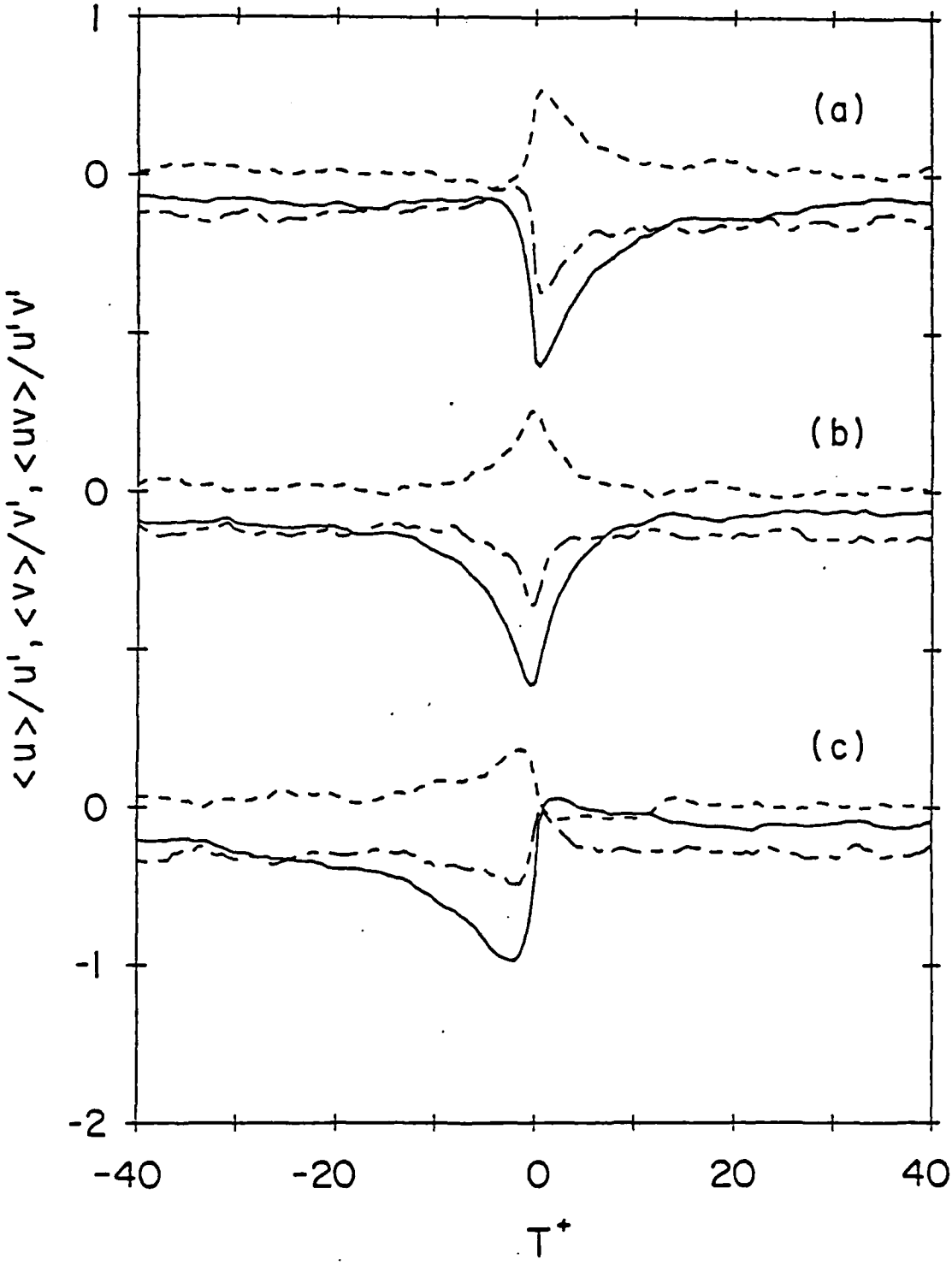

Figure 12. Conditionally averaged velocity signals for the water flow centered on a) leading edge, b) middle, c) trailing edge of an ejection; ——— <u>, ---- <v>, —·—·— <uv>.

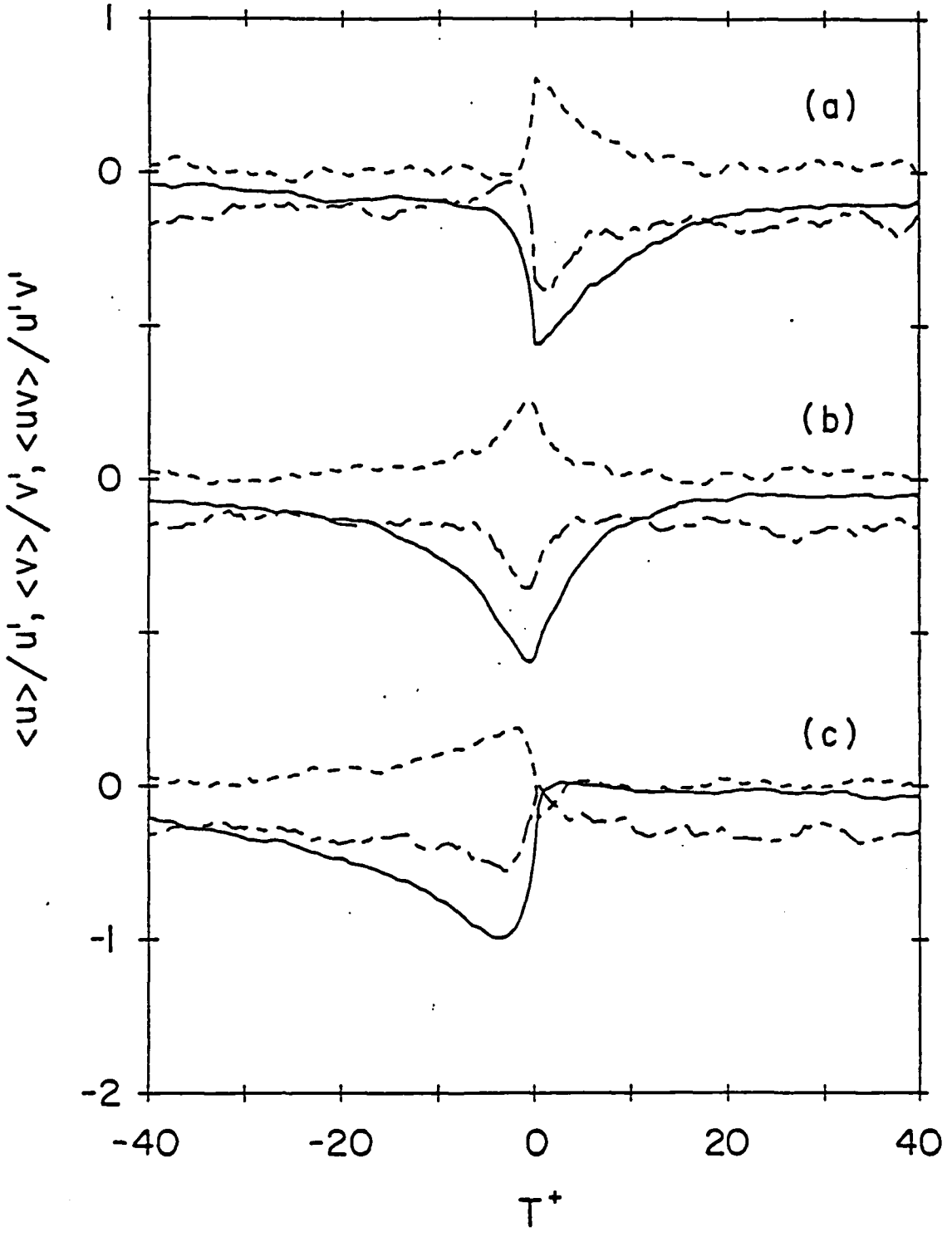

Figure 13. Conditionally averaged velocity signals for case DR1 centered on a) leading edge, b) middle, c) trailing edge of an ejection; —— <u>, ---- <v>, —·—·— <uv>.

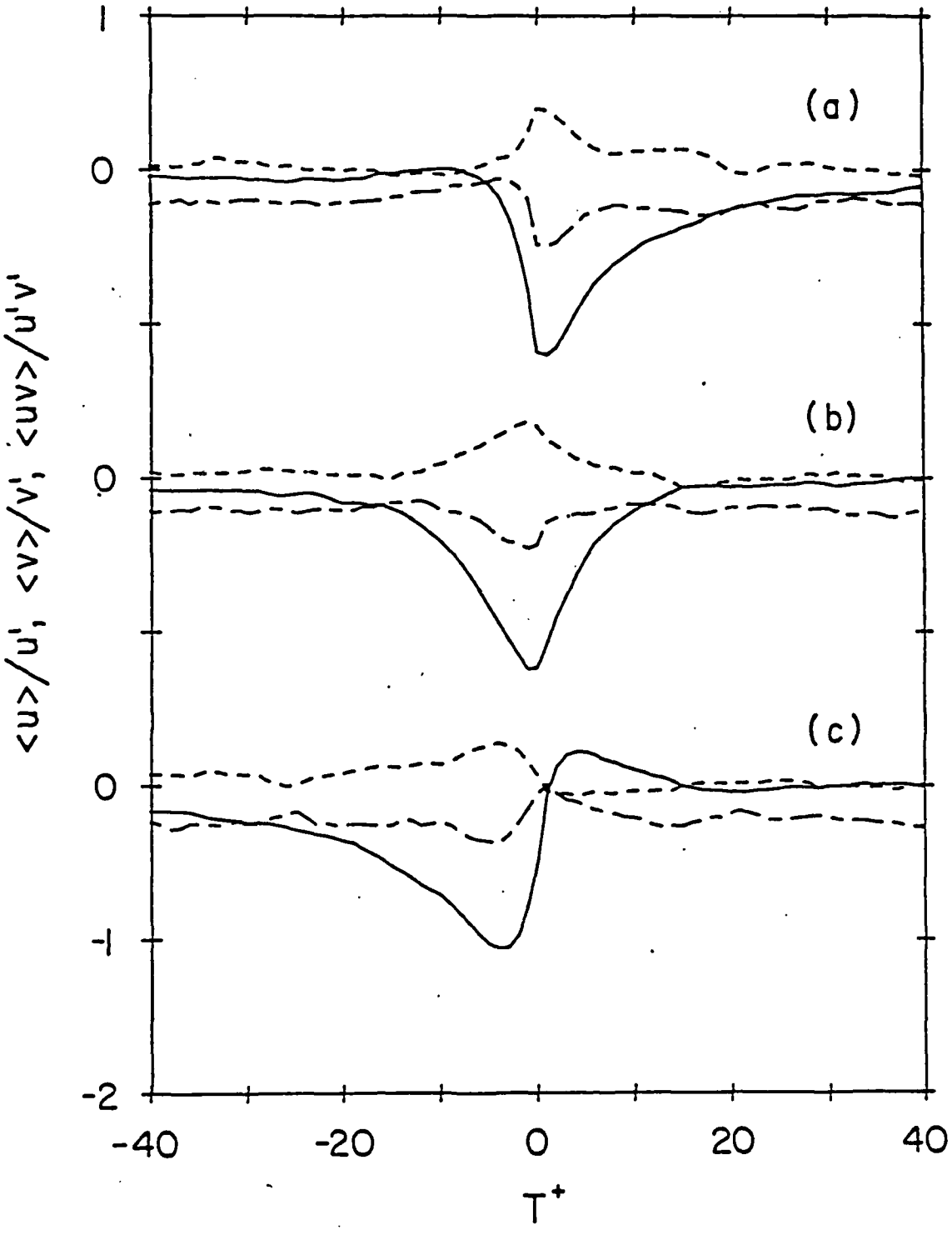

Figure 14. Conditionally averaged velocity signals for case DR2 centered on a) leading edge, b) middle, c) trailing edge of an ejection; —— <u>, ---- <v>, —·—·— <uv>.

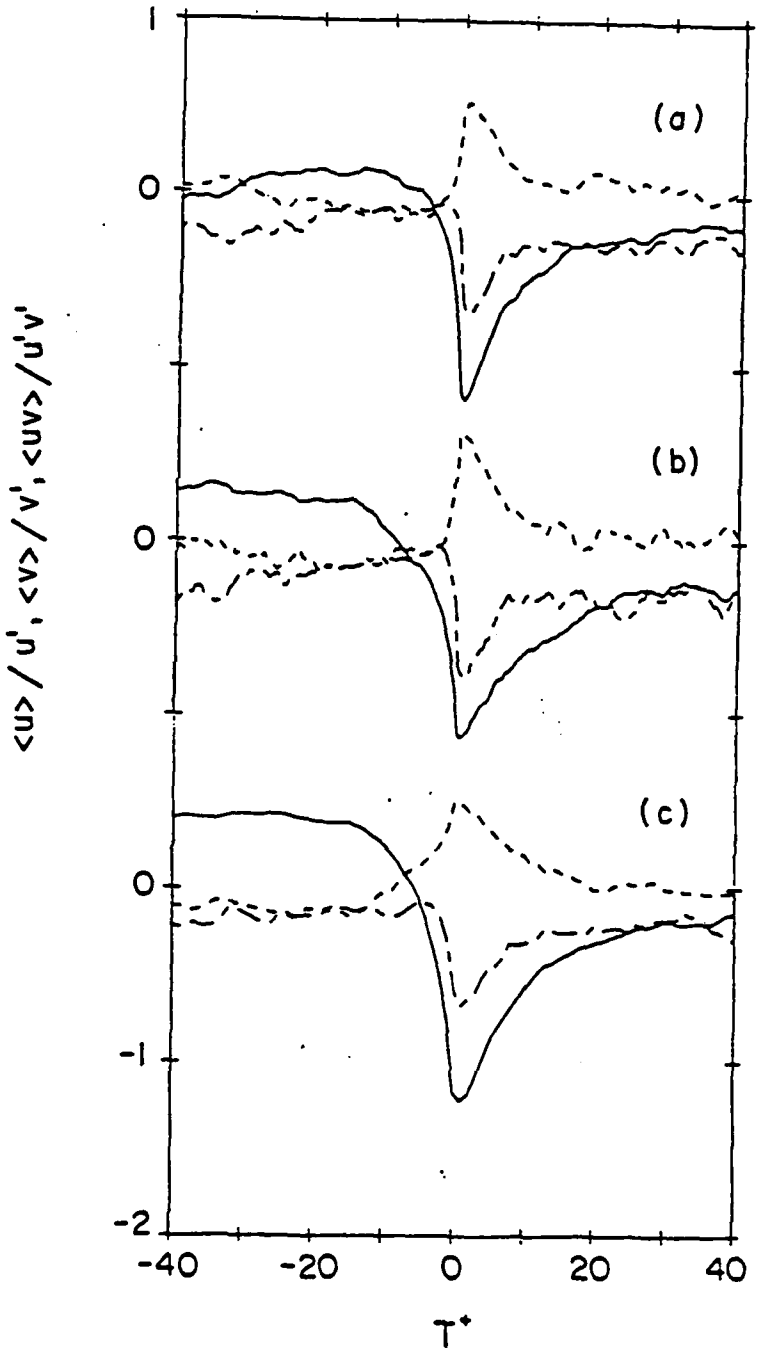

Figure 15. Conditionally averaged velocity signals centered on the leading edge of a burst for a) water flow, b) Case DR1, c) Case DR2; ——— <u>, ---- <v>, ——·——<uv>.

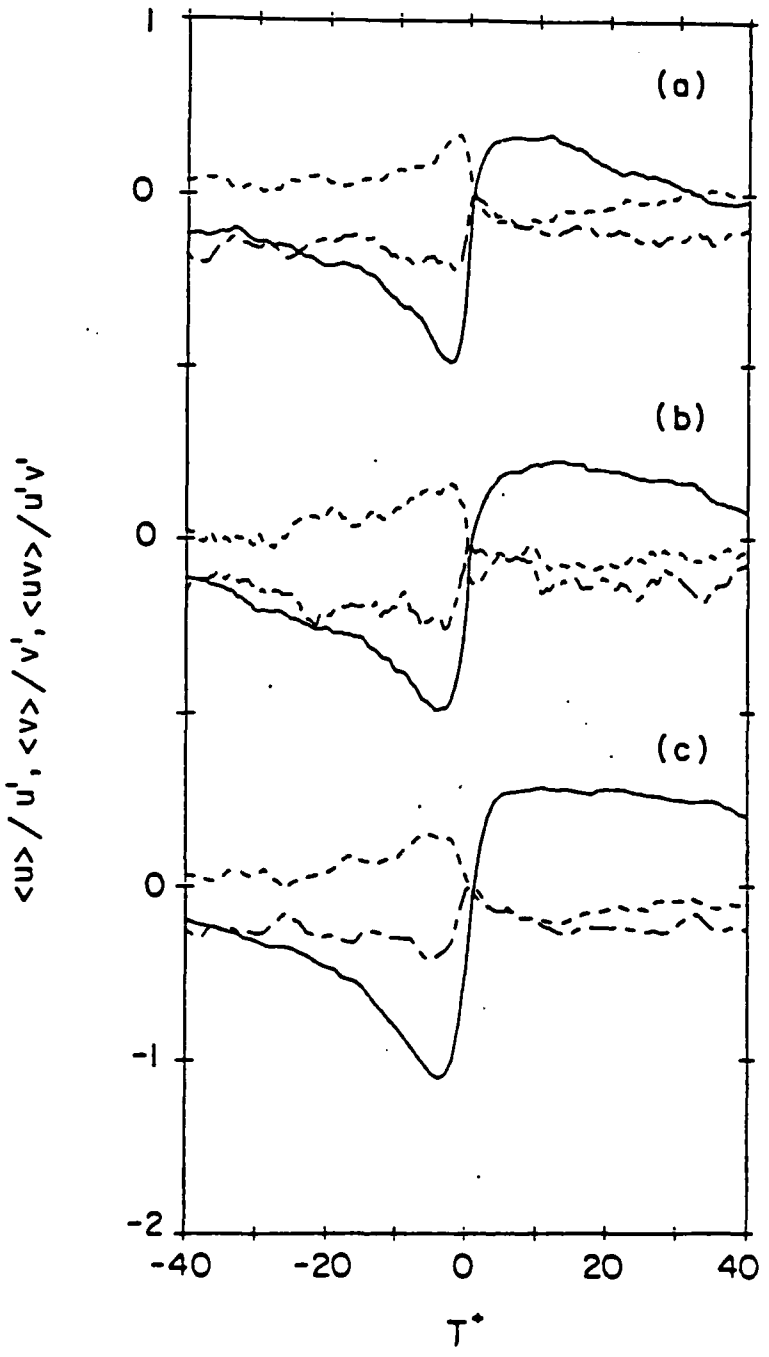

Figure 16. Conditionally averaged velocity signals centered on the trailing edge of a burst for a) water flow, b) Case DR1, c) Case DR2;——— <u>, ---- <v>,— - — <uv>.

APPENDIX C

List of Publications, Presentations and Degrees Granted to Participants.

Publications

1. Tiederman, W.G., Luchik, T.S. and Bogard, D.G., "Wall layer structure and drag reduction," J. Fluid Mechanics, 156 pp. 419-437, July 1985.

2. Luchik, T.S. and Tiederman, W.G., "Effect of spanwise probe volume length on laser velocimeter measurements in wall bounded turbulent flows," Experiments in Fluids, 3, pp. 339-341, 1985.

3. Walker, D.T., Tiederman, W.G. and Luchik, T.S., "Optimization of the injection process for drag-reducing additives," Experiments in Fluids, 4, pp. 114-120, 1986.

Presentations

1. T.S. Luchik, "Turbulent Channel Flows," Fluid Mechanics Seminar, School of Mechanical Engineering, Purdue University, April 26, 1985.

2. W.G. Tiederman, "Turbulent Structure in Low Concentration Drag-Reducing Channel Flows," Drag Reduction and Boundary Layer Control Symposium, National Academy of Sciences, Washington, DC, October 23, 1985.

3. T.S. Luchik, "Eulerian Techniques for Detecting Bursts in Turbulent Wall Flows," 38th Annual Meeting of the Division of Fluid Dynamics, American Physical Society, Tucson, AZ, November 25, 1985.

Degrees Granted

1. D.T. Walker, MSME, School of Mechanical Engineering, Purdue University, May 1985.

2. T.S. Luchik, Ph.D., School of Mechanical Engineering, Purdue University, August 1985.

APPENDIX D

Distribution List

Dr. Michael M. Reischman, Code 432
Office of Naval Research
800 North Quincy Street
Arlington, VA 22217

Office of Naval Research
Resident Representative
536 S. Clark Street, Rm 286
Chicago, IL 60605-1588

Director
Naval Research Laboratory
ATTN: Code 2627
Washington, DC 20375
(6 copies)

Defense Technical Information Center
Building. 5, Cameron Station
Alexandria, VA 22314
(12 copies)

Mechanical Engineering Business Office
Purdue University
West Lafayette, IN 47907

Dr. Steve Deutsche
ARL
Pennsylvania State University
P. O. Box 30
State College, PA 16801

James H. Green, Code 634
Naval Ocean System Center
San Diego, CA 92152

Dr. R. J. Hansen, Code 5844
Naval Research Laboratory
Washington, DC 20375

Dr. D. L. Hunston
Polymer Sciences & Standards Division
National Bureau of Standards
Washington, DC 20234

Mr. G. W. Jones
Code 55W3
Naval Sea Systems Command
Washington, DC 20362

Dr. O. Kim, Code 6124
Naval Research Laboratory
Washington, DC 20375

G. Leal
Department of Chemistry and
Chemical Engineering
California Institute of Technology
Pasadena, CA 91125

Justin H. McCarthy
Code 1540
David Taylor Naval Ship R&D Center
Bethesda, MD 20084

Professor E. W. Merrill
Department of Chemical Engineering
Massachusetts Institute of Technology
Cambridge, MA 02139

Dr. T. E. Pierce
Code 63R31
Naval Sea Systems Command
Washington, DC 20362

Professor W. W. Willmarth
Department of Aerospace Engineering
University of Michigan
Ann Arbor, MI 48109

END

DTIC

6-86